Summer 2019

Performance of Cognitive Radio Networks with Unknown Dynamic Primary User Signals

Sara L. MacDonald
Old Dominion University, smacd006@odu.edu

PERFORMANCE OF COGNITIVE RADIO NETWORKS WITH UNKNOWN DYNAMIC PRIMARY USER SIGNALS

by

Sara L. MacDonald
B.S.May 2000, South Dakota School of Mines and Technology
M.S. May 2013, Old Dominion University

A Dissertation Submitted to the Faculty of
Old Dominion University in Partial Fulfillment of the
Requirements for the Degree of

DOCTOR OF PHILOSOPHY

ELECTRICAL & COMPUTER ENGINEERING

OLD DOMINION UNIVERSITY
August 2019

Approved by:

Dimitrie C. Popescu (Director)

W. Steven Gray (Member)

Dean J. Krusienski (Member)

Otilia Popescu (Member)

ABSTRACT

PERFORMANCE OF COGNITIVE RADIO NETWORKS WITH UNKNOWN DYNAMIC PRIMARY USER SIGNALS

Sara L. MacDonald
Old Dominion University, 2019
Director: Dr. Dimitrie C. Popescu

The current static assignment of RF spectrum in the United States and other parts of the world has led to a large portion of the RF spectrum to be geographically and temporally underutilized. While the amount of RF spectrum is finite, the demand for spectrum continues to increase making it necessary to increase utilization of many bands. Several innovative methods for allowing licensed primary users (PUs) to share spectrum with unlicensed secondary users (SUs) have being proposed. Of these methods Cognitive Radio (CR) has emerged as a promising technology thatenables SUs to dynamically access spectrum after first sensing the spectrum to ensure the PU is not active. Sensing performance is critical to a successful CR implementation, and within the last decade there has been significant CR research examining various sensing challenges and methods to improve sensing performance. The majority of this research has focused on PUs that utilize spectrum with relatively long idle and transmission periods which in turn allows for SU sensing periods with an extended duration.

The work presented in this dissertation focuses on CR systems where the PU is highly dynamic and addresses several issues that arise when attempting to access this spectrum. In the case of a highly dynamic PU, it is not possible for the SU to increase the sensing period to improve performance, resulting in suboptimal sensing performance. A proposed hybrid framework is described which allows for suboptimal sensing performance by limiting the SU transmission power dependent on the sensing capabilities. In order to quantify sensing capabilities, a mathematical model for describing the PU activity with respect to the SU sensing period is derived using the mean active and idle durations of the PU. Using this PU activity model, closed form mathematical expressions for sensing performance are provided for two different hypothesis tests. Finally, the PU activity model and corresponding expressions for sensing performance depend on knowing the mean PU active and idle durations; because the SU may not know these PU parameters, a modified expectation maximization algorithm is proposed to estimate these parameters and corresponding sensor performance.

ACKNOWLEDGEMENTS

Though this dissertation is an individual work, I was able to complete it with the guidance and support of numerous people.

First, I would like to express my deepest gratitude to my advisor, Dr. Dimitrie C. Popescu, for his outstanding technical guidance and mentoring, unfailing support, and of course patience during my Ph.D. studies. On a few occasions he reminded me that I was capable of completing my doctorate degree and provided me the encouragement to keep going.

I owe a large debt of gratitude to all the faculty and staff, past and present, in the Electrical and Computer Engineering Department at Old Dominion University. I would like to particularly thank Dr. W. Steven Gray, Dr. Dean J. Krusienski, and Dr. Otilia Popescu for serving on my committee. Each member played a critical role in the direction of my Ph.D. studies as the work described in this dissertation is centered on wireless communication systems, probability theory and signal processing. My interest in these topics flourished while taking graduate courses from my committee members.

I would like to thank MITRE for funding the majority of my education. Additionally, I would like to thank my supervisors and colleagues at MITRE for their flexibility in allowing me to pursue my education by permitting me to take leaves of absence in various forms over the last several years.

I would like to thank my family for supporting me during my Ph.D. studies. To my children Tiffany and Rusty, thank you for being understanding of your very busy and tired mother and for making many small sacrifices while I pursued my doctoral degree. Finally and most importantly, thank you to my husband Chris. Without his support and encouragement I would not have been able to balance being a working mother and graduate student.

TABLE OF CONTENTS

Page

LIST OF TABLES vii

LIST OF FIGURES x

Chapter

1. INTRODUCTION 1
   - 1.1 PROBLEM STATEMENT 2
   - 1.2 DISSERTATION CONTRIBUTIONS 3
   - 1.3 DISSERTATION OUTLINE 5

2. BACKGROUND AND RELATED WORK 7
   - 2.1 UNDERLYING TECHNOLOGIES 7
   - 2.2 COGNITIVE RADIO WITH DYNAMIC PRIMARY USERS 17

3. HYBRID SPECTRUM SHARING PARADIGM 20
   - 3.1 SPECTRUM SHARING SYSTEM MODEL 21
   - 3.2 PROBABILITY OF COLLISION 23
   - 3.3 CALCULATING PRIMARY USER PERFORMANCE 25
   - 3.4 DEFINING SECONDARY USER OPERATING REGION 29
   - 3.5 EXAMPLE 4-QAM PRIMARY USER SYSTEM 34
   - 3.6 CHAPTER SUMMARY 41

4. DYNAMIC PRIMARY USER MODEL 46
   - 4.1 DYNAMIC PRIMARY USER SYSTEM MODEL 46
   - 4.2 MARKOV CHAIN DYNAMIC PRIMARY USER MODEL 47
   - 4.3 HYPOTHESIS TESTING 50
   - 4.4 JOINT AND CONDITIONAL PROBABILITIES 53
   - 4.5 VERIFICATION OF DYNAMIC PRIMARY USER MODEL 58
   - 4.6 CHAPTER SUMMARY 59

5. DYNAMIC PRIMARY USERS SENSING PERFORMANCE 62
   - 5.1 SPECTRUM SENSING SYSTEM MODEL 62
   - 5.2 STATIC PRIMARY USER DETECTION PERFORMANCE 63
   - 5.3 DYNAMIC PRIMARY USER MIXTURE MODELS 64
   - 5.4 ANY SAMPLE HYPOTHESES DETECTION PERFORMANCE 66
   - 5.5 N^{TH} SAMPLE HYPOTHESES DETECTION PERFORMANCE 67
   - 5.6 VERIFICATION OF DYNAMIC SENSING PERFORMANCE 69
   - 5.7 CHAPTER SUMMARY 71

Page

6. ESTIMATING SENSING PERFORMANCE 76
6.1 PERFORMANCE ESTIMATION SYSTEM MODEL 76
6.2 INCREMENTAL EXPECTATION MAXIMIZATION ALGORITHM 77
6.3 ESTIMATING PERFORMANCE STATISTICS 81
6.4 INCREMENTAL EXPECTATION MAXIMIZATION VERIFICATION . . . 82
6.5 CHAPTER SUMMARY 86

7. CONCLUSIONS AND FUTURE RESEARCH 87
7.1 CONCLUSIONS 87
7.2 FUTURE WORK 88

BIBLIOGRAPHY 90

VITA 95

LIST OF TABLES

Table Page

1. Operating parameters for 4-QAM PU system. 35

2. Summary of Any Sample probabilities. 53

3. Summary of N^{th} sample probabilities. 56

LIST OF FIGURES

Figure Page

1. Transmission patterns for two primary users, both with a 20% duty cycle but with the latter representing a more dynamic PU. 2

2. Three dimensional spectral hole. 9

3. Hidden Node problem caused by geographic position of PU and SU transmitters and receivers may cause collisions as in the bottom half of the figure. 10

4. Spectrum sharing paradigms. 11

5. Example receiver operating characteristic curve. 12

6. Example of probability of sensing error versus λ. 13

7. Energy detector block diagram. 15

8. Waveform based detector block diagram. 15

9. Cyclostationary detector block diagram. 16

10. Sensing-throughput analysis time slot structure. 19

11. Illustration of a dynamic PU state which switches from ON to OFF at random time instance, and the SU state which switches between ON, OFF, and Blocked depending on the SU traffic and sensing data. 22

12. Illustration of a dynamic PU signal which switches from ON to OFF at random time instances,along the SU for spectrum sensing. 23

13. Venn diagram depicting the events related to SU interference 24

14. Acceptable SU operating range defined by a piecewise linear boundary. 30

15. Acceptable SU operating range defined by a piecewise polynomial boundary. . . . 30

16. $\widetilde{\mathcal{P}_b}$ for 4-QAM with $\text{SINR}_{nc} = 12$ dB and select $\mathcal{P}_c$ and P_{SU} combinations. 36

17. Contour of $\widetilde{\mathcal{P}_b}$ for 4-QAM with $\text{SINR}_{nc}=12$ dB over a range of $\mathcal{P}_c$ and P_{SU} values. 37

18. Comparison of four boundary equations. 40

19. Comparison of four variant boundary equation over contour map where areas less than 10^{-4} are shaded. 40

Figure Page

20. PU performance with a fixed SU value $\mathcal{P}_Y = .9$ and a range of SU $(\mathcal{P}_c, P_{SU})$ operating pairs on the linear boundary. 42

21. PU performance with a fixed SU value $\mathcal{P}_Y = .9$ and a range of SU $(\mathcal{P}_c, P_{SU})$ operating pairs on the 2nd-order polynomial boundary. 42

22. PU performance with a fixed SU value $\mathcal{P}_Y = .9$ and a range of SU $(\mathcal{P}_c, P_{SU})$ operating pairs on the 4th-order polynomial boundary. 43

23. PU performance with a fixed SU value $\mathcal{P}_d = 0.25$ and a range of SU $(\mathcal{P}_c, P_{SU})$ operating pairs on the linear boundary. 43

24. PU performance with a fixed SU value $\mathcal{P}_d = 0.25$ and a range of SU $(\mathcal{P}_c, P_{SU})$ operating pairs on the 2nd-order polynomial boundary. 44

25. PU performance with a fixed SU value $\mathcal{P}_d = 0.25$ and a range of SU $(\mathcal{P}_c, P_{SU})$ operating pairs on the 4th-order polynomial boundary. 44

26. Illustration of a dynamic PU signal which switches from ON to OFF at random time instances, along with the sampling approach used by the SU for spectrum sensing. 47

27. Markov chain representation of PU activity. 48

28. Two-state trellis representation of an N-step Markov chain evolution. 49

29. Spectrum sensing hypotheses H_{free} and H_{busy} due to dynamic PU activity during a sensing period starting at $n = 1$ and ending at $n = N$. 51

30. Spectrum sensing hypotheses H_{N0} and H_{N1} due to dynamic PU activity during a sensing period starting at $n = 1$ and ending at $n = N$. 53

31. Theoretical vs simulated comparison of Φ_x with $N = 20$, $\rho = 50$, and (a) $\tau = 5$, (b) $\tau = 10$,(c) $\tau = 20$,(d) $\tau = 50$. 60

32. Theoretical vs simulated comparison of $N_{i|s_N}$ with $N=20$, $\rho=50$, $\tau \in \{5, 10, 20, 50\}$. 61

33. Theoretical vs simulated comparison of $N_{i|A}$ with $N=20$, $\rho=50$, $\tau \in \{5, 10, 20, 50\}$. 61

34. Examples of mixed chi-squared distributions with $N=4$, weights $\mathbf{\Phi} = \{0.2, 0.2, 0.2, 0.2, 0.2\}$, and (a) $\gamma = 6dB$, (b) $\gamma = -3dB$. 66

Figure Page

35. H_{free} and H_{busy} dynamic PU ROC with $\rho = 50$,$\tau = 10$, $N = 20$ and SNR values (a) $\gamma = 0$dB, (b) $\gamma = -6$dB, and (c) $\gamma = -12$dB. 72

36. H_{N0} and H_{N1} dynamic PU ROC with $\rho = 50$,$\tau = 10$, $N = 20$ and SNR values (a) $\gamma = 0$dB, (b) $\gamma = -6$dB, and (c) $\gamma = -12$dB. 73

37. H_{free} and H_{busy} dynamic PU ROC with $\rho = 50$,$\tau = 10$, $N = 20$ and SNR values (a) $\gamma = 0$dB, (b) $\gamma = -6$dB, and (c) $\gamma = -12$dB. 74

38. H_{N0} and H_{N1} dynamic PU ROC with $\rho = 50$,$\tau = 10$, $N = 20$ and SNR values (a) $\gamma = 0$dB, (b) $\gamma = -6$dB, and (c) $\gamma = -12$dB. 75

39. Illustrating different subsets of a chi-squared distribution with a total of $N = 10$ components. 79

40. $\hat{\gamma}$ for $N=20$, $\rho=50$, $\tau=10$, and $\gamma=-12$, -9, -6, -3, and 0 dB. 83

41. $\hat{\mathbf{\Phi}}$ for $N=20$, $\rho=50$, $\tau=10$, and $\gamma=-12$, -9, -6, -3, and 0 dB. 83

42. Estimated ROC for for $N=20$, $\rho=50$, $\tau=10$, and $\gamma=-12$, -9, -6, -3, and 0 dB. 84

43. $\hat{\gamma}$ for $N=20$, $\rho=50$, $\tau=50$, and $\gamma=-12$, -9, -6, -3, and 0 dB. 85

44. $\hat{\mathbf{\Phi}}$ for $N=20$, $\rho=50$, $\tau=50$, and $\gamma=-12$, -9, -6, -3, and 0 dB. 85

45. Estimated ROC for $N=20$, $\rho=50$, $\tau=50$, and $\gamma=-12$, -9, -6, -3, and 0 dB. . 86

CHAPTER 1

INTRODUCTION

The RF spectrum in the United States and other parts of the world appears to be overcrowded. Wireless devices are growing in number and in data rate requirements. The ever-growing bandwidth demands of commercial and military users have resulted in a spectrum shortage. It is no longer the case that hardware is the limiting factor in the achievable data rate of a wireless device; rather, it is spectrum availability. However, according to measurements taken by the FCC's Spectrum Policy Task Force, utilization ranges geographically and temporally from 15% to 85% [1]. Ideally, the duty cycle would be much higher, but the current static spectrum allocation policy provides exclusive rights to the spectrum holder. If the licensed spectrum holder is not using the frequency, it remains idle. Therefore, spectrum shortage is partially an artifact of the current spectrum allocation policy.

In order to increase spectral utilization, several paradigms have been proposed that allow licensed primary users (PUs) to share spectrum with unlicensed secondary users (SUs). Of the proposed spectrum sharing paradigms the interweave paradigm has emerged as a viable option as it minimizes impact to PUs and requires no changes to the current spectrum allocation process. The interweave paradigm is reliant on Cognitive Radio (CR) technology which enables SUs to first sense the spectrum to determine whether it is in use by a PU and only dynamically access spectrum when it is idle [2]. In recent years there has been significant research in the area of CR exploring topics such as network security [3–5], sensor performance [6–9], and collaborative sensing [10–13]. The focus of this dissertation is on CR networks where the PU is highly dynamic, a topic that has received limited research attention but is increasingly relevant as the Internet of Things (IoT) has increased the need for sensor networks to share data in short bursts. Additionally, multi-access techniques such Orthogonal frequency-division multiple access (OFDMA) and Single-carrier frequency-division multiple access (SC-FDMA), employed by wireless standards such as LTE, result in licensed users accessing portions of the licensed spectrum on a dynamic basis.

Numerous problems arise in CR networks when the PU is highly dynamic. This dissertation attempts to address some of these problems and sheds light on other areas yet to be addressed in order to effectively utilize idle spectrum licensed to a dynamic PU.

1.1 PROBLEM STATEMENT

The presence of a highly dynamic PU poses several issues to CR networks. When the licensed PU is highly dynamic, the resulting spectrum idle periods are shorter and less predictable. In order to efficiently use these idle periods the SU must adjust its sensing behavior accordingly. The complexity of sensing and accessing spectrum licensed to a highly dynamic PU is apparent in Figure 1 which shows the transmission patterns for two different PUs, each with a 20% duty cycle but with very different transmission patterns. An SU attempting to exploit the idle periods on the top time axis, where the time scale may be in hours, would not require the same constraints as an SU attempting to exploit the idle periods on the bottom time axis, where the time scale may be in ms. Existing spectrum sharing paradigms are not well suited for highly dynamic PUs, and there is a need to develop a framework that is suitable for exploiting the idle spectrum of a highly dynamic PU.

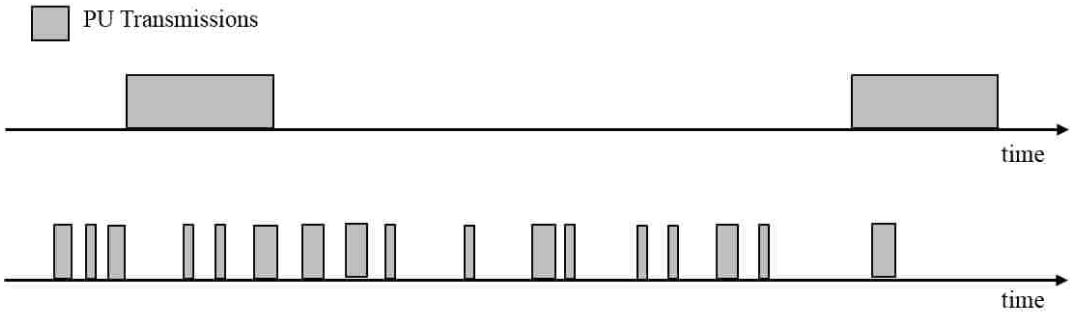

Figure 1. Transmission patterns for two primary users, both with a 20% duty cycle but with the latter representing a more dynamic PU.

In a CR network the SU periodically senses the spectrum in order to determine if an active PU is present. The effectiveness of CR, both in the ability of the SU to not interfere

with the PU and the ability of the SU to utilize idle spectrum, relies on the accuracy with which the SU senses the spectrum. There are well-established closed-form analytical expressions for spectrum sensing under various channel conditions [14–17]. However, these expressions assume a static context, with a PU signal that is either active or inactive for the entire duration of spectrum sensing, and become inaccurate in scenarios where the PU signal may switch from active to inactive or vice versa while spectrum sensing is in progress. It is therefore necessary to quantify spectrum sensor performance not just in context to the channel conditions but also in context to the PU activity dynamics.

One of the appealing aspects of CR over other spectrum sharing paradigms is it not necessary for the PU to share all information about it's transmissions with prospective SUs. It is therefore likely that the parameters dictating the PU activity may not be known to the SU. Because the performance of the SU spectrum sensing is contingent on the SU's knowledge of the PU dynamics, mechanisms for SU estimation of PU dynamics should be explored.

1.2 DISSERTATION CONTRIBUTIONS

The dissertation is composed of four major contributions, all related to the utilization, detection, and performance of CR networks with highly dynamic PUs. The first major contribution is a hybrid spectrum sharing framework that adequately supports a dynamic PU. We propose a hybrid interweave and underlay paradigm where the PU allows some SU interference which arises from a reduced ability to accurately perform spectrum in the presence of a dynamic PU. In order to achieve this type of sharing the PU sets guidelines which limit the SU power dependent on the SU sensing performance and duty cycle. Verified analytic expressions built upon the PU threshold performance requirements are provided for bounding SU operating parameters.

The second contribution is a model for the dynamic PU activity with respect to the SU sensing period. The model considers a PU that switches between being active and idle during the sensing period. A Markov chain is used to model the two-state PU signal activity and the evolution of this chain for the duration of the sensing period is considered. Unlike prior research, no assumptions are made regarding the number of PU signal changes during the

sensing period. The resulting PU model is considered in context to an energy detector at the SU receiver. The derived energy detector test statistic in the presence of a dynamic PU is a chi-squared mixture where the number of components in the mixture is proportional to the length of the SU sensing period, and the component weights are dependent on the parameters dictating the PU dynamic activity, specifically the mean active and idle durations.

The third contribution of this dissertation is analytic expressions for the probabilities of detection $\mathcal{P}_d$ and false alarm $\mathcal{P}_f$ that take into account all potential changes in the PU signal during an SU sensing period. Traditionally, $\mathcal{P}_d$ and $\mathcal{P}_f$ are derived from the Neyman-Pearson approach to signal detection where H_0, or the null hypothesis, indicates the signal is absent during the entire sensing period and H_1 indicates the signal is present during the entire sensing period. Because a dynamic PU can be both present and absent during a sensing period, two alternative sets of hypotheses are described. The first set of dynamic PU hypotheses, termed the *Any Sample Hypotheses*, considers a conservative set of hypotheses H_{free} and H_{busy} where the null hypothesis H_{free} corresponds to a PU that is absent during the entire sensing duration and H_{busy} corresponds to a PU that is present at any point during a sensing duration. The second set assumes that at the end of the sensing period the SU would either transmit or remain silent based on the formulated hypothesis. We refer to this set as the N^{th} *Sample Hypotheses* where N refers to the last sample in the sensing period. In this case the null hypothesis H_{N0} corresponds to the PU being idle at the end of the sensing period and H_{N1} corresponds to a PU that is active at the end of the sensing period. For both sets of hypotheses closed-form analytic expressions for $\mathcal{P}_d$ and $\mathcal{P}_f$ are derived using the chi-squared mixture energy detector test statistic. The performance statistics are verified through simulation, and the expressions are precise across PU dynamic activity levels and PU signal to noise ratio (SNR) at the SU receiver. Further, because the expressions for $\mathcal{P}_d$ and $\mathcal{P}_f$ can be complex, particularly with extended sensing periods, we present approximate expressions of $\widetilde{\mathcal{P}_d}$ and $\widetilde{\mathcal{P}_f}$ for both sets of hypotheses and through simulation explore the validity of the approximate performance statistics.

The verified closed-form expressions for $\mathcal{P}_d$ and $\mathcal{P}_f$ derived in this dissertation assume both the PU SNR at the SU receiver and the PU dynamic activity, specifically the mean active and idle durations, are known. The fourth contribution is a proposed method to

estimate the sensor performance statistics $\mathcal{P}_d$ and $\mathcal{P}_f$ in the presence of a dynamic PU with unknown parameters. We develop an incremental expectation maximization (EM) algorithm to estimate the weights of the chi-squared mixture as well as estimating the SNR using a set of observations from the output of the SU energy detector. Because the EM algorithm converges to a local rather than the global optimum its performance can be poor when the number of components in the mixture is large. The number of components in the chi-squared mixture is proportional to the length of the SU sensing period so it typically contains a large number of components. We therefore propose an incremental EM algorithm which starts with a subset of components and adds components incrementally. With the estimated weights and SNR determined by the incremental EM algorithm we then estimate the performance of the energy detector and compare the results to the expressions for $\mathcal{P}_d$ and $\mathcal{P}_f$ using the actual PU transmission parameters.

1.3 DISSERTATION OUTLINE

The following chapters of this dissertation are organized as follows. Chapter 2 provides an overview of underlying technologies relevant to this work. A brief overview of CR and spectrum sharing paradigms is provided followed by a discussion of spectrum sensing performance and techniques. Chapter 2 also provides a literature review of relevant research, focusing on CR research which considers dynamic PUs.

A framework for spectrum sharing is proposed in Chapter 3 which considers a dynamic PU as well as the potential for a dynamic SU. The proposed framework allows the PU to provide a two dimensional boundary for SU operation using the probability of collusion and SU power. The two dimensional boundary limits interference to the PU while still obfuscating details of its own transmissions. An example 4-QAM PU system is considered, and simulations are performed with SUs operating at various points on the SU operating boundary.

Chapter 4 provides a mathematical model for describing the dynamic PU state using a Markov chain. The evolution of the Markov chain over the SU sensing period is used to develop a distribution for the test statistic at the output of an energy detector. Chapter 4 also introduces the dynamic PU *Any Sample* and N^{th} *Sample* hypotheses. The dynamic PU

test statistic is applied to alternative hypotheses, and corresponding joint and conditional probabilities are derived and verified through simulation.

Building upon the verified dynamic PU model, Chapter 5 derives closed-form expressions for an energy detector test statistic and spectrum sensing performance statistics in the presence of a dynamic PU. Because of the complexity of the expressions derived, particularly for extended sensing periods, approximations for sensing performance are considered. Simulations provided verify the expressions for sensing performance and provide limitations on the use of the approximated expressions.

In Chapter 6 a novel incremental EM algorithm is proposed to estimate PU transmission parameters using observations from the output of the SU energy detector. The estimated parameters are then used to estimate the SU sensing parameters. The approach is validated through simulation for a range of SNR values.

Finally, this dissertation concludes with Chapter 7. A summary of the dissertation is provided as well as concluding remarks. Further, because the topic of CR networks with dynamic PUs is in its early stages there are several areas of future work that should be explored based on the advances made in this dissertation. Chapter 7 also provides a discussion of this proposed future work.

We note that the work presented in this dissertation, particularly in Chapters 3 through 6, builds upon the work and verified results from previous chapters. At the introduction of these chapters a system model for the research described in the chapter is provided including a review of critical and verified components from prior chapters.

CHAPTER 2

BACKGROUND AND RELATED WORK

This chapter provides background information relevant to the work presented in this dissertation. The chapter contains two major sections. Section 2.1 provides an overview of the underlying technologies considered in this dissertation. Section 2.2 provides a description of the limited research related to the CR networks in which a dynamic PU is considered.

2.1 UNDERLYING TECHNOLOGIES

A brief history of CR is first provided in Section 2.1.1 followed a description of sharing dimensions and paradigms in Section 2.1.2. An overview of common spectrum sensing techniques and sensor performance quantization is provided in Section 2.1.3.

2.1.1 COGNITIVE RADIO SYSTEMS

Cognitive Radio (CR) is an emerging concept that is expected to contribute to spectrum sharing and more efficient use of the frequency spectrum in future generations of wireless systems by enabling dynamic access to idle spectrum. While there are many variations on the definition of a CR, the FCC's definition has been widely adopted:

> "Cognitive Radio: A radio or system that senses its operational electromagnetic environment and can dynamically and autonomously adjust its radio operating parameters to modify system operation, such as maximize throughput, mitigate interference, facilitate interoperability, access secondary markets." [1].

Using this definition of CR, techniques for detecting the radio environment are clearly a key component of CR technology. However, CR is a broad interdisciplinary topic, involving spectral analysis, control systems, computer networking, game theory, and formal languages, amongst other technical disciplines [18].

Dr. Joseph Mitola III led research and development in the area of CR. His early work in software-defined radios led to his concept of CR. Mitola's vision of CR was more robust than the FCC's definition. He first described software-defined radios that were fully aware of not only spectrum availability but other aspects of the communication system as well [19]. Between 2002 and 2005, Mitola served as Special Assistant to the Director of the Defense Advanced Research Projects Agency (DARPA) to develop the Next Generation (XG) and Wireless Network after Next (WNaN) programs. DARPAs XG and WNAN programs focused on the development of low cost military handheld terminals that utilize CR techniques. The WNaN military radios are capable of sensing spectrum, opportunistically utilizing unused spectrum, and dynamically shifting utilized spectrum to optimize spectrum utilization across the entire channel.

Outside of military applications, there are several commercial applications that make use of CR. In the 2.4 and 5.725 GHz unlicensed bands, several devices are beginning to implement CR technology. IEEE 802.11k is an update to the WLAN standard that includes spectrum sensing to help determine which access point a WLAN device should connect to. Additionally, Bluetooth now includes Adaptive Frequency Hopping (AFH) as a way of reducing interference with the numerous other devices operating in this band. AFH senses which portions of the band are busy and does not transmit on those frequencies. This reduces interference and thus increases performance for both the Bluetooth device and other wireless devices operating in the band.

An additional commercial application of CR is the work being done by the IEEE 802.22 Working Group on Wireless Regional Area Networks (WRAN). IEEE802.22 has a goal of developing a standard for unlicensed access to white spaces in UHF TV bands (400-800 MHz). The FCC indicates that in most geographical areas there are multiple unused 6 MHz channels. Because of the long range propagation characteristics in this band, the aim of this technology is to provide wireless broadband access in rural areas.

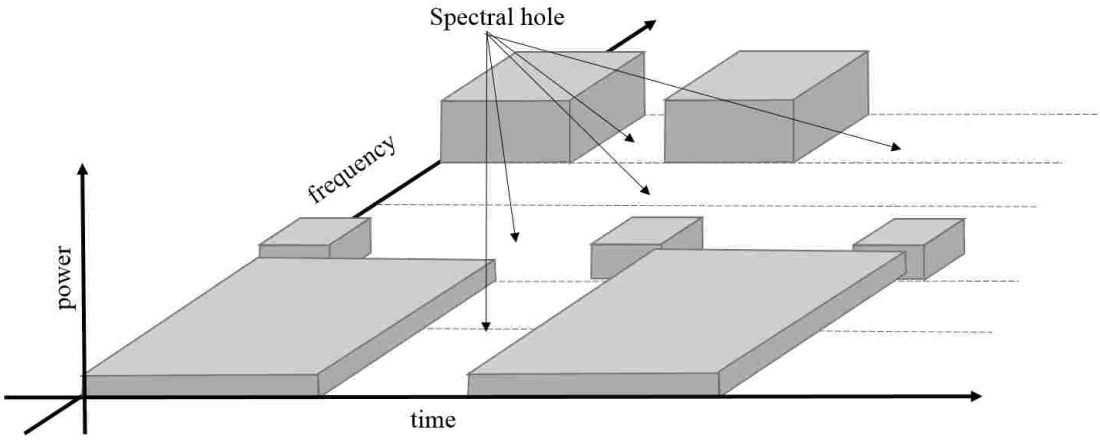

Figure 2. Three dimensional spectral hole.

2.1.2 SPECTRUM SHARING DIMENSIONS AND PARADIGMS

There are multiple dimensions in which SUs may transmit without interfering with the PU as shown in Figure 2 and described below. SUs may take advantage of spectrum opportunities, or spectrum holes, in one or more of these dimensions [20].

A. Frequency: If the spectrum allocation is broken into multiple narrow bands of spectrum, some of these smaller bands may go unused by the PU. These smaller bands of spectrum could potentially be used by SUs. The UHF TV bands are an extreme example of opportunities within the frequency domain; these opportunities are relatively static over time and can be exploited with negligible impact to PUs.

B. Time: If the PU is not transmitting constantly, there are periods when the spectrum is idle and a SU could access the spectrum. Because network loading generally varies greatly over time, certain times of the day may have extended opportunities in the time domain while others may have relatively few opportunities. This dissertation explores a highly dynamic PU with a duty cycle depicted in the bottom half of Figure 1.

C. Power: Extremely low PU power levels are generally an indication of geospatial separation. If an SU is an adequate distance from the PU, then that SU may be able to transmit

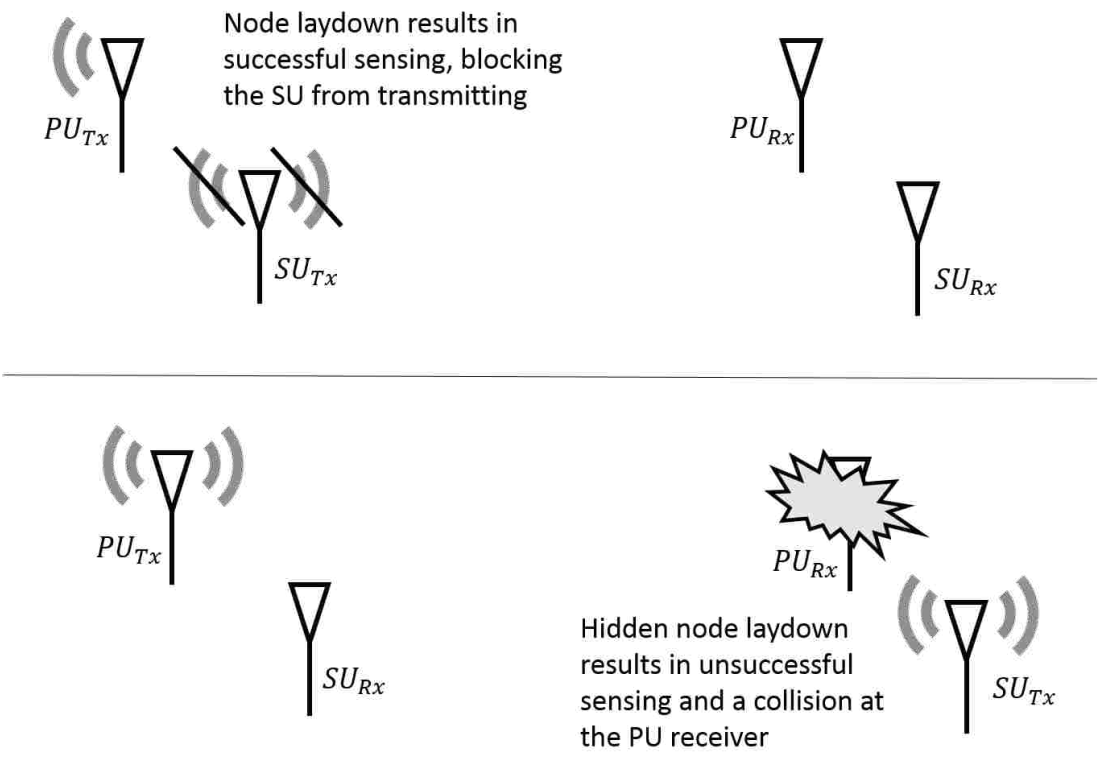

Figure 3. Hidden Node problem caused by geographic position of PU and SU transmitters and receivers may cause collisions as in the bottom half of the figure.

without interfering with the PU's transmission. Geospatial separation can also take advantage of directional transmissions and often relies on power control of the SU. It is important to note that CR is susceptible to the hidden node problem as illustrated in Figure 3. The top of Figure 3 illustrates successful sensing by the SU transmitter to avoid SU transmission and collision. In the scenario depicted in the bottom of Figure 3 the SU transmitter is close to the PU receiver but too far from the PU transmitter for successful detection, potentially causing a collision at the PU receiver.

Three primary paradigms for spectrum sharing are described in the literature: underlay, interweave, and overlay [18, 21–23]. The underlay paradigm dictates that the interference caused by a secondary user (SU) at the primary user (PU) receiver is kept below a certain threshold such that both the PU and SU may operate simultaneously in the same space-time-frequency domain. The interweave paradigm, from which cognitive radio was originally conceived, allows temporary space, time, or frequency voids, referred to as spectrum holes, to

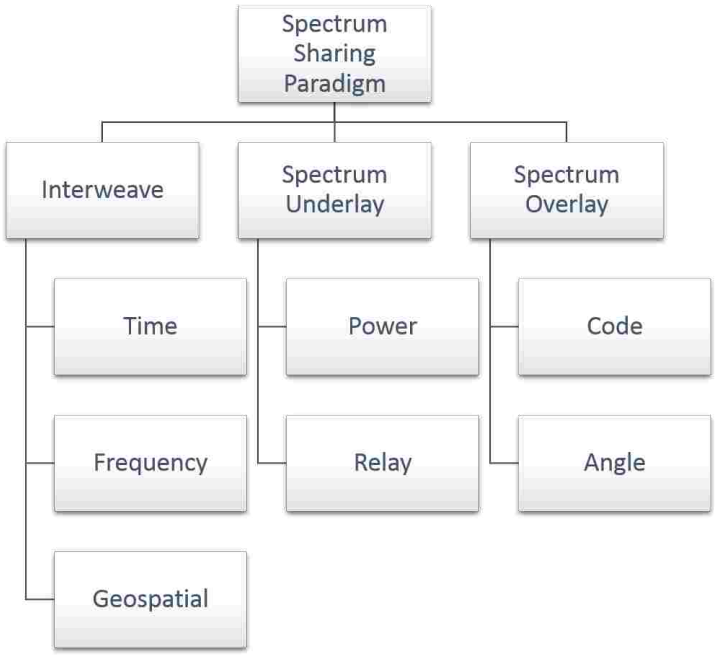

Figure 4. Spectrum sharing paradigms.

be exploited and utilized opportunistically. Finally, the overlay paradigm requires that the SU has extensive knowledge of the PU message, the channel between the SU and PU receiver, as well as the channel between the PU transmitter and receiver. With this information the SU is then able to precode its own transmissions and other SU as well as all the channels between them. While these paradigms are discussed in literature as three distinct cases, it is likely that specific applications of spectrum sharing between RF systems will require a combination or modification of the paradigms. This dissertation focuses on a highly dynamic PU and in Chapter 3 a hybrid interweave and underlay paradigm is proposed to accommodate a dynamic PU. We note that [24] also proposes a hybrid paradigm that allows the SU to transition between the interweave and underlay paradigms in order to optimize spectral utilization. In contrast, the hybrid paradigm proposed in Chapter 3 addresses the issue of suboptimal sensing performance that is inherent with a dynamic PU and provides a method for the PU to bound SU operation to minimize interference to the PU. The hybrid paradigm proposed considers that the SU may take advantage of spectrum sensing in order to reduce interference to the PU despite the performance of the spectrum sensing being reduced because

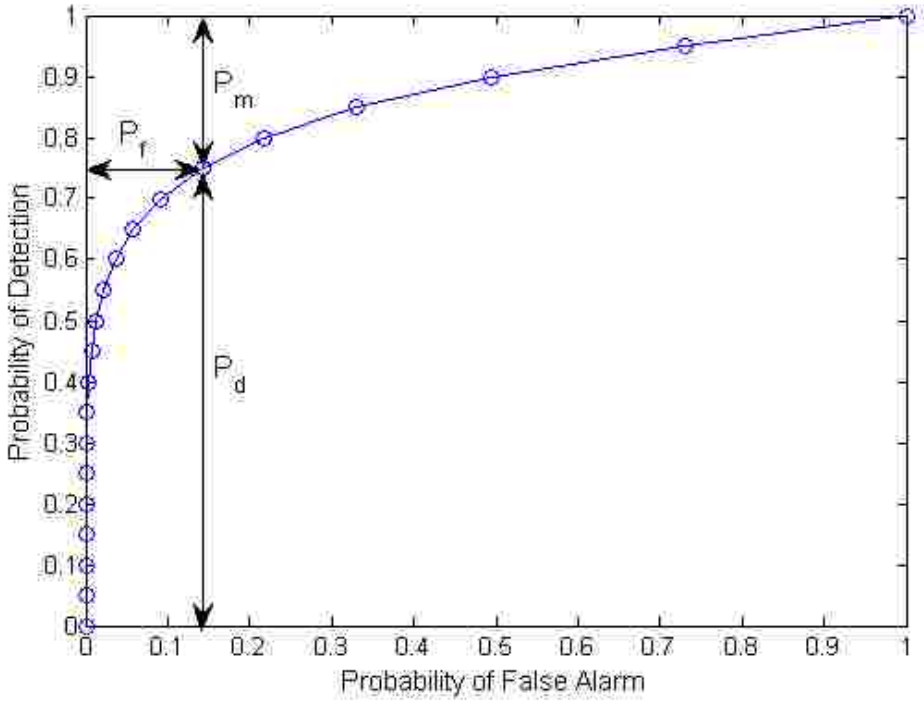

Figure 5. Example receiver operating characteristic curve.

of PU dynamics. The following section provides an overview of spectrum sensing.

2.1.3 SPECTRUM SENSING TECHNIQUES AND PERFORMANCE

When examining spectrum sensing performance, the two probabilities discussed in the prior section are of concern. The first is the probability of detection, $\mathcal{P}_d$, which is the probability of the SU accurately detecting the PU. The other probability of concern is the probability of false alarm, $\mathcal{P}_f$, or the probability of the SU falsely determining that the PU is active. These values are often plotted against each other in a receiver operating characteristic (ROC) curve. Figure 5 provides an example ROC curve.

The spectrum sensing techniques described are dependent on the threshold value λ. Different values of λ will result in different points on the ROC curve. If λ is set too large then the probability of false alarm will also be high resulting in missed opportunities to access the spectrum. However, if λ is set too low then the probability of missed identification, $\mathcal{P}_m = 1 - \mathcal{P}_d$, will be high. A high $\mathcal{P}_m$ value could result in interference to the PUs.

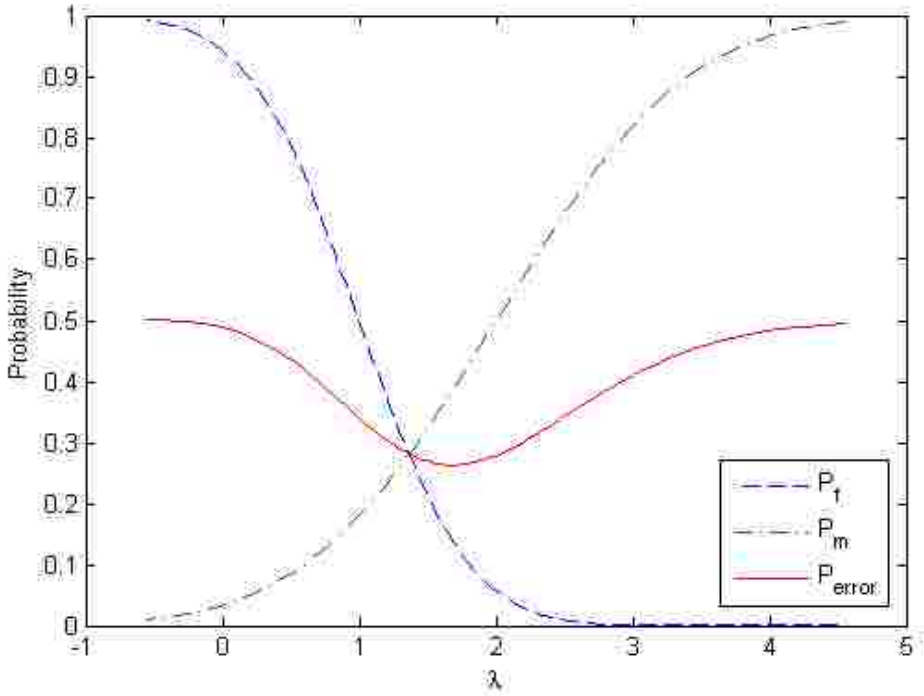

Figure 6. Example of probability of sensing error versus λ.

In addition to utilizing ROC curves, spectrum sensing performance is often evaluated based on the probability of sensing error $\mathcal{P}_{error}$ which is described as

$$\mathcal{P}_{error} = \alpha \cdot \mathcal{P}_m + (1 - \alpha) \cdot \mathcal{P}_f. \tag{1}$$

where α is a weighing factor which determines the weight of the individual contributions. Figure 6 illustrates an example $\mathcal{P}_{se}$ versus λ where α is set to 0.5. Examining sensing performance in this manner facilitates the selection of the proper threshold value of λ.

2.1.4 SPECTRUM SENSING TECHNIQUES

Spectrum sensing is the general term used to describe methods in which SUs sense PU transmissions. The objective of spectrum sensing is for the SU to decide between the two

hypotheses:

$$H_0 \rightarrow \text{PU signal OFF, channel is AVAILABLE}$$
$$H_1 \rightarrow \text{PU signal ON, channel is BLOCKED.} \quad (2)$$

These two hypotheses may likewise be expressed mathematically in terms of the SU received signal $r(n)$ as

$$H_0 : r(n) = u(n) \quad (3)$$
$$H_1 : r(n) = s(n) + u(n), \quad (4)$$

where $u(n)$ is the noise, and $s(n)$ is the signal transmitted by the PU. Many approaches to spectrum sensing have been identified. These techniques range in complexity and accuracy. The most popular of these approaches are summarized in the following sections.

Energy Detection

The most basic and most common form of spectrum sensing is energy detection. It requires no knowledge of the PU's waveform, so it is more universal than other forms of spectrum sensing. However, it is less accurate and does not work with CDMA systems [16]. An energy detector will compare the power spectral density (PSD) of the received signal to a threshold level λ. The value of λ is critical as it determines the success of the opportunity identification using the probabilities [14]

$$\mathcal{P}_d = Pr\{|r(n)|^2 > \lambda | H_1\} \quad (5)$$
$$\mathcal{P}_f = Pr\{|r(n)|^2 > \lambda | H_0\}, \quad (6)$$

where $\mathcal{P}_d$ is the probability of successfully detecting a transmitted signal and $\mathcal{P}_f$ is the probability of a false alarm. Figure 7 is a block diagram of a basic energy detector.

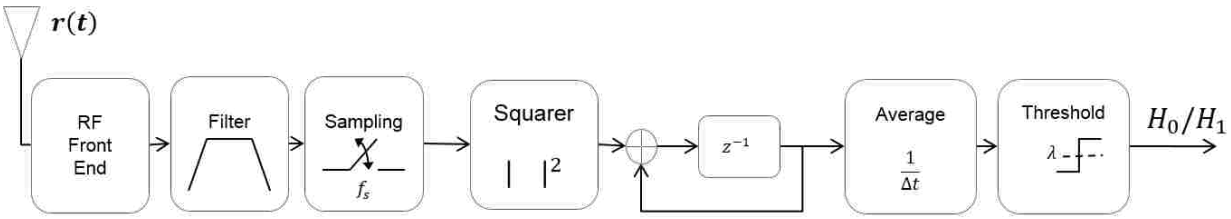

Figure 7. Energy detector block diagram.

Waveform-Based Sensing

Also called coherent sensing, this method requires knowledge of the PU's waveform. It utilizes preambles, spreading sequences, and other patterns. These pilot patterns allow the waveform to be detected by correlating the received signal with a copy of itself. Using the same hypothesis in (3) and (4), the values of $\mathcal{P}_d$ and $\mathcal{P}_f$ are [17]

$$\mathcal{P}_d = Pr\{r(n)s^*(n) > \lambda | H_1\} \tag{7}$$

$$\mathcal{P}_f = Pr\{r(n)s^*(n) > \lambda | H_0\}. \tag{8}$$

Just as in energy detection, setting the threshold level λ is critical to the performance of the both the primary and secondary users. Figure 8 is a block diagram of a basic waveform based detector.

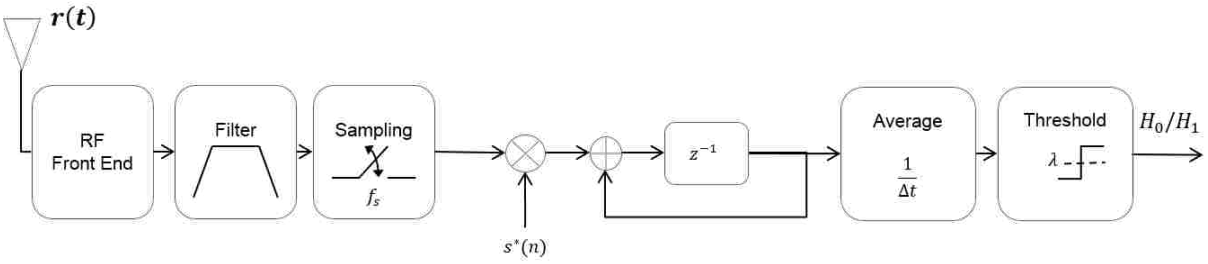

Figure 8. Waveform based detector block diagram.

Cyclostationary Sensing

Also called feature detection, cyclostationary sensing does not use the power spectral density of the receive signal but instead uses a cyclic correlation function. Cyclostationary detection is capable of differentiating noise from the transmitted signal. This is possible because AWGN is wide sense stationary with no correlation and transmitted signals are typically spectrally correlated. Cyclostationary sensing uses a spectral correlation density (SCD) function [25],

$$S(f,\alpha) = \sum_{-\infty}^{\infty} R_y^{\alpha} e^{-j2\pi f\tau} \tag{9}$$

where

$$R_y^{\alpha} = E[y(n+\tau)y^*(n-\tau)e^{-j2\pi f\tau}]. \tag{10}$$

Therefore the decision probabilities are

$$\mathcal{P}_d = Pr\{S(f,\alpha) > \lambda | H_1\} \tag{11}$$

$$\mathcal{P}_f = Pr\{S(f,\alpha) > \lambda | H_0\}. \tag{12}$$

Figure 9 is a block diagram of a basic cyclostationary detector.

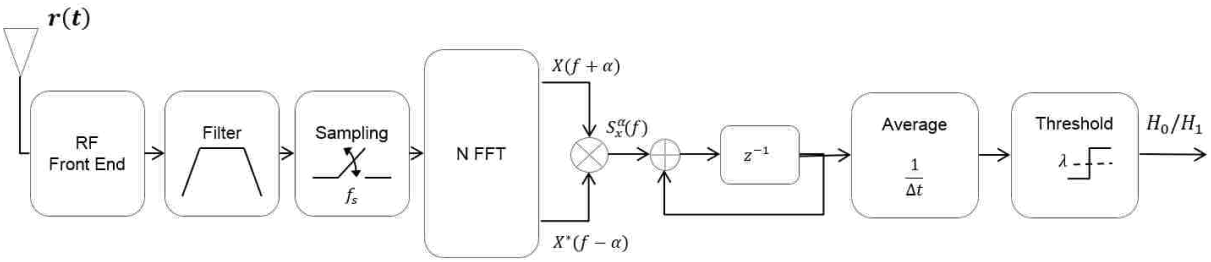

Figure 9. Cyclostationary detector block diagram.

The work in this dissertation considers an SU which utilizes an energy detector. This is ideal as the energy detector requires no knowlege of the PU signal. However, if information were known about the PU signal such that an alternative detector could be used, the work presented in this dissertation could readily be extended to consider either a waveform-based or cyclostationary detector.

2.2 COGNITIVE RADIO WITH DYNAMIC PRIMARY USERS

The performance of the sensing methods in Section 2.1.4 have been analyzed and validated closed-form expressions for sensing performance exist. However, these expressions assume a static context with a PU signal that is either active or idle for the entire duration of a spectrum sensing period. This dissertation covers CR networks with a highly dynamic PU and the static PU expressions become inaccurate in scenarios where the PU signal may switch from active to idle or vice versa while spectrum sensing is in progress. While there is significant CR research, scenarios with a dynamic PU have received limited attention. The dynamic PU research that does exist focuses on sensing performance using various constraints. Scenarios where the PU signal is not static during sensing are described in [26–30] and are briefly described below.

A dynamic PU which may potentially change state a single time during the sensing period is considered in [26]. Because the dynamic PU may be both active and inactive during a single sensing window the standard hypothesis used for spectrum sensing, H_0 when the PU is absent and H_1 when the PU is present, is not applicable. The potential single PU state switch during the sensing window results in four potential cases: $H_{0,1}$ the PU is absent during the entire sensing window; $H_{1,2}$ the PU is absent at the beginning of the sensing window and switches on by the end of the sensing window; $H_{0,2}$ the PU is present at the beginning of the sensing window and switches off by the end of the sensing window; and $H_{1,1}$ the PU is present during the entire sensing window. These four cases are then mapped to the hypotheses H_0 and H_1 based on the PU state at the end of the sensing period with $H_{0,1}$ and $H_{0,2}$ mapping to H_0 and $H_{1,1}$ and $H_{1,2}$ mapping to H_1. Closed form expressions are provided for the $\mathcal{P}_d$ and $\mathcal{P}_f$ which are reliant on the probability of cases $H_{0,1}$, $H_{0,2}$, $H_{1,1}$ and $H_{1,2}$ occurring. Because a specific PU traffic distribution was not assumed, the probabilities

$\mathcal{P}_d$ and $\mathcal{P}_f$ were not calculated. A scenario similar to [26] is provided in [27, 28] with an exponential PU traffic profile assumed allowing for the calculation of the probability that each of the four cases occur.

In [29] the problem of detecting signals characterized by a discontinuous presence in the detection window is also addressed. As in [26] alternative hypothesis are defined but instead of considering the PU state at the end of the sensing period, [29] defines the hypothesis as H_{free} when the signal is absent for the entire duration of the sensing window and H_{busy} when the signal is present at any point during the sensing window. In the case of H_{busy} the PU is assumed to be present for a percentage of the sensing window corresponding to the PU duty cycle. This assumption limits the application of this work to scenarios where the sensing window is relatively large in comparison to the PU transmission which results in very few H_{free} sensing windows and which limited SU transmission opportunities.

Unlike prior research, [30] considers a PU that may switch states active/inactive more than once during a sensing window. However, an upper limit on number of switches, derived using a maximum likelihood estimation, is assumed for the PU signal during the spectrum sensing interval. The closed-form expressions presented in Chapter 5 removes this assumption on the number of PU signal changes during the sensing interval by using a Markov chain to model the two-state PU signal activity. In this context we derive analytical expressions for the probabilities of detection $\mathcal{P}_d$ and false alarm $\mathcal{P}_f$ that take into account all potential changes in the PU signal from active to inactive and/or vice versa.

The aforementioned papers all note a reduced sensing performance as a result of the dynamic PU and many address the optimal duration of the sensing period to maximize the number of samples while minimizing the probability of the PU switching states during the sensing interval. However, none of these papers analyze the overall impact to CR network performance. There is considerable research that examines overall CR network throughput as it relates to the duration of the sensing window, notably [7,31,32]. The scenario presented in these papers assumes a time slotted system where the SU must determine the variable α which determines the percentage of the slots used for sensing and SU transmission as in Figure 10. While none of these papers consider the possibility of the PU switching during a sensing window, [31] considers the possibility that the PU may switch states between the

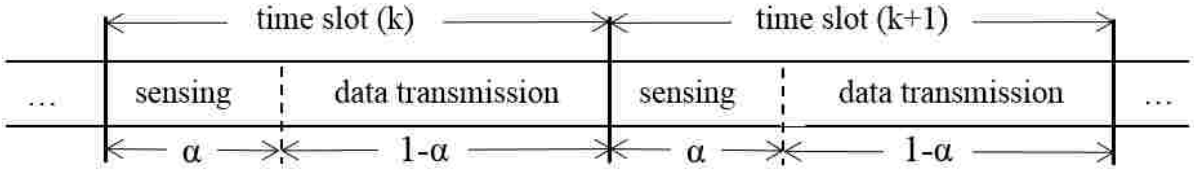

Figure 10. Sensing-throughput analysis time slot structure.

sensing and data transmission portion of the time slot. As the PU becomes more dynamic, the overall throughput of the system is then reduced. There is no known analysis of the impact of reduced sensing performance, resulting from a PU state switch during sensing, on CR network throughput.

Research using machine learning to estimate dynamic PU activity models in CR networks is limited. However, the estimation of dynamic PU activity is studied in [33], where hidden Markov models and a modified EM approach are used to evaluate the parameters of PU activity and its SNR. We note that [33] assumes that the activity of the PU is static for the entire sensing period and therefore the PU dynamics is estimated between sensing intervals.

CHAPTER 3

HYBRID SPECTRUM SHARING PARADIGM

In this chapter we consider a highly dynamic PU with a low temporal spectrum utilization such that there is a significant opportunity to temporally share the spectrum with other RF systems. CR is built upon the interweave paradigm, discussed in Section 2.1.2, which allows for the temporal sharing of spectrum by requiring the SU to first sense the spectrum to determine the presence of the PU prior to transmitting. Traditionally, the interweave paradigm assumes that the PU has no knowledge of the SU and therefore the SU must not interfere with the operation of active PUs. This requires that the SU has the ability to detect the PU with very high accuracy, i.e. $P_d \approx 1$. As noted in Section 2.1.3, optimal ROCs rise quickly such that a very small $\mathcal{P}_f$ results in a near perfect $\mathcal{P}_d$. In a system where the PU is either active or inactive for long periods of time, it is possible for the SU to have extended sensing periods and for the $\mathcal{P}_d \to 1$ with a small $\mathcal{P}_f$. However, in the case of a highly dynamic PU the SU must have a shortened sensing period resulting in reduced sensing performance. With suboptimal sensing performance an underlay sharing paradigm would work, but this assumes the SU is always transmitting and has no sensing capability. Therefore, if the SU is also highly dynamic with a small duty cycle or has some ability to sense the spectrum, the SU power will be artificially limited. The proposed hybrid framework allows for variable SU power depending on the probability of an SU transmission and the SU sensor performance.

All RF systems, regardless of whether spectrum sharing is employed, must consider interference from distant transmitters and adjacent spectrum channels. This type of interference is assumed to be at a very low-power level and always present. The maximum acceptable interference level is referred to as the interference threshold I_T and guidelines exist for calculating I_T. The Communications Receiver Performance Degradation Handbook published by Defense Information Systems Agency [34] provides guidance on calculating the effects of noise and interference on RF communications receivers and includes calculations for determining I_T. Additionally, the IEEE 1900 Series defines standards for Dynamic Spectrum

Access (DSA) systems including providing technical guidance for analyzing the potential for interference between RF systems. IEEE 1900.2-2008 [35] refers to interference above I_T as harmful interference and uses I_T to determine coexistence boundaries or the frequency and geographic separation required by two systems. We note that while I_T as defined by [34] and [35] is a sufficient metric when considering static low-power interference, it is not sufficient when the interference is from a dynamic higher-power source such as an SU. In this chapter we propose appropriate metrics for protecting a dynamic PU from harmful SU interference while still enabling spectrum sharing.

3.1 SPECTRUM SHARING SYSTEM MODEL

We consider a PU which is a non-sensing system and one or more SUs which employ CR to first sense the spectrum to determine availability before transmitting. The PU traffic profile is dynamic and when the PU has traffic to send it accesses the spectrum dynamically, switching from ON (active transmissions) to OFF (idle) at random time instances. Figure 11(a) illustrates an example of the PU traffic model. Here we note that the PU traffic profile is equivalent to the PU state.

The SU performs spectrum sensing on an ongoing basis so that the SU maintains one of the following two possible hypotheses:

$$\begin{aligned} H_0 &\rightarrow \text{PU signal OFF, channel is AVAILABLE} \\ H_1 &\rightarrow \text{PU signal ON, channel is BLOCKED.} \end{aligned} \tag{13}$$

The method used by the SU to sense the spectrum is not relevant; the SU maintains a hypotheses concerning channel availability. The top time axis in Figure 11(b) illustrates an example of a SU sensor output where B indicates the channel is BLOCKED (H_1) and A indicates the channel is AVAILABLE (H_0). The figure includes both an example of a false alarm and a missed detection, respectively $\mathcal{P}_f$ and $\mathcal{P}_m$, which are determined by comparing the sensor output to the PU traffic in Figure 11(a). Similar to the PU, the SU also has a dynamic traffic profile as shown in the second time axis in Figure 11(b). Unlike the PU, the SU does not transmit whenever it has traffic to send and instead must first verify that the

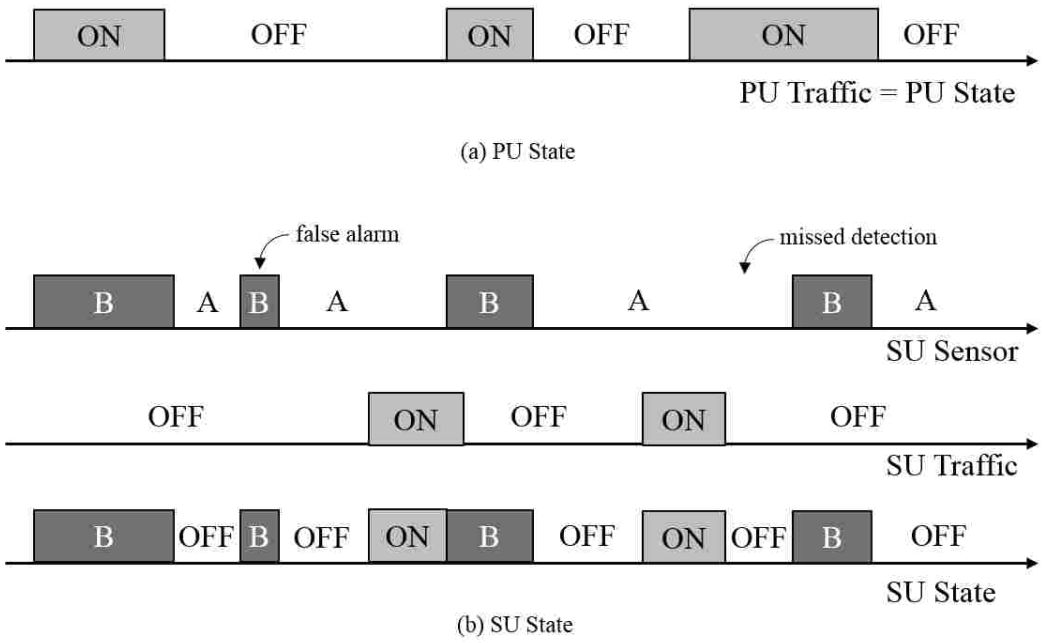

Figure 11. Illustration of a dynamic PU state which switches from ON to OFF at random time instance, and the SU state which switches between ON, OFF, and Blocked depending on the SU traffic and sensing data.

channel is available. If the SU sensing hypothesis indicates that the channel is available when the SU has traffic, the data is sent. Otherwise, if the SU sensing hypothesis indicates that the channel is blocked when the SU has data to transmit, the data is dropped. The system does not employ any queuing at the SU. The bottom time axis in Figure 11(b) represent the overall SU state, a combination of the SU traffic pattern and sensor output. The PU and SU activity shown in Figure 11 can also be represented by the finite state machines in Figure 12. In Chapter 4 we will expand the PU state machine to include state transition probabilities, but this level of detail is not necessary for the hybrid framework proposed in this chapter.

Prior sensing performance analysis with a dynamic PU reveals a lower $\mathcal{P}_d$ than is generally required for an interweave paradigm [26–30]. The low $\mathcal{P}_d$ increases the probability of collision and it is therefore desirable to consider an alternative framework which allows for a slightly lower $\mathcal{P}_d$. While the rest of this chapter focuses on the case of a dynamic PU, this framework is relevant to any scenario where the PU is difficult to detect.

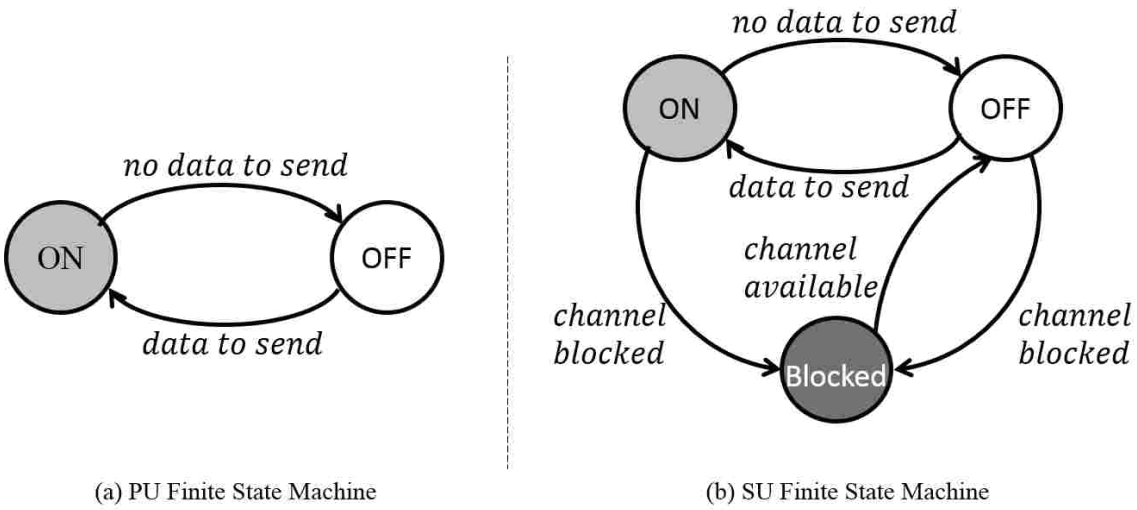

Figure 12. Illustration of a dynamic PU signal which switches from ON to OFF at random time instances,along the SU for spectrum sensing.

3.2 PROBABILITY OF COLLISION

We use the Venn diagram in Figure 13 to illustrate the following events: X={PU is active}, Y={SU wants to transmit}, and Z={SU sensor indicates channel is available}. The probabilities of each event can defined in terms of the PU and SU duty cycles, respectively $\mathcal{P}_X$ and $\mathcal{P}_Y$, and SU sensor performance, $\mathcal{P}_d$ and $\mathcal{P}_f$.

$$\begin{aligned} Pr\{X\} &= \mathcal{P}_X \\ Pr\{Y\} &= \mathcal{P}_Y \\ Pr\{Z\} &= \mathcal{P}_X\,\overline{\mathcal{P}_d} + \overline{\mathcal{P}_X}\,\overline{\mathcal{P}_f} \end{aligned} \tag{14}$$

We note that the events X and Y is independent, but Z is dependent on X as reflected by $\mathcal{P}_d$ and $\mathcal{P}_f$.

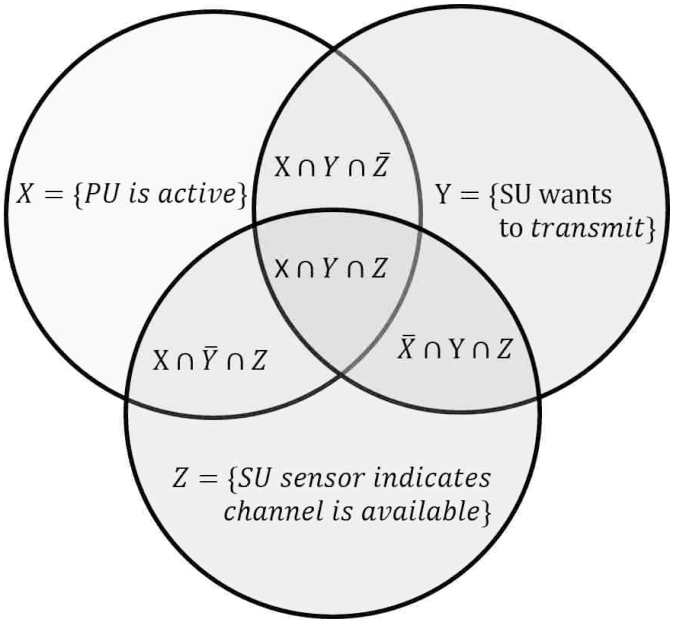

Figure 13. Venn diagram depicting the events related to SU interference

The intersection of these events and the relation to the PU and SU states illustrated in Figures 11 are:

$\{X \cap Y \cap Z\} = \{\text{PU ON, SU ON}\}$

$\{X \cap Y \cap \overline{Z}\} = \{\text{PU ON, SU Blocked}\}$

$\{X \cap \overline{Y}\} = \{\text{PU ON, SU OFF}\}$

$\{\overline{X} \cap Y \cap Z\} = \{\text{PU OFF, SU ON}\}$

$\{\overline{X} \cap Y \cap \overline{Z}\} = \{\text{PU OFF, SU Blocked}\}$

$\{\overline{X} \cap \overline{Z}\} = \{\text{PU OFF, SU OFF}\}.$

The event $\{X \cap Y \cap Z\}$ represents an event where the PU is transmitting, the SU has traffic, and the SU falsely determined the channel was available. This is the only event in which

both the PU and SU are transmitting and the probability of $\{X \cap Y \cap Z\}$ occurring is

$$\begin{aligned} Pr\{X \cap Y \cap Z\} &= Pr\{X \cap Z\} \cdot Pr\{Y\} \\ &= Pr\{Z|X\} \cdot Pr\{X\} \cdot Pr\{Y\} \\ &= \overline{\mathcal{P}_d} \cdot \mathcal{P}_X \cdot \mathcal{P}_Y. \end{aligned} \tag{15}$$

The probability of $\{X \cap Y \cap Z\}$ in (15) provides a method to determine the probability of the PU and SU simultaneously transmitting with respect to all time. In order to protect the PU transmissions, the PU is interested specifically in the periods of time when the PU is transmitting. The probability of a collision occurring during a PU transmission can thus be expressed as

$$\begin{aligned} \mathcal{P}_c &= Pr\{X \cap Y \cap Z|X = 1\} \\ &= \overline{\mathcal{P}_d} \cdot \mathcal{P}_Y. \end{aligned} \tag{16}$$

From (16) we see that the SU can reduce the $\mathcal{P}_c$ by either reducing its own duty cycle or increasing $\mathcal{P}_d$. The consideration of the SU duty cycle is unique to the proposed hybrid framework. In the next section we use $\mathcal{P}_c$ along with the SU power to quantify the PU performance.

3.3 CALCULATING PRIMARY USER PERFORMANCE

In a CR network with a dynamic PU it is necessary to consider the signal to noise plus interference ratio (SINR) at the PU receiver during a collision when both the SU and PU are transmitting and also when there is no collision. During a collision the PU receiver will receive the signal from the PU transmitter along with interference from the SU transmitter. During the collision the SINR expressed as

$$\text{SINR}_c = \frac{P_{PU}}{P_{SU} + I + N} \tag{17}$$

where P_{PU} and P_{SU} are respectively the PU and signal power at the PU receiver, I is

interference from distant transmitters and adjacent channels, and N is the receiver noise. Likewise when there is no collision the SINR is expressed as

$$\text{SINR}_{nc} = \frac{P_{PU}}{I + N}. \tag{18}$$

We also introduce the ratio P_{PU}/P_{SU}. Defining the PU system in terms of SINR_{nc} and P_{PU}/P_{SU} is often more convenient than using SINR_c, SINR_{nc}. Additionally, the ratio P_{PU}/P_{SU} provides a more meaningful ratio for the CR network designer. The relationship between SINR_c, SINR_{nc} and P_{PU}/P_{SU} is

$$\text{SINR}_c = \frac{\frac{P_{PU}}{P_{SU}} \cdot \text{SINR}_{nc}}{\frac{P_{PU}}{P_{SU}} + \text{SINR}_{nc}} \tag{19}$$

$$\text{SINR}_{nc} = \frac{\frac{P_{PU}}{P_{SU}} \cdot \text{SINR}_c}{\frac{P_{PU}}{P_{SU}} - \text{SINR}_c} \tag{20}$$

$$\frac{P_{PU}}{P_{SU}} = \frac{\text{SINR}_{nc} \cdot \text{SINR}_c}{\text{SINR}_{nc} - \text{SINR}_c}. \tag{21}$$

Achieving a desired SINR at the PU receiver is critical as it determines whether the information in PU signal is able to be received accurately. Regardless of interference levels or the types of interference present, all RF systems will experience some information loss. The probability of information error that is considered tolerable is dependent on the RF system. Some example of information error probability measures are:

- symbol error rate (SER), packet error rate (PER), or bit error rate (BER) used in digital communication systems
- track error rate or target detection probability for tracking radar systems

- speech intelligibility or articulation index in legacy analog voice communication systems.

Functions for calculating threshold SINR based on the threshold probability of information error are system dependent and covered in corresponding textbooks [36–39]. Thus far this chapter has been independent of the type of PU system, digital communications, radar, or analog communications. In order to proceed we focus on a digital communications PU system.

Digital communication systems define a threshold probability of bit error $\mathcal{P}_b$, or BER, as a method of limiting information error. Depending on the coding and modulation scheme used the digital communication system defines a function for $\mathcal{P}_b$,

$$\mathcal{P}_b = f\left(\frac{E_b}{N_0}\right), \tag{22}$$

where E_b/N_0 is the energy per bit to noise power spectral density ratio. We note that $f(\cdot)$ is generally a non-linear function and is defined assuming the absence of interference. Because we are interested in how interference impacts $\mathcal{P}_b$ and E_b/N_0 does not consider interference, it is necessary to examine the relationship between E_b/N_0 and SINR. We note that the relationship between E_b/N_0 and SNR is

$$\frac{S}{N} = \frac{E_b}{N_0}\,\frac{R}{B} \tag{23}$$

where B is the bandwidth and R is the bit rate. The noise power spectral density N_0 relates to the total noise power N by

$$N_0 = \frac{N}{B}. \tag{24}$$

To include interference we use the definition for interference power spectral density I_0 for non-SU interference power and define an SU interference power spectral density P_{SU0} as

$$I_0 = \frac{I}{B} \qquad \text{and} \qquad P_{SU0} = \frac{P_{SU}}{B}. \tag{25}$$

We can then define an energy per bit to noise plus interference power spectral density with and without collision respectively as

$$\zeta_{nc} = \frac{E_b}{N_0 + I_0} \qquad \text{and} \qquad \zeta_c = \frac{E_b}{N_0 + I_0 + P_{SU0}}. \tag{26}$$

SINR can be written with respect to ζ as

$$\text{SINR}_{nc} = \zeta_{nc} \frac{R}{B} \qquad \text{and} \qquad \text{SINR}_c = \zeta_c \frac{R}{B}, \tag{27}$$

with the inverse equation for ζ with respect to SINR

$$\zeta_{nc} = \text{SINR}_{nc} \frac{B}{R} \qquad \text{and} \qquad \zeta_c = \text{SINR}_c \frac{B}{R}. \tag{28}$$

As long as I and P_{SU} have a distribution similar to N such that the three terms can be added together, we can express the approximate $\mathcal{P}_b$ using (22) as a combination of the $\mathcal{P}_b$ values with and without collision

$$\widetilde{\mathcal{P}_b} = \mathcal{P}_c \cdot f(\zeta_c) + \overline{\mathcal{P}_c} \cdot f(\zeta_{nc}), \tag{29}$$

noting that because $f(\cdot)$ is not typically a linear function $\widetilde{\mathcal{P}_b} \neq f(\mathcal{P}_c \cdot \zeta_c + \overline{\mathcal{P}_c} \cdot \zeta_{nc})$. We can further expand (29) using the relationships in (17), (18), and (28)

$$\begin{aligned}
\widetilde{\mathcal{P}_b} &= \mathcal{P}_c \cdot f(\zeta_c) + \overline{\mathcal{P}_c} \cdot f(\zeta_{nc}) \\
&= \mathcal{P}_c \cdot f\left(\text{SINR}_c \frac{B}{R}\right) + \overline{\mathcal{P}_c} \cdot f\left(\text{SINR}_{nc} \frac{B}{R}\right) \\
&= \mathcal{P}_c \cdot f\left(\frac{P_{PU}}{P_{SU} + I + N} \frac{B}{R}\right) + \overline{\mathcal{P}_c} \cdot f\left(\frac{P_{PU}}{I + N} \frac{B}{R}\right)
\end{aligned} \tag{30}$$

Finally, we define a value $\widetilde{\zeta}$ which relates to $\widetilde{\mathcal{P}_b}$ using the inverse of (22)

$$\widetilde{\zeta} = f^{-1}(\widetilde{\mathcal{P}_b}). \tag{31}$$

Again the non-linearity of $f(\cdot)$ means $\widetilde{\zeta} \neq \mathcal{P}_c \cdot \zeta_c + \overline{\mathcal{P}_c} \cdot \zeta_{nc}$. The values of $\widetilde{\zeta}$ represents the equivalent ζ required to meet $\widetilde{\mathcal{P}_b}$ in a non-hybrid scenario.

3.4 DEFINING SECONDARY USER OPERATING REGION

In order for a PU to meet the desired $\mathcal{P}_b$ threshold it must place constraints on the SU operation. Because a PU may want to share spectrum while obfuscating waveform details, ideally these constraints reveal as little about the PU operation as possible. From (29) it is apparent that there are a range of $\mathcal{P}_c$, ζ_{nc}, and ζ_c that would result in the same value of $\widetilde{\mathcal{P}_b}$. The expanded equation in (30) reveals how the PU and SU each contribute to $\widetilde{\mathcal{P}_b}$. The PU determines P_{PU}, I, N, and B while the SU determines $\mathcal{P}_c$ and P_{SU}. The proposed framework defines an the boundary for acceptable SU operating range using ($\mathcal{P}_c$, P_{SU}) pairs. In the most basic case this SU operating boundary is a piecewise linear equation formed from the points (1, $P_{SU\text{-}min}$) and ($\mathcal{P}_{c\text{-}min}$, $P_{SU\text{-}max}$) as illustrated in Figure 14. The equation for piecewise linear boundary between the two SU operating regions is

$$P_{SU} = \begin{cases} P_{SU\text{-}max}, & \mathcal{P}_c \leq \mathcal{P}_{c\text{-}min} \\ (\mathcal{P}_c - 1) \cdot \frac{P_{SU\text{-}min} - P_{SU\text{-}max}}{1 - \mathcal{P}_{c\text{-}min}} + P_{SU\text{-}min}, & \mathcal{P}_c > \mathcal{P}_{c\text{-}min}. \end{cases} \tag{32}$$

As noted, (32) is linear while $\widetilde{\mathcal{P}_b}$ is linear only if $f(\cdot)$ is linear. Often if $\mathcal{P}_{c\text{-}min}$ is large enough a localized linear approximation is sufficient even if $f(\cdot)$ is non-linear. If the linear approximation in not sufficient, the points (1, $P_{SU\text{-}min}$) and ($\mathcal{P}_{c\text{-}min}$, $P_{SU\text{-}max}$) are still used and additional points are added between $\mathcal{P}_{c\text{-}min}$ and 1 to generate a polynomial that better defines the desired SU operation. A non-linear boundary is depicted in Figure 15.

For the non-linear case the boundary between the two SU operating regions is defined by

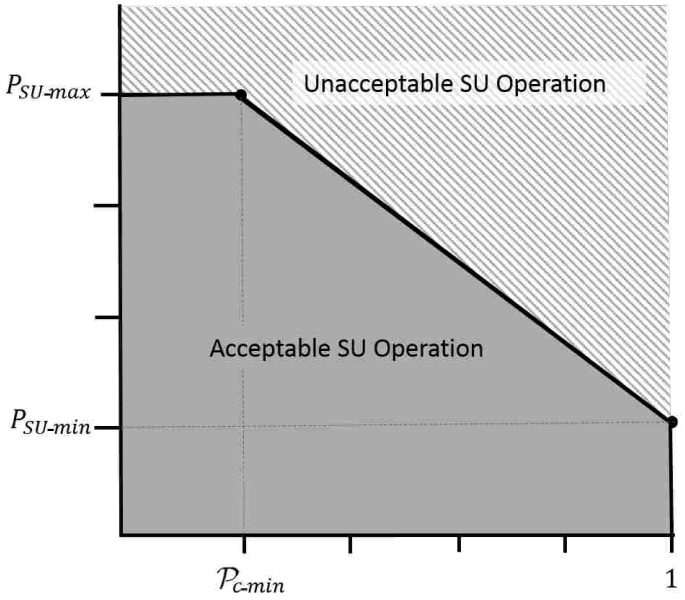

Figure 14. Acceptable SU operating range defined by a piecewise linear boundary.

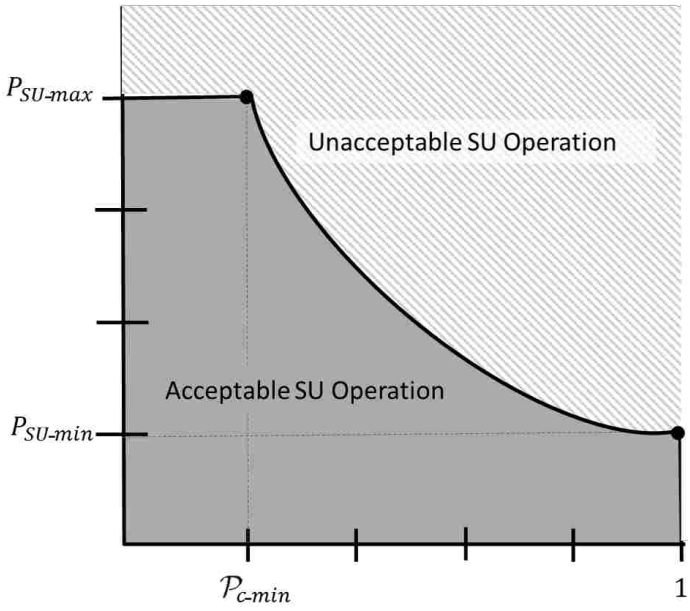

Figure 15. Acceptable SU operating range defined by a piecewise polynomial boundary.

the polynomial

$$P_{SU} = \begin{cases} P_{SU\text{-}max}, & \mathcal{P}_c \leq \mathcal{P}_{c\text{-}min} \\ a_0 \mathcal{P}_c^{\,n} + a_1 \mathcal{P}_c^{\,n-1} + \ldots + a_n, & \mathcal{P}_c > \mathcal{P}_{c\text{-}min}. \end{cases} \tag{33}$$

where there are n+1 defined points including (1, $P_{SU\text{-}min}$) and ($\mathcal{P}_{c\text{-}min}$, $P_{SU\text{-}max}$). We note that the linear boundary is equivalent to the polynomial boundary with two points. If the PU is attempting to obfuscate waveform details it should use as few points as possible which means using linear boundary if possible. The steps in defining the SU operating region are as follows:

1. Determine (1,$P_{SU\text{-}min}$)
2. Determine ($\mathcal{P}_{c\text{-}min}$,$P_{SU\text{-}max}$)
3. Evaluate the boundary
4. Add additional point if current boundary is insufficient

Steps 3 and 4 are repeated until the boundary is adequate.

3.4.1 DETERMINE (1,$P_{SU\text{-}MIN}$)

In determining the pairs that bound the SU operating range, the PU must first define ψ, the threshold value for $\mathcal{P}_b$. The value of $P_{SU\text{-}min}$ corresponding to $\mathcal{P}_c = 1$ in Figure 14 can be found by first inserting $\mathcal{P}_c = 1$ into (30) and using the threshold ψ which results in

$$\psi = f\left(\frac{P_{PU}}{P_{SU} + I + N}\,\frac{B}{R}\right)$$

$$= f\left(\mathrm{SINR}'_c\,\frac{B}{R}\right) \tag{34}$$

Using the inverse of (22), we can solve for SINR'_c

$$\mathrm{SINR}'_c = f^{-1}(\psi)\,\frac{R}{B}. \tag{35}$$

We assume SINR_{nc} and P_{PU} are known to the PU so use (21) to convert SINR'_c in (35) to $P_{SU\text{-}min}$,

$$P_{SU\text{-}min} = P_{PU} \cdot \frac{\text{SINR}_{nc} - \text{SINR}'_c}{\text{SINR}_{nc} \cdot \text{SINR}'_c}. \tag{36}$$

3.4.2 DETERMINE ($\mathcal{P}_{c\text{-}min}$,$P_{SU\text{-}MAX}$)

We can see from (29) that when $\mathcal{P}_c = 0$ the value of P_{SU} does not matter, so bounding the lower edge of the SU operating range by $\mathcal{P}_c = 0$ is not particularly useful. Additionally as noted in Section 3.2 this would require the $\mathcal{P}_d = 1$ and because the proposed framework is specifically for difficult to detect PUs a $\mathcal{P}_c = 0$ is not realistic. Instead of $\mathcal{P}_c = 0$ the PU selects a value for $\mathcal{P}_{c\text{-}min}$ to be the lower bound. The value of $P_{SU\text{-}max}$ corresponding to $\mathcal{P}_{c\text{-}min}$ in Figure 14 can be found by first inserting $\mathcal{P}_{c\text{-}min}$ into (30) and using the threshold ψ which results in

$$\psi = \mathcal{P}_{c\text{-}min} \cdot f\left(\frac{P_{PU}}{P_{SU} + I + N}\,\frac{B}{R}\right) + (1 - \mathcal{P}_{c\text{-}min}) \cdot f\left(\frac{P_{PU}}{I + N}\,\frac{B}{R}\right)$$

$$f\left(\text{SINR}''_c\,\frac{B}{R}\right) \geq \frac{\psi - (1 - \mathcal{P}_{c\text{-}min}) \cdot f\left(\text{SINR}_{nc}\,\dfrac{B}{R}\right)}{\mathcal{P}_{c\text{-}min}}$$

$$\text{SINR}''_c = f^{-1}\left(\frac{\psi - (1 - \mathcal{P}_{c\text{-}min}) \cdot f\left(\text{SINR}_{nc}\,\dfrac{B}{R}\right)}{\mathcal{P}_{c\text{-}min}}\right)\frac{R}{B} \tag{37}$$

Again SINR_{nc} and P_{PU} are known so (21) is used to convert SINR_c in (37) to $P_{SU\text{-}max}$,

$$P_{SU\text{-}max} = P_{PU} \cdot \frac{\text{SINR}_{nc} - \text{SINR}''_c}{\text{SINR}_{nc} \cdot \text{SINR}''_c}. \tag{38}$$

3.4.3 VERIFY BOUNDARY

At minimum the boundary is defined by two points, (1,$P_{SU\text{-}min}$) and ($\mathcal{P}_{c\text{-}min}$,$P_{SU\text{-}max}$), resulting in a linear boundary defined by substituting (32) for P_{SU} in (30). The resulting equation for $\widetilde{\mathcal{P}_{b\text{-}bd}}$ has one independent variable $\mathcal{P}_c$,

$$\widetilde{\mathcal{P}_{b\text{-}bd}} = \begin{cases} \mathcal{P}_c \cdot f\left(\dfrac{P_{PU}}{P_{SU\text{-}max}+I+N}\dfrac{B}{R}\right) + \overline{\mathcal{P}_c}\cdot f\left(\dfrac{P_{PU}}{I+N}\dfrac{B}{R}\right), & \mathcal{P}_c \le \mathcal{P}_{c\text{-}min} \\ \mathcal{P}_c \cdot f\left(\Psi\cdot\dfrac{B}{R}\right) + \overline{\mathcal{P}_c}\cdot f\left(\dfrac{P_{PU}}{I+N}\cdot\dfrac{B}{R}\right), & \mathcal{P}_c > \mathcal{P}_{c\text{-}min} \end{cases} \tag{39}$$

where

$$\Psi = \frac{P_{PU}}{\dfrac{(\mathcal{P}_c - 1)\,(P_{SU\text{-}min} - P_{SU\text{-}max})}{1-\mathcal{P}_{c\text{-}min}} + P_{SU\text{-}min} + I + N}\,. \tag{40}$$

We note that while (30) applies to any combination of ($\mathcal{P}_c$,P_{SU}), (39) applies specifically to the ($\mathcal{P}_c$,P_{SU}) pairs that lie on the SU operating boundary.The linear boundary is sufficient if $\max(\widetilde{\mathcal{P}_{b\text{-}bd}}) \le \psi + \epsilon,$ for $\mathcal{P}_c < 1$ where ϵ is a small error factor determined by the PU. If $\max(\widetilde{\mathcal{P}_{b\text{-}bd}}) > \psi + \epsilon$, additional points are added.

After each new point is added, an interpolating polynomial which passes through all defined points is determined and used to define the piecewise polynomial SU boundary in (33). Here we use the Vandermonde method for polynomial interpolation [40] by specifying $n-1$ points on the boundary along with points (1,$P_{SU\text{-}min}$) and ($\mathcal{P}_{c\text{-}min}$,$P_{SU\text{-}max}$):

$$\begin{bmatrix} a_0 \\ a_1 \\ \vdots \\ a_{(n-1)} \\ a_n \end{bmatrix} = \begin{bmatrix} \mathcal{P}_{c\text{-}min}^n & \cdots & \mathcal{P}_{c\text{-}min} & 1 \\ \mathcal{P}_{c\text{-}1}^n & \cdots & \mathcal{P}_{c\text{-}1} & 1 \\ \vdots & \cdots & \vdots & \vdots \\ \mathcal{P}_{c\text{-}(n-1)}^n & \cdots & \mathcal{P}_{c\text{-}(n-1)} & 1 \\ 1 & \cdots & 1 & 1 \end{bmatrix}^{-1} \begin{bmatrix} P_{SU\text{-}max} \\ P_{SU\text{-}1} \\ \vdots \\ P_{SU\text{-}(n-1)} \\ P_{SU\text{-}min} \end{bmatrix}. \tag{41}$$

Similar to (39), a boundary equation $\widetilde{\mathcal{P}_{b\text{-}bd}}$ is derived,

$$\widetilde{\mathcal{P}_{b\text{-}bd}} = \begin{cases} \mathcal{P}_c \cdot f\left(\dfrac{P_{PU}}{P_{SU\text{-}max}+I+N}\,\dfrac{B}{R}\right) + \overline{\mathcal{P}_c}\cdot f\left(\dfrac{P_{PU}}{I+N}\,\dfrac{B}{R}\right) & \mathcal{P}_c \le \mathcal{P}_{c\text{-}min} \\ \mathcal{P}_c \cdot f\left(\dfrac{P_{PU}}{(a_0\mathcal{P}_c^{\,n}+a_1\mathcal{P}_c^{\,n-1}+\ldots+a_n)+I+N}\,\dfrac{B}{R}\right) + \overline{\mathcal{P}_c}\cdot f\left(\dfrac{P_{PU}}{I+N}\,\dfrac{B}{R}\right) & \mathcal{P}_c > \mathcal{P}_{c\text{-}min}. \end{cases} \tag{42}$$

Additional points are added until $\max(\widetilde{\mathcal{P}_{b\text{-}bd}}) \le \psi + \epsilon$.

3.4.4 ADDITIONAL POINTS

Additional points are labeled $(\mathcal{P}_{c\text{-}i},\ P_{SU\text{-}i})$ for $i \in \{1,2,3,\ldots\}$. The value of $\mathcal{P}_{c\text{-}i}$ for each new point should be between $\mathcal{P}_{c\text{-}min}$ and 1 and should correspond to the $\max(\widetilde{\mathcal{P}_{b\text{-}bd}})$ from the previous iteration. The value of $P_{SU\text{-}i}$ is found using the same method as $P_{SU\text{-}max}$ substituting $\mathcal{P}_{c\text{-}i}$ for $\mathcal{P}_{c\text{-}min}$,

$$\mathrm{SINR}_c^i = f^{-1}\left(\frac{\psi - \overline{\mathcal{P}}_{c\text{-}i}\cdot f\left(\mathrm{SINR}_{nc}\,\dfrac{B}{R}\right)}{\mathcal{P}_{c\text{-}i}}\right)\frac{R}{B} \tag{43}$$

$$P_{SU\text{-}i} = P_{PU}\cdot\frac{\mathrm{SINR}_{nc}-\mathrm{SINR}_c^i}{\mathrm{SINR}_{nc}\cdot\mathrm{SINR}_c^i}. \tag{44}$$

In the following sections we provide an example of a digital communications PU system and walk through the process of calculating SU operating boundaries and provide simulations to support the validity of the sharing framework.

3.5 EXAMPLE 4-QAM PRIMARY USER SYSTEM

We consider a 10 KHz 4-QAM digital communication system with threshold $\mathcal{P}_b$ value, $\psi = 10^{-4}$. We consider an ideal system with $B = 10$ KHz and $R = log_2(M)\cdot B = 20$ kbps. The system has an $\mathrm{SINR}_{nc} = 12$ dB and the value of P_{PU}, generally referred to as the receiver sensitivity in wireless communications systems, is $P_{PU} = -97$ dBm. These PU parameters are summarized in Table 1.

Table 1. Operating parameters for 4-QAM PU system.

PU Parameter	Value
SINR_{nc}	12 dB
P_{PU}	-97 dBm
B	10 KHz
f_B	20 kbps
$\mathcal{P}_x$	.30
ψ	10^{-4}
ϵ	5×10^{-7}

We assume I and P_{SU} are Gaussian distributed when they arrive at the PU receiver; this is the case when there are multiple sources of interference and/or the interference arrives via multipath channel conditions. In the presence of Gaussian interference and assuming AWGN, $\mathcal{P}_b$ for a QAM signal is defined as [39]

$$\mathcal{P}_b = f(\zeta) = \frac{4}{log_2(M)} \cdot \left(1 - \frac{1}{\sqrt{M}}\right) \cdot Q\left(\sqrt{\frac{3 \cdot log_2(M)}{M-1} \cdot \zeta}\right) \tag{45}$$

where M is the modulation order, in this example $M = 4$. The inverse of this function is

$$\zeta = f^{-1}(\mathcal{P}_b) = \left[Q^{-1}\left(\frac{\mathcal{P}_b \cdot log_2(M)}{4 \cdot \left(1 - \frac{1}{\sqrt{M}}\right)}\right)\right]^2 \cdot \frac{M-1}{3 \cdot log_2(M)}. \tag{46}$$

The function in (45) and its inverse in (46) are shown by the solid curve in Figure 16.

In a CR scenario with a dynamic PU the value of $\widetilde{\mathcal{P}_b}$, as determined by (29), is dependent on P_{PU}, P_{SU}, and $\mathcal{P}_c$. The multiple points in Figure 16 indicate the $\widetilde{\mathcal{P}_b}$ for select SU combinations ($\mathcal{P}_c$, P_{SU}) and a fixed $\text{SINR}_{nc} = 12$ dB. P_{SU} is represented by the ratio P_{PU}/P_{SU} rather than an absolute power but is readily converted given a value for P_{PU}. The x-axis is $\widetilde{\zeta}$ or the equivalent ζ required to meet the calculated $\widetilde{\mathcal{P}_b}$ in a non-hybrid scenario as defined in (31).

There are a two items worth observing in Figure 16, one related to SINR_{nc} and the other to SINR_c. First as expected the value of P_{SU} is irrelevant when $\mathcal{P}_c = 0$. This point represents an $\text{SINR}_{nc} = 12$ dB, or equivalently $\zeta_{nc} = 8.99$ dB, which yields $\mathcal{P}_b = 3.43 \times 10^{-5}$ using (45). Figure 16 also illustrates two points, each with $\mathcal{P}_c = 1$, corresponding to SINR_c. When $\text{SINR}_{nc} = 12$ dB and $P_{PU}/P_{SU} = 12$ dB, (19) results in a $\text{SINR}_c = 8.99$ dB, or equivalently $\zeta_c = 5.99$ dB; this yields a $\mathcal{P}_b = 2.4 \times 10^{-3}$ using (45). Likewise, when $\text{SINR}_{nc} = 12$ dB and $P_{PU}/P_{SU} = 0$ dB results in a

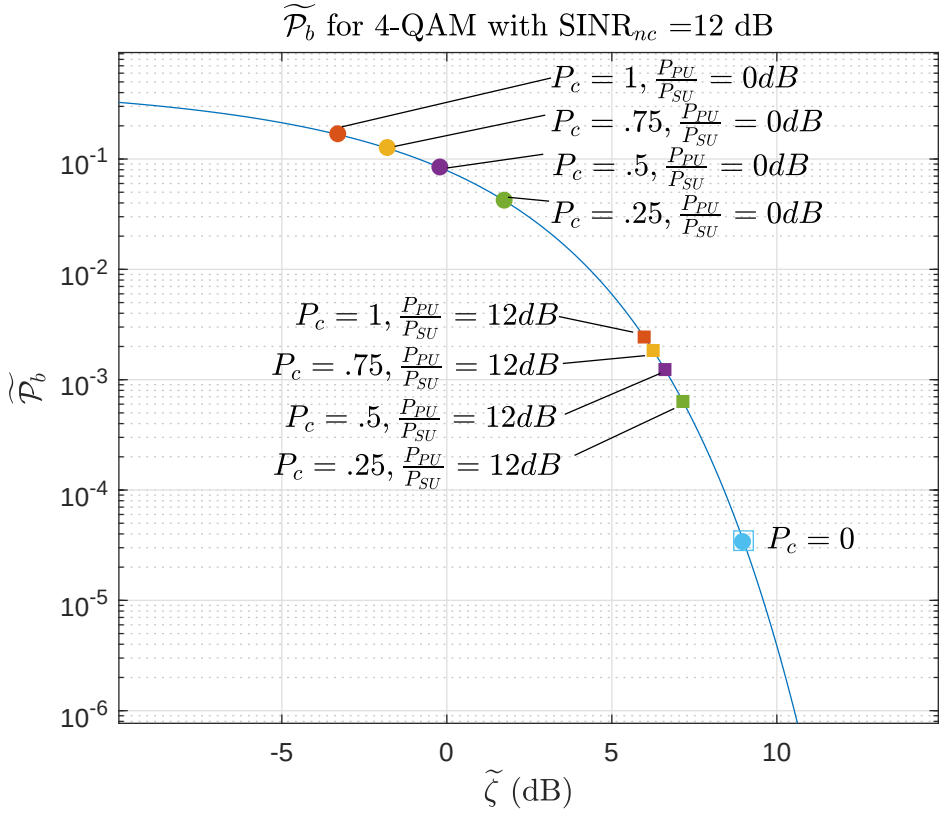

Figure 16. $\widetilde{\mathcal{P}_b}$ for 4-QAM with SINR$_{nc} = 12$ dB and select $\mathcal{P}_c$ and P_{SU} combinations.

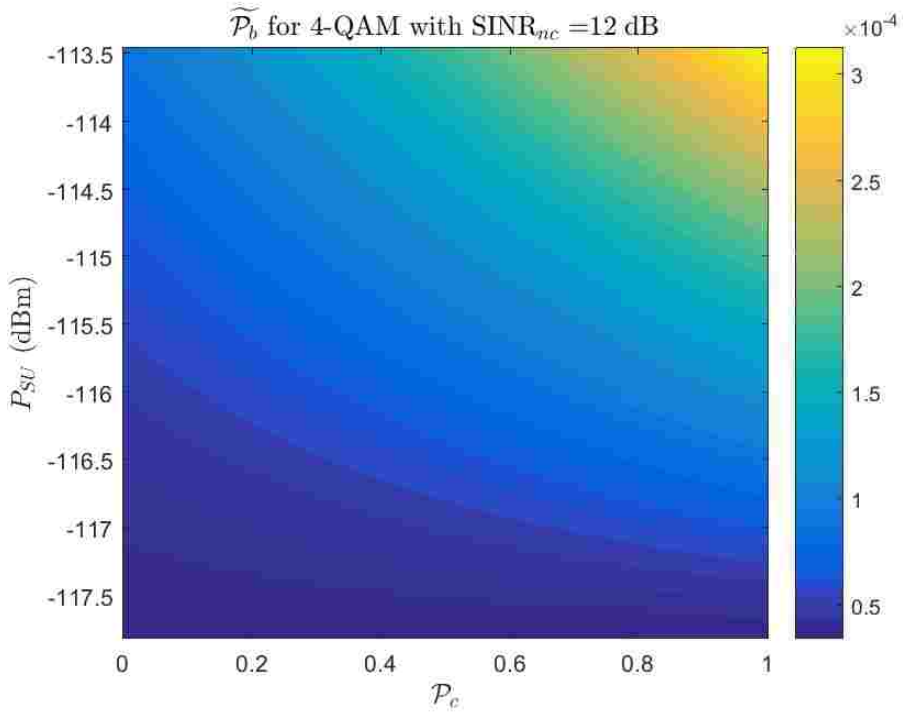

Figure 17. Contour of $\widetilde{\mathcal{P}_b}$ for 4-QAM with $\text{SINR}_{nc} = 12$ dB over a range of $\mathcal{P}_c$ and P_{SU} values.

$\text{SINR}_c = -0.27$ dB, or equivalently $\zeta_c = -3.28$ dB, and $\mathcal{P}_b = 0.17$.

3.5.1 SECONDARY USER OPERATION REGION FOR 4-QAM SYSTEM

Figure 17 shows a contour of $\widetilde{\mathcal{P}_b}$ for the example 4-QAM system using values from Table 1. The contour provides general idea of where the boundary for the SU operating range will be. To determine a precise SU operating boundary that will allow the PU to achieve the desired $\mathcal{P}_b \leq 10^{-4}$ we follow the process outlined in Sections 3.4.1 through 3.4.4.

Determine (1,$P_{SU\text{-}min}$)

When $\mathcal{P}_c = 1$ we use (35) to find SINR_c. Using the values for ψ, B, and R from Table 1 results in an $\text{SINR}_c = 11.41$ dB, or $\zeta_c = 8.40$ dB. Using (21) with $\text{SINR}_c = 11.41$ dB and $\text{SINR}_{nc} = 12$ dB results in a $P_{PU}/P_{SU} = 20.37$ dB. Finally, using $P_{PU} = -97$ dBm from Table 1 results in $P_{SU\text{-}min} = -117.37$ dBm. The point (1,-117.37 dBm) is the first point required to bound the SU operating range. This PU combination corresponds with an underlay sharing paradigm.

Determine ($\mathcal{P}_{c\text{-}min}$,$P_{SU\text{-}max}$)

The PU may select any $\mathcal{P}_{c\text{-}min} > 0$, noting that as $\mathcal{P}_{c\text{-}min} \to 1$ the SU will likely abandon attempts to detect the SU signal and operate solely using the underlay paradigm. Smaller values of $\mathcal{P}_{c\text{-}min}$ allow the SU flexibility to operate using an interweave, underlay, or a hybrid combination or the two paradigms. Assuming the SU has some detection capability and/or a duty cycle less than one, a $\mathcal{P}_{c\text{-}min} = 0.25$ is used. Using values from Table 1 and $\mathcal{P}_{c\text{-}min} = 0.25$, (35) results in $\text{SINR}_c = 10.72$ dB, or $\zeta_c = 7.70$ dB. A $\text{SINR}_c = 10.72$ dB and $\text{SINR}_{nc} = 12$ dB results in a $P_{PU}/P_{SU} = 16.65$ dB using (21). Again we use $P_{PU} = -97$ dBm from Table 1 resulting in $P_{SU\text{-}max} = -113.65$ dBm. The point (0.25,-113.65 dBm) is the second point required to bound the SU operating range.

Verify Boundary

Following the process outlined in Section 3.4.3 we define the piecewise linear boundary values for $P_{SU\text{-}min}$ and $P_{SU\text{-}max}$ found in steps 1 and 2 along with $\mathcal{P}_{c\text{-}min} = 0.25$ such that,

$$P_{SU} = \begin{cases} 4.32 \cdot 10^{-12} \text{ mW}, & \mathcal{P}_c \leq 0.25 \\ (-3.31\,\mathcal{P}_c + 5.14) \cdot 10^{-12} mW, & 0.25 < \mathcal{P}_c \leq 1. \end{cases} \tag{47}$$

Figure 18 illustrates $\widetilde{\mathcal{P}_{b\text{-}bd}}$ as defined in (39) using the piecewise linear boundary defined in (47). We can see that below $\mathcal{P}_c = 0.25$ where the P_{SU} is limited to $P_{SU\text{-}max}$ the $\widetilde{\mathcal{P}_{b\text{-}bd}}$ is below 10^{-4}. As expected $\widetilde{\mathcal{P}_{b\text{-}bd}} = 10^{-4}$ at $\mathcal{P}_c = 0.25$, it then rises above 10^{-4} with a peak value of 1.26×10^{-4} and returns to 10^{-4} at $\mathcal{P}_c = 1$. Using the $\epsilon = 5 \times 10^{-7}$ from Table 1, we determine it is appropriate to add a third point.

Add Additional Point

The third point should be added at the value of $\mathcal{P}_c$ corresponding to $\max(\widetilde{\mathcal{P}_{b\text{-}bd}})$. This can be done by setting the derivative of $\widetilde{\mathcal{P}_{b\text{-}bd}}$ equal to zero and solving for $\mathcal{P}_c$. Because of the complexity of (39) we instead find a numeric approximation of the max point which is at $\mathcal{P}_c = 0.5792$. Using $\mathcal{P}_{c\text{-}1} = 0.5792$ in (44) results in $P_{SU\text{-}1} = -115.78$ dBm.

Reevaluate Boundary

Using the Vandermonde method with the points (1,-117.37 dBm), (0.25,-113.65 dBm), and (0.5792,-115.78 dBm) results in the quadratic boundary

$$P_{SU} = \begin{cases} 4.32 \cdot 10^{-12} \text{ mW}, & \mathcal{P}_c \leq 0.25 \\ (4.27\,\mathcal{P}_c^2 - 8.67\,\mathcal{P}_c + 6.27) \cdot 10^{-12} \text{ mW}, & 0.25 < \mathcal{P}_c \leq 1. \end{cases} \tag{48}$$

Figure 18 illustrates $\widetilde{\mathcal{P}_{b\text{-}bd}}$ as defined in (42) using the piecewise 2nd-order or quadratic boundary defined in (48). The maximum value of $\widetilde{\mathcal{P}_{b\text{-}bd}}$ using the second order boundary is 1.046×10^{-4} which still exceeds the desired $\psi + \epsilon = 1.005 \times 10^{-4}$ limit.

We continue this process adding a fourth point at (0.3788,-114.65 dBm) and fifth point at (0.8557,-116.89 dBm). The resulting 3rd- and 4th-order polynomial boundaries are respectively

$$P_{SU} = \begin{cases} 4.32 \cdot 10^{-12} \text{ mW}, & \mathcal{P}_c \leq 0.25 \\ (-8.49\,\mathcal{P}_c^3 + 19.81\,\mathcal{P}_c^2 - 16.93\,\mathcal{P}_c + 7.46) \cdot 10^{-12} \text{ mW}, & 0.25 < \mathcal{P}_c \leq 1 \end{cases} \tag{49}$$

$$P_{SU} = \begin{cases} 4.32 \cdot 10^{-12} \text{ mW}, & \mathcal{P}_c \leq 0.25 \\ (8.90\,\mathcal{P}_c^4 - 28.14\,\mathcal{P}_c^3 + 34.63\,\mathcal{P}_c^2 - 21.50\,\mathcal{P}_c + 7.94) \cdot 10^{-12} \text{ mW}, & 0.25 < \mathcal{P}_c \leq 1. \end{cases} \tag{50}$$

We note that the 3rd-order boundary has a $\max \widetilde{\mathcal{P}_{b\text{-}bd}} = 1.049 \times 10^{-4}$ and is not an improvement over the 2nd-order boundary. However, the 4th-order boundary has a $\max \widetilde{\mathcal{P}_{b\text{-}bd}} = 1.004 \times 10^{-4}$ which meets the $\psi + \epsilon$ threshold. A comparison of the four alternative boundaries is illustrated in Figure 18. We can see that the 4th-order polynomial is a good fit to achieve the desired $\mathcal{P}_b \leq 10^{-4}$. Figure 19 is a variant of Figure 17 where areas less than 10^{-4} are shaded gray. Note that the x-axis in this figure is from $\mathcal{P}_{c\text{-}min}$ to 1. The boundaries illustrated in Figure 18 are imposed onto the contour. Again this plot shows the 4th-order polynomial boundary is the best fit.

Depending on the level at which the PU would like to obfuscate its waveform and its ability to relax ϵ, it can share any of the boundary equations with potential SUs wishing to exploit spectral holes. An $\epsilon \approx 5 \times 10^{-6}$ would allow for the 2nd-order boundary while the linear boundary would require $\epsilon \approx 3 \times 10^{-5}$. In the next section we simulate the 4-QAM PU operation and evaluate its performance with various SU values of $(\mathcal{P}_c, P_{SU})$ considering the linear, 2nd-order, and 4th-order polynomial boundaries.

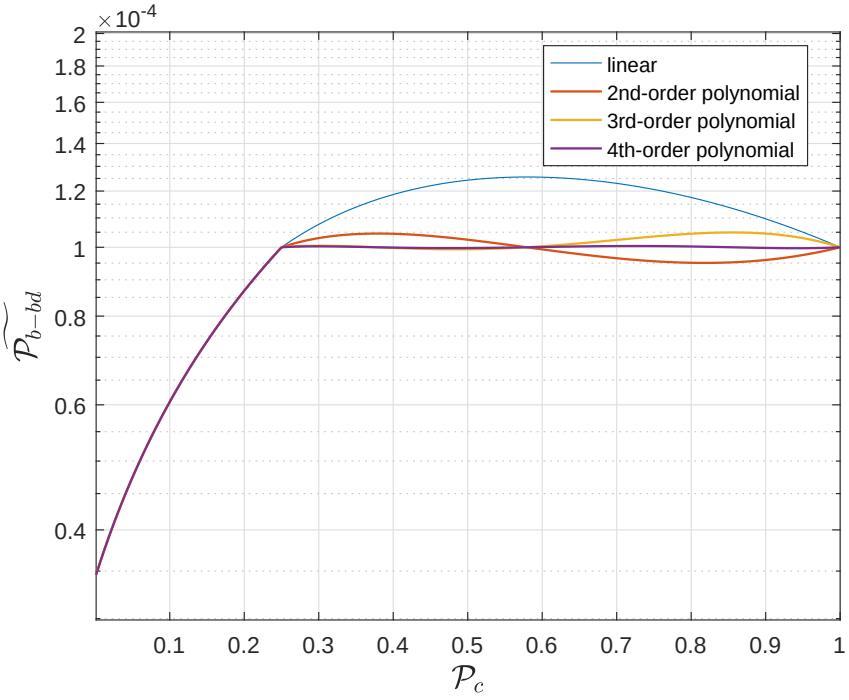

Figure 18. Comparison of four boundary equations.

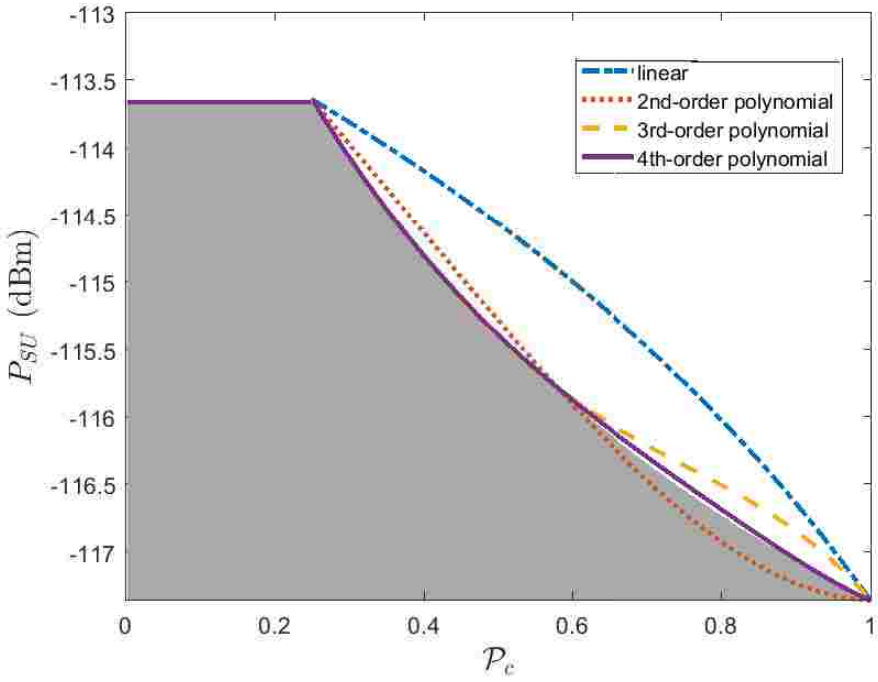

Figure 19. Comparison of four variant boundary equation over contour map where areas less than 10^{-4} are shaded.

3.5.2 SIMULATED PRIMARY USER PERFORMANCE

In this section we examine the performance of a simulated 4-QAM PU in a CR network. We consider the impact of SUs with $(\mathcal{P}_c, P_{SU})$ operating parameters derived from the linear, 2nd-order, and 4th-order polynomial boundaries.

For the first simulation we used a fixed $\mathcal{P}_Y = 0.9$. Noting that $\mathcal{P}_c$ can not exceed $\mathcal{P}_Y$, we evaluated 10 values of $\mathcal{P}_c \in \{0.1 : 0.9\}$. The value of $\mathcal{P}_d$ was calculated using (16). From the value of $\mathcal{P}_c$, we calculated the corresponding value of P_{SU} according to the boundary equation provided by the PU. The simulation was for 10,000s, with a PU duty cycle of $\mathcal{P}_X = 0.3$ turning on and off with a mean PU transmission duration of 1.5 ms and a mean time between PU transmissions of 3.5 ms. The SU achieved the duty cycle of $\mathcal{P}_Y = 0.9$ with a mean available traffic duration of 4.5 ms and a mean time with no available traffic of 0.5 ms. The SU sensor was simulated by forcing the SU into the blocked state, thus dropping any available traffic, according to the calculated value of $\mathcal{P}_d$. The results for this simulation are illustrated in Figure 20, Figure 21 and Figure 22 for the respective linear, 2nd-order, and 4th-order polynomial boundaries. The simulated values of P_{SU} are also shown in each figure for reference. The three figures show that the simulated PU value of $\mathcal{P}_b$ is very close to the expected theoretical boundary. These results illustrate that the SU will not interfere with the PU across a range of $\mathcal{P}_d$ values so long as the value of P_{SU} is bound accordingly.

For the second simulation we used a fixed $\mathcal{P}_d = 0.25$ and varied the SU duty cycle. In this case the value of $\mathcal{P}_c$ cannot exceed 1-$\mathcal{P}_d$ so we evaluated 10 values of $\mathcal{P}_c \in \{0.1 : 0.75\}$. The value of $\mathcal{P}_Y$ was calculated using (16) and in each case the desired duty cycle was achieved by fixing the mean available traffic duration of 1.5 ms and adjusting the duration between transmissions. The results for this simulation are provided for the linear, 2nd-order, and 4th-order polynomial boundaries respectively in Figure 23, Figure 24, and Figure 25. Again, the simulated value of P_{SU} is also shown for reference. As in the first simulation, the PU value of $\mathcal{P}_b$ was very close to the expected theoretical boundary. These results illustrate that the SU can avoid interfering with the PU by adjusting its power and duty cycle.

3.6 CHAPTER SUMMARY

In this chapter a hybrid method for sharing spectrum was proposed that allows for sensors that perform suboptimally. The proposed method only requires that the PU share the equation for the SU operating boundary with potential SUs. The SU operating boundary provides a limit

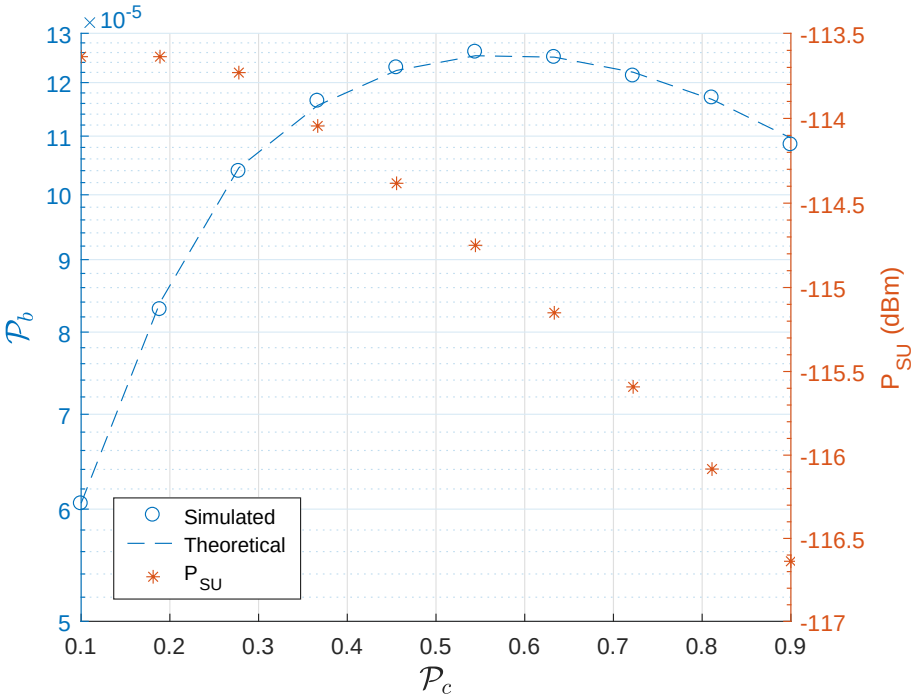

Figure 20. PU performance with a fixed SU value $\mathcal{P}_Y = .9$ and a range of SU $(\mathcal{P}_c, P_{SU})$ operating pairs on the linear boundary.

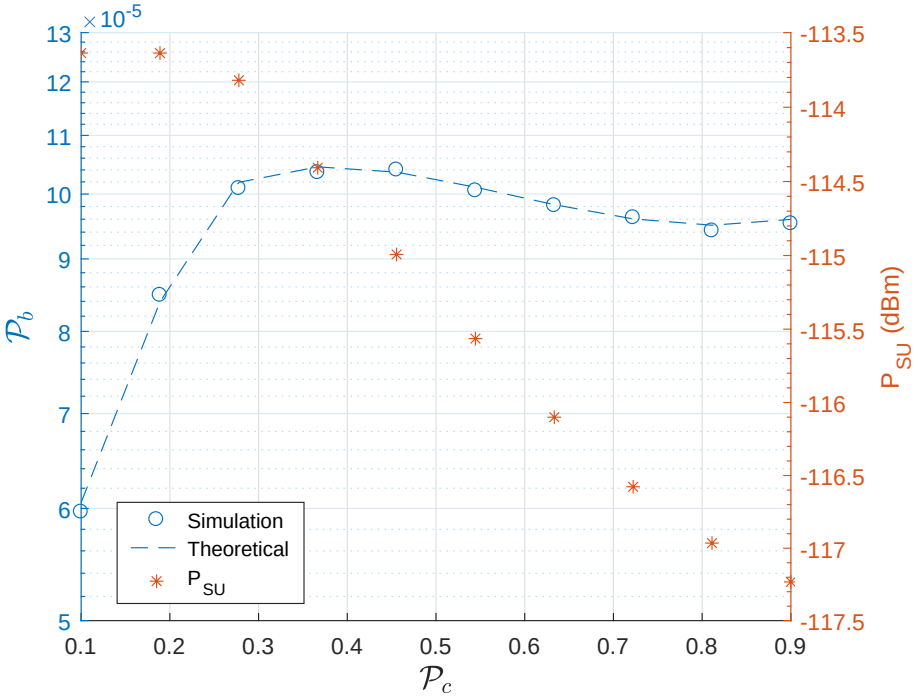

Figure 21. PU performance with a fixed SU value $\mathcal{P}_Y = .9$ and a range of SU $(\mathcal{P}_c, P_{SU})$ operating pairs on the 2nd-order polynomial boundary.

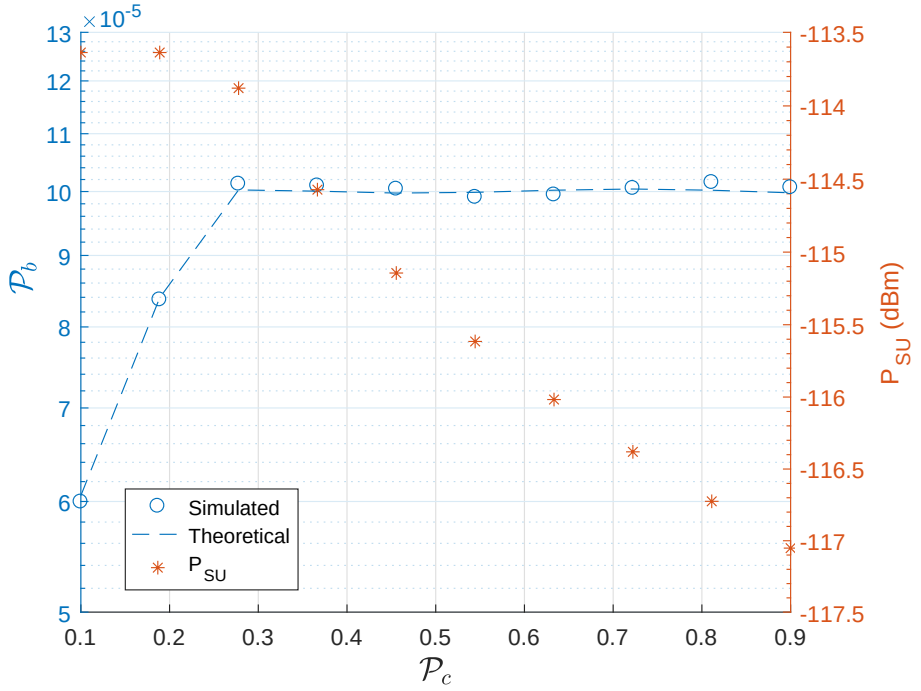

Figure 22. PU performance with a fixed SU value $\mathcal{P}_Y = .9$ and a range of SU $(\mathcal{P}_c, P_{SU})$ operating pairs on the 4th-order polynomial boundary.

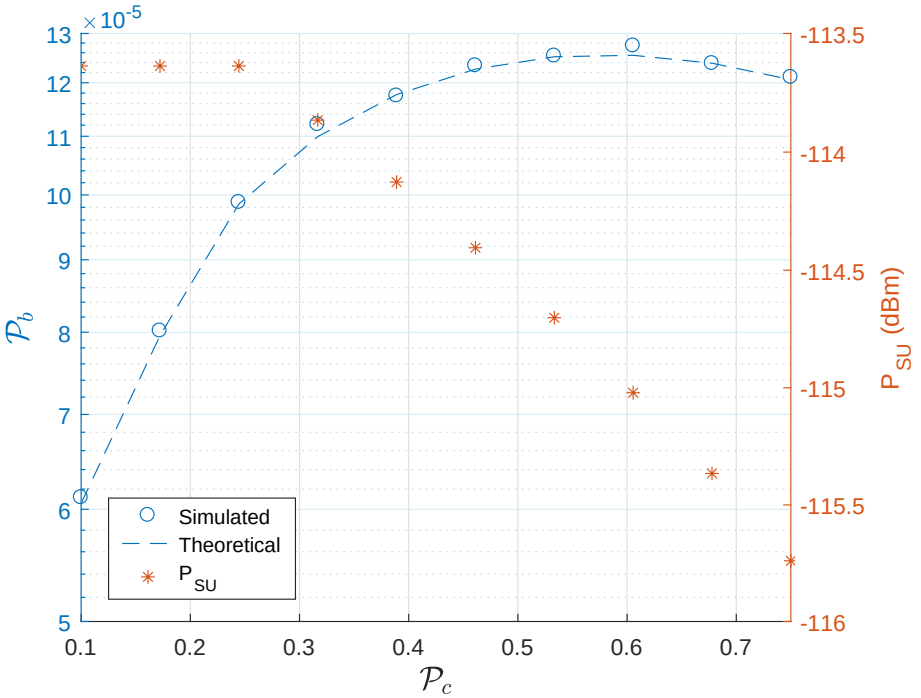

Figure 23. PU performance with a fixed SU value $\mathcal{P}_d = 0.25$ and a range of SU $(\mathcal{P}_c, P_{SU})$ operating pairs on the linear boundary.

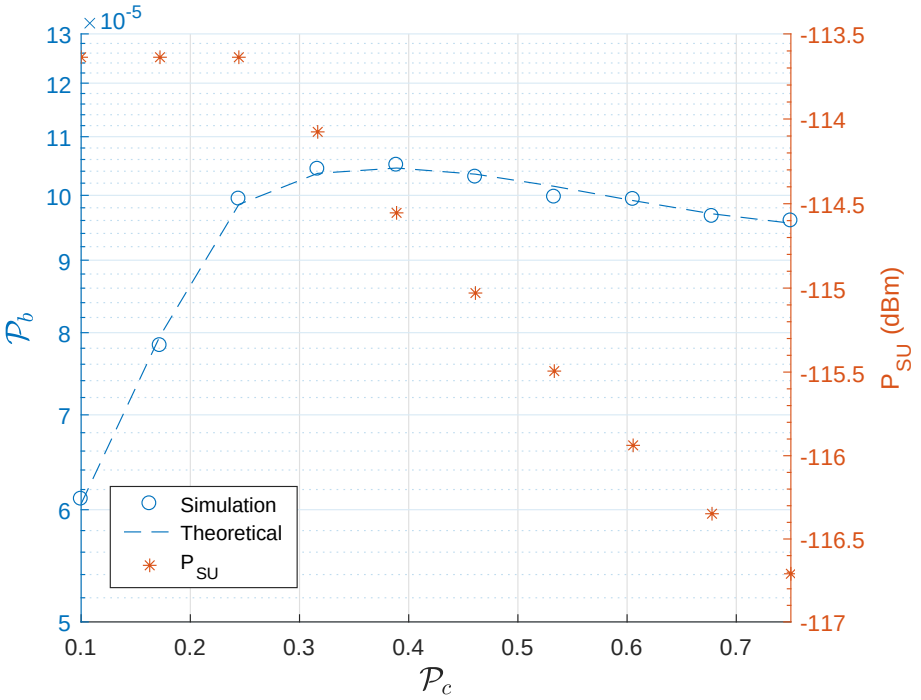

Figure 24. PU performance with a fixed SU value $\mathcal{P}_d = 0.25$ and a range of SU $(\mathcal{P}_c, P_{SU})$ operating pairs on the 2nd-order polynomial boundary.

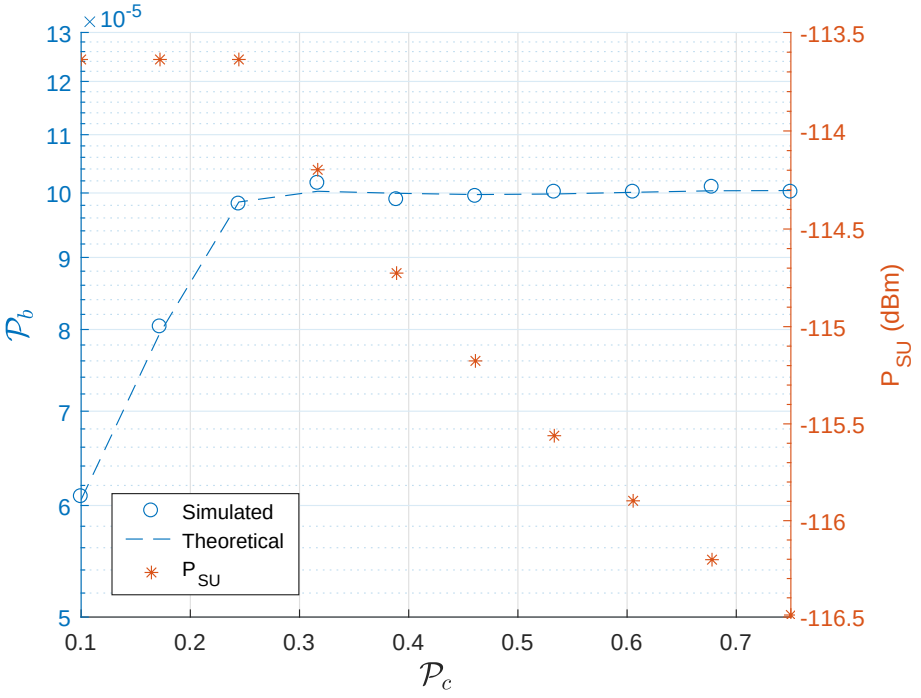

Figure 25. PU performance with a fixed SU value $\mathcal{P}_d = 0.25$ and a range of SU $(\mathcal{P}_c, P_{SU})$ operating pairs on the 4th-order polynomial boundary.

for P_{SU} given $\mathcal{P}_c$ or vice versa. Depending on the level at which the PU would like to obfuscate its waveform, the boundary equation can range from a simple linear equation defined by two points or may be a higher fidelity polynomial. This chapter also provided an alternate formula for the probability of collision $\mathcal{P}_c$ which considers both the SU duty cycle $\mathcal{P}_Y$ and the probability of missed detection $\overline{\mathcal{P}_d}$. In the case that the SU sensor is not able to achieve the desired $\overline{\mathcal{P}_d}$, the SU has the option of backing off on it's duty cycle to achieve the desired $\mathcal{P}_c$. This chapter did not address how an SU can calculate or estimate it's sensor performance, which is discussed in detail in Chapters 4 through 6.

CHAPTER 4

DYNAMIC PRIMARY USER MODEL

The previous chapter proposed a hybrid framework for use with dynamic PUs. The hybrid framework allowed for flexibility with the SU transmission and sensing performance while still ensuring the PU meets its desired $\mathcal{P}_b$. One SU variable considered in meeting the PU desired $\mathcal{P}_b$ is the SU sensing performance statistic $\mathcal{P}_d$. It is therefore critical for the SU to be able to accurately estimate its sensing capabilities, specifically the probability of detection, in the presence of a dynamic PU. Validated analytical expressions for $\mathcal{P}_d$ are provided for the sensing methods in Section 2.1.4 under the assumption of a static PU. Additionally expressions for $\mathcal{P}_d$ with a dynamic PU have been provided in prior research as described in Section 2.2. This former research has assumed varying constraints on they dynamic nature of the PU. In this chapter we consider a scenario similar to that in [30], with a dynamic PU. However, the analysis in [30] models the dynamic activity of the PU as a $1-0$ random process and assumes a maximum number of switches active/inactive of the PU signal during the spectrum sensing period. In this analysis we use a two-state Markov chain to model the PU signal activity and make no assumption on the number of PU signal changes during the sensing period. The closed-form expression for $\mathcal{P}_d$ and the corresponding probability $\mathcal{P}_f$ derived in Chapter 5 remove all assumptions concerning PU activity. This is accomplished by first deriving an analytical expression for the PU traffic model with respect to the SU sensing period.

4.1 DYNAMIC PRIMARY USER SYSTEM MODEL

We consider a CR scenario in which an SU performs spectrum sensing by collecting samples of the received signal during sensing period of equal duration in order to establish if the sensed frequency band, which is licensed for PU transmissions, is idle and may be used by the SU. The PU signal is assumed to be dynamic, switching from ON to OFF at random time instances as shown in Figure 26. The PU activity is assumed to be independent of the SU sensing period, such that the beginning and ending instances of the sensing period are not correlated with the beginning and ending of active/inactive periods of PU transmissions.

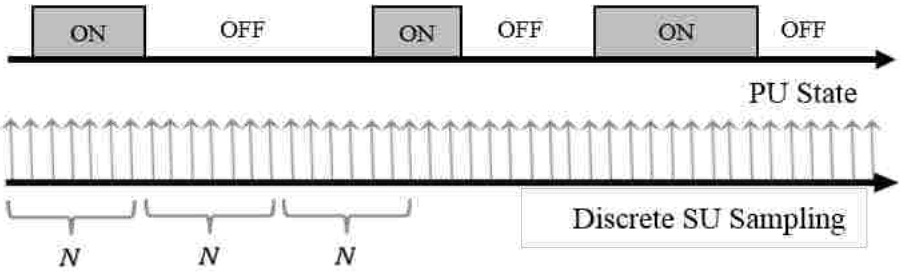

Figure 26. Illustration of a dynamic PU signal which switches from ON to OFF at random time instances, along with the sampling approach used by the SU for spectrum sensing.

The SU samples its received signal at a sampling rate f_s such that, over a sensing period with duration T a total of $N = T \cdot f_s$ samples are collected. Because the two possible states of the PU signal, active (ON) and idle (OFF) are mutually exclusive, each sample of the received signal $r(n)$ at the SU is described by one of the following two possible hypotheses:

$$\begin{aligned} H_0 &\rightarrow \text{PU signal OFF} : r(n) = u(n) \\ H_1 &\rightarrow \text{PU signal ON} : r(n) = s(n) + u(n), \end{aligned} \tag{51}$$

where $u(n)$ is the white Gaussian noise with zero mean and variance σ_u^2 corrupting the signal at the SU receiver. The PU signal $s(n)$ can be real or complex and has variance σ_s^2.

4.2 MARKOV CHAIN DYNAMIC PRIMARY USER MODEL

In order to model the dynamic activity of the PU we assume that, when the PU is active, the duration of its signal is exponentially distributed with mean τ, while the PU idle periods are exponentially distributed with mean ρ. In the context of discrete time processing by the SU where the received signal is sampled with frequency f_s, the values of τ and ρ represent the average number of samples corresponding to PU transmissions and idle periods.

Because the periods when the PU signal is ON, respectively OFF, are mutually exclusive, the PU activity may be modeled by a two-state Markov chain [41] as shown in Figure 27. The PU is either OFF (state 0) or ON (state 1) and the sojourn times in each state are independent exponential random variables represented by the average number of samples for the idle and active PU are ρ and τ, respectively. The probability of the PU signal to be in a given state, OFF or ON, at any

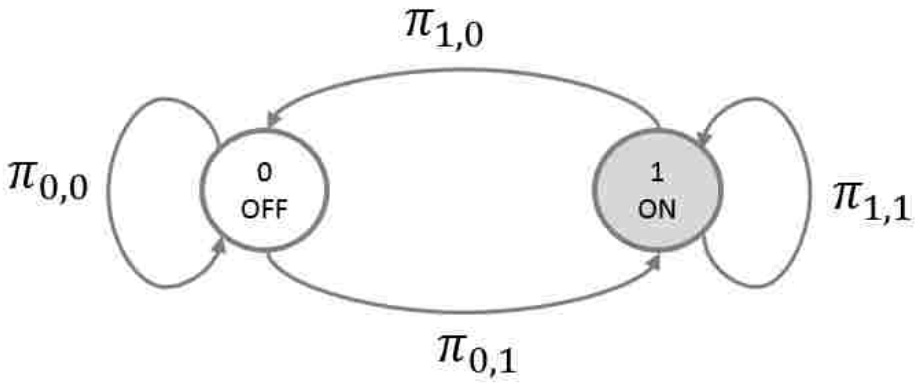

Figure 27. Markov chain representation of PU activity.

given time is determined by the limiting state probabilities, $\mathcal{P}_{off}$ and $\mathcal{P}_{on}$, respectively,

$$\mathcal{P}_{off} = \frac{\rho}{\tau + \rho} \quad \text{and} \quad \mathcal{P}_{on} = \frac{\tau}{\tau + \rho}. \tag{52}$$

In context to the PU duty cycle in Chapter 3, $\mathcal{P}_{on} = \mathcal{P}_X$ and $\mathcal{P}_{off} = 1 - \mathcal{P}_X$.

We note the exponential distribution for sojourn time corresponding to the number of samples is $\lambda e^{-\lambda}$ where $\lambda = 1/\rho$ when the state is 0 or OFF and $\lambda = 1/\tau$ when the PU state is 1 or ON. These distribution are used to derive the one-step transition probabilities of the two-state Markov chain in Figure 27. The transition probabilities $\pi_{i,j}$ represent the probability that the PU signal is in state $i \in \{0, 1\}$ at SU sample n and state $j \in \{0, 1\}$ at SU sample $n + 1$ and are given by [42]

$$\Pi = \begin{bmatrix} \pi_{0,0} & \pi_{0,1} \\ \\ \pi_{1,0} & \pi_{1,1} \end{bmatrix} = \frac{\rho\tau}{\rho + \tau} \begin{bmatrix} \frac{1}{\tau} + \frac{1}{\rho}\, e^{-\left(\frac{1}{\tau}+\frac{1}{\rho}\right)} & \frac{1}{\rho} - \frac{1}{\rho}\, e^{-\left(\frac{1}{\tau}+\frac{1}{\rho}\right)} \\ \\ \frac{1}{\tau} - \frac{1}{\tau}\, e^{-\left(\frac{1}{\tau}+\frac{1}{\rho}\right)} & \frac{1}{\rho} + \frac{1}{\tau}\, e^{-\left(\frac{1}{\tau}+\frac{1}{\rho}\right)} \end{bmatrix}. \tag{53}$$

4.2.1 INDIVIDUAL PATH PROBABILITIES

We are interested in examining the PU activity in context to the SU sensing period of N samples. Therefore, we consider the N-step evolution of the Markov chain as illustrated by the two-state trellis in Figure 28, noting that there are $K = 2^N$ possible evolutions or paths the model

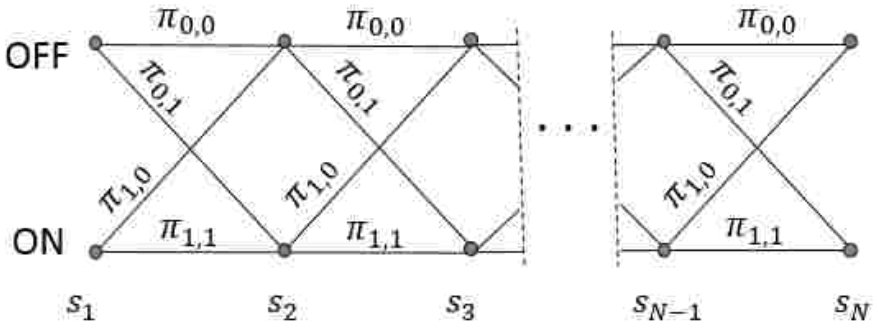

Figure 28. Two-state trellis representation of an N-step Markov chain evolution.

allows for during the sensing period. Each path probability is determined by the product of the initial state probability, $\mathcal{P}_{init}$, and the $N-1$ transition probabilities corresponding to the path. Specifically the probability of the k^{th} path occurring in a sensing window is

$$\mathcal{P}_k = \mathcal{P}_{init}^{(k)} \prod_{n=1}^{N-1} \pi_{s_n^{(k)}, s_{n+1}^{(k)}}, \tag{54}$$

where $\mathcal{P}_{init}^{(k)}$ is the initial state probability and $\pi_{s_n^{(k)}, s_{n+1}^{(k)}}$ is the one-step transition probability between the sampling instants n and $n+1$. We note that for the k^{th} path the probability $\mathcal{P}_{init}^{(k)}$ is equal to either $\mathcal{P}_{off}$ or $\mathcal{P}_{on}$ depending on whether the PU is OFF or ON, respectively, at the beginning of the sensing window.

4.2.2 DISTRIBUTION OF x ON SAMPLES

In deriving a model for PU activity with respect to the SU sensing period it is important to understand the distribution of x, where x indicates the number of samples that the PU is ON during the sensing period and $N-x$ represent the number of samples where the PU is OFF. Therefore, for each of the $k \in \{1, 2, \ldots, K\}$ paths we consider the number of samples that PU is either ON or OFF in that path along with the probability of that path occurring. We partition the K paths into $N+1$ subsets $K_x \in \{K_0, K_1, \ldots, K_N\}$ where each path in the K_x subset has x samples where the PU is ON. The individual path probabilities $\mathcal{P}_{k_x}$ in the K_x subset are calculated as in (54) and summing the $\binom{N}{x}$ path probabilities in the K_x subset provides the probability that the PU will be

ON for x samples in a N sample sensing period,

$$\Phi_x = \sum_{k_x=1}^{\binom{N}{x}} \mathcal{P}_{k_x}. \tag{55}$$

We note that

$$\sum_{x=0}^{N} \Phi_x = 1, \tag{56}$$

which is critical in forming proper probability distributions.

4.3 HYPOTHESIS TESTING

The PU activity model described in this chapter is independent of the sensing technique employed by the SU. However, we present the hypotheses in this section in context to an energy detector for clarity. It is important to note that the use of a waveform-based sensor or cyclostationary detector described in Section 2.1.4 can also be used with the proposed dynamic PU hypotheses and dynamic PU activity model.

When an energy detector similar to that in Section 2.1.4 is used to distinguish between the H_0 and H_1 hypotheses the test statistic is [14, 15]

$$Y(N) = \sum_{n=1}^{N} \left| \frac{r(n)}{\sigma_u} \right|^2. \tag{57}$$

The single sample hypotheses in (51) where H_0 and H_1 indicates the PU is respectively OFF or ON, is traditionally extended to the entire sensing period. That is, the hypothesis H_0 traditionally represents the PU being OFF during the entire sensing period while H_1 traditionally represents the PU being ON during the entire sensing period. The energy detector test statistic is then,

$$Y(N) = \begin{cases} \sum_{n=1}^{N} \left| \frac{u(n)}{\sigma_u} \right|^2, & H_0 \\ \sum_{n=1}^{N} \left| \frac{s(n)+u(n)}{\sigma_u} \right|^2, & H_1. \end{cases} \tag{58}$$

Due to the dynamic nature of the PU during a single sensing period the PU can be in both OFF and ON. It is therefore necessary to redefine the hypotheses that apply to a sensing period. Because

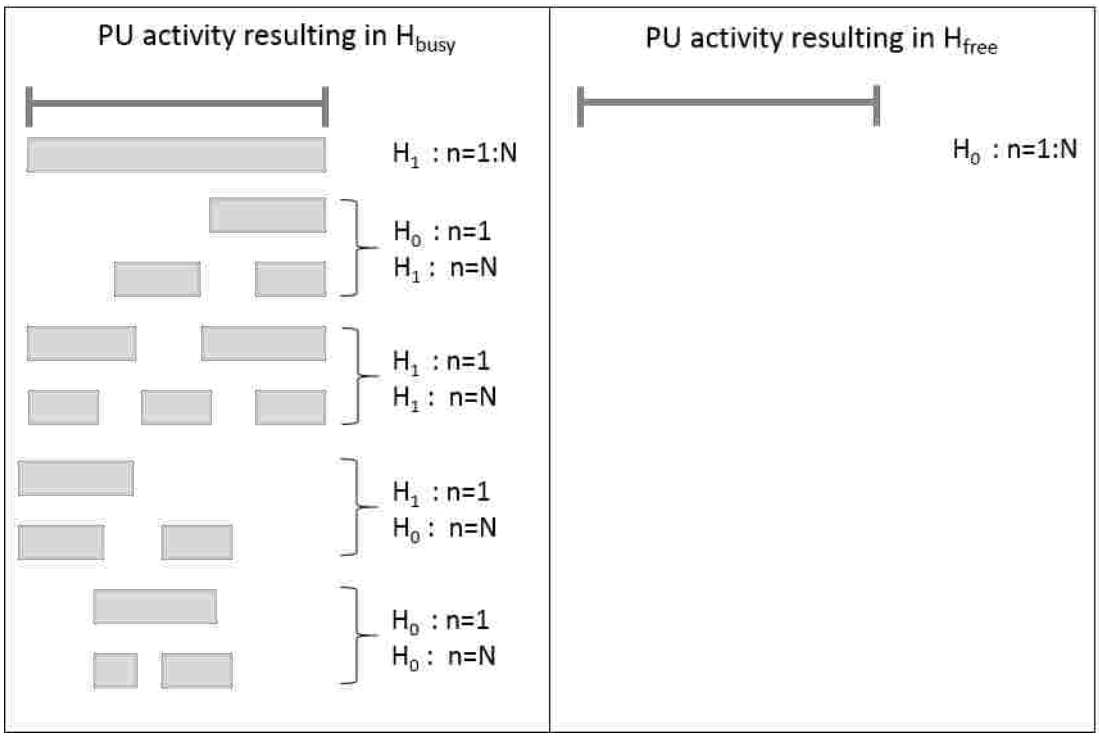

Figure 29. Spectrum sensing hypotheses H_{free} and H_{busy} due to dynamic PU activity during a sensing period starting at $n = 1$ and ending at $n = N$.

the needs of different CR networks may vary, we consider two alternative sets of hypotheses.

4.3.1 ANY SAMPLE HYPOTHESES

We first consider a conservative set of hypotheses H_{free} and H_{busy} as first defined by [29] where the null hypothesis H_{free} corresponds to a PU that is OFF during the entire sensing duration and H_{busy} corresponds to a PU that is ON at one or more samples during a sensing period. Figure 29 illustrates how various PU activity relates to the hypotheses H_{free} and H_{busy}. Clearly there is only one PU activity pattern that results in H_{free} while all others are categorized as H_{busy}.

In the case of H_{busy} the dynamic behavior will directly influence the value of the test statistic while H_{free} will remain the same as in (58). We revise the test statistic for H_{busy} to account for the dynamic nature of the PU. To do this we consider the cumulative number of samples where the PU is ON during a sensing period, x, and the cumulative number of samples where the PU is OFF, $N - x$. In context to the energy detector which sums the square of the N samples in the sensing period, the order of the N received samples is irrelevant. The test statistic for any given sensing

period is given by

$$Y(N) = \begin{cases} \sum_{n=1}^{N} \left| \frac{u(n)}{\sigma_u} \right|^2, & H_{free} \\ \sum_{n=1}^{x} \left| \frac{s(n)+u(n)}{\sigma_u} \right|^2 + \sum_{n=N-x}^{N} \left| \frac{u(n)}{\sigma_u} \right|^2, & H_{busy}. \end{cases} \tag{59}$$

4.3.2 N$^{\text{TH}}$ SAMPLE HYPOTHESES

The second set of hypotheses considered assume that at the end of the sensing period the SU will either transmit or remain silent based on the formulated hypothesis. From the perspective of SU spectral utilization, the SU is therefore interested in establishing which hypothesis is true at the end of the sensing period, or SU sample $n = N$. Accordingly, we define the hypothesis H_{N0} corresponding to the PU being OFF at the end of the sensing period and H_{N1} corresponding to a PU that is ON at the end of the sensing period. Figure 30 illustrates how various PU activity relates to the hypotheses H_{N0} and H_{N1} and when compared with Figure 29 there is a clear difference in the two sets of proposed dynamic PU hypotheses. In fact, Figure 30 illustrates that in some instances the hypothesis H_{N0} could apply to a sampling period where the PU is predominately ON and alternatively the hypothesis H_{N1} could apply to a sampling period where the PU is predominately OFF.

Using the hypotheses H_{N0} and H_{N1} the test statistic for any given sensing period is

$$Y(N) = \begin{cases} \sum_{n=1}^{x} \left| \frac{s(n)+u(n)}{\sigma_u} \right|^2 + \sum_{n=N-x}^{N} \left| \frac{u(n)}{\sigma_u} \right|^2, & H_{N0} \\ \sum_{n=1}^{x} \left| \frac{s(n)+u(n)}{\sigma_u} \right|^2 + \sum_{n=N-x}^{N} \left| \frac{u(n)}{\sigma_u} \right|^2, & H_{N1}. \end{cases} \tag{60}$$

We note the formulas for $Y(N)$ under H_{N0} and H_{N1} are identical when considering a single sensing period. It is therefore important to develop distribution functions for $Y(N)$ which consider how the average number of samples where the PU is ON varies between the hypothesis H_{N0} and H_{N1}.

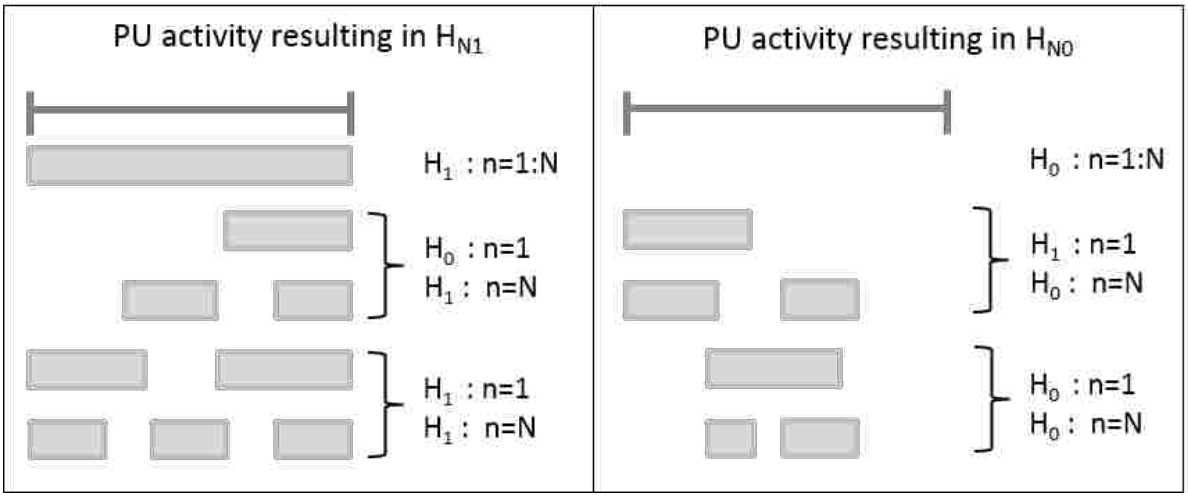

Figure 30. Spectrum sensing hypotheses H_{N0} and H_{N1} due to dynamic PU activity during a sensing period starting at $n = 1$ and ending at $n = N$.

4.4 JOINT AND CONDITIONAL PROBABILITIES

In this section we use the probabilities for p_k and Φ_x, defined respectively as (54) and (55) in Section 4.2, to formulate conditional and joint probabilities corresponding to the two alternative sets of dynamic PU hypotheses described in Section 4.3.

4.4.1 ANY SAMPLE HYPOTHESES PROBABILITIES

In this section we derive the probabilities summarized in Table 2 with respect to the hypotheses H_{free} and H_{busy}.

Table 2. Summary of Any Sample probabilities.

Probability	Description
$\Phi_{x,A}$	Probability the PU is ON $x \in \{0, 1, \ldots N\}$ samples and $A \in \{free, busy\}$
$\Phi_{x\|A}$	Probability the PU is ON $x \in \{0, 1, \ldots N\}$ samples given $A \in \{free, busy\}$
$\mathcal{P}_{i,A}$	Probability $s_n = i$ for $i \in \{0, 1\}$ and $A \in \{free, busy\}$
$\mathcal{P}_{i\|A}$	Probability $s_n = i$ for $i \in \{0, 1\}$ given $A \in \{free, busy\}$

We first consider $\Phi_{x,A}$, the joint probability of PU is ON x of N samples and $A \in \{free, busy\}$. We note that the hypothesis H_{free} corresponds to $x = 0$ and H_{busy} corresponds to $x > 0$. The

probabilities are intuitively,

$$\Phi_{x,A} = \begin{cases} \Phi_0, & A = free,\ x = 0 \\ 0, & A = free,\ x > 0 \\ 0, & A = busy,\ x = 0 \\ \Phi_x, & A = busy,\ x > 0. \end{cases} \tag{61}$$

Using the joint probability we can calculate the corresponding conditional probabilities using the Kolmogorov definition

$$\Phi_{x|A} = \frac{\Phi_{x,A}}{\Pr\{A\}}. \tag{62}$$

We use the values of Φ_x in (55) to calculate $\Pr\{A\}$ for $A \in \{free, busy\}$

$$\Pr\{free\} = \Pr\{x{=}0\} = \Phi_0 \tag{63}$$

$$\Pr\{busy\} = \Pr\{x{>}0\} = \sum_{x=1}^{N} \Phi_x = 1 - \Phi_0. \tag{64}$$

Expanding (62) to consider the hypotheses separately results in

$$\Phi_{x|A} = \begin{cases} 1, & A = free,\ x = 0 \\ 0, & A = free,\ x > 0 \\ 0, & A = busy,\ x = 0 \\ \dfrac{\Phi_x}{1 - \Phi_0}, & A = busy,\ x > 0. \end{cases} \tag{65}$$

We next consider the joint probability $\mathcal{P}_{i,A}$ where $i \in \{0, 1\}$ represents the dynamic PU state s_n at sampling instant $n \in \{1, 2, \ldots, N\}$. We use the calculated joint probabilities $\Phi_{x,A}$ so that

$$\mathcal{P}_{i,A} = \begin{cases} \displaystyle\sum_{x=0}^{N} \Phi_{x,A}\ \frac{N - x}{N}, & i = 0 \\ \displaystyle\sum_{x=0}^{N} \Phi_{x,A}\ \frac{x}{N}, & i = 1. \end{cases} \tag{66}$$

Again, we expand the equation to consider the hypotheses separately

$$\mathcal{P}_{i,A} = \begin{cases} \Phi_0, & A = free,\ i = 0 \\ 0, & A = free,\ i = 1 \\ \sum_{x=1}^{N} \Phi_x \ \dfrac{N-x}{N}, & A = busy,\ i = 0 \\ \sum_{x=1}^{N} \Phi_x \ \dfrac{x}{N}, & A = busy,\ i = 1. \end{cases} \tag{67}$$

To calculate the joint probabilities we again the Kolmogorov definition

$$\mathcal{P}_{i|A} = \frac{\mathcal{P}_{i,A}}{\Pr\{A\}}, \tag{68}$$

which expanded to consider specificall $\mathcal{P}_{i|free}$ and $\mathcal{P}_{i|busy}$ is

$$\mathcal{P}_{i|A} = \begin{cases} 1, & A = free,\ i = 0 \\ 0, & A = free,\ i = 1 \\ \dfrac{\sum_{x=1}^{N} \Phi_x \ \dfrac{N-x}{N}}{1-\Phi_0}, & A = busy,\ i = 0 \\ \dfrac{\sum_{x=1}^{N} \Phi_x \ \dfrac{x}{N}}{1-\Phi_0}, & A = busy,\ i = 1. \end{cases} \tag{69}$$

Using the conditional probabilities in (69) we can also evaluate the expected number of samples collected during the sensing period that correspond to a given PU state to be $i \in \{0, 1\}$ at SU sampling instant $n \in \{1, 2, \ldots, N\}$ given that the PU state is $A \in \{free, busy\}$ to be

$$N_{i|A} = \mathcal{P}_{i|A} \cdot N. \tag{70}$$

We note that while N is inherently an integer, this is not necessarily the case for $N_{i|A}$.

4.4.2 N$^{\text{TH}}$ SAMPLE HYPOTHESES PROBABILITIES

In this section we derive the probabilities summarized in Table 3 with respect to the hypotheses H_{N0} and H_{N1}. Here we use $s_N \in \{0,1\}$ to represent the state of the PU in the N^{th} sample where $s_N = 0$ and $s_N = 1$ represent the hypotheses respectively H_{N0} and H_{N1}.

Table 3. Summary of N^{th} sample probabilities.

Probability	Description
Φ_{x,s_N}	Probability the PU is ON $x \in \{0,1,\dots N\}$ samples and $s_N \in \{0,1\}$
$\Phi_{x\|s_N}$	Probability the PU is ON $x \in \{0,1,\dots N\}$ samples given $s_N \in \{0,1\}$
$\mathcal{P}_{i,s_N}$	Probability $s_n = i$ for $i \in \{0,1\}$ and $s_N \in \{0,1\}$
$\mathcal{P}_{i\|s_N}$	Probability $s_n = i$ for $i \in \{0,1\}$ given $s_N \in \{0,1\}$

For the hypotheses H_{N0} and H_{N1} it is necessary to further divide the K_x subsets depending on the state of the PU at the end of the sensing period. We label these subsets, K_{x,s_N} resulting in $K_{x,s_N} \in \{K_{0,0}, K_{0,1}, K_{1,0}, K_{1,1} \dots, K_{N,0}, K_{N,1}\}$. We note that the subsets K_0 and K_N are each composed of a single path, respectively all OFF and all ON; thus, the subsets $K_{0,1}$ and $K_{N,0}$ are empty resulting in $2N$ non-empty subsets. We sum the paths in the corresponding K_{x,s_N} subset to form the joint probability that the PU will be ON for x samples in a N sample sensing period is

$$\Phi_{x,s_N} = \begin{cases} \sum_{k_x=1}^{\binom{N-1}{x}} \mathcal{P}_{k_x}, & s_N = 0,\ x \in \{0,1,\dots,N-1\} \\ 0, & s_N = 0,\ x = N \\ 0, & s_N = 1,\ x = 0 \\ \sum_{k_x=1}^{\binom{N-1}{x-1}} \mathcal{P}_{k_x}, & s_N = 1,\ x \in \{1,2,\dots,N\}. \end{cases} \tag{71}$$

We note that

$$\sum_{x=0}^{N} \Phi_{x,0} = \Pr\{s_N = 0\} = \mathcal{P}_{off} \qquad \text{and} \tag{72}$$

$$\sum_{x=0}^{N} \Phi_{x,1} = \Pr\{s_N = 1\} = \mathcal{P}_{on}, \tag{73}$$

and we use these values to calculate the conditional probabilities with respect to the hypotheses

H_{N0} and H_{N1},

$$\Phi_{x|s_N} = \frac{\Phi_{x,s_N}}{\Pr\{s_N\}} = \begin{cases} \dfrac{\Phi_{x,0}}{\mathcal{P}_{off}} & s_N = 0,\ x \in \{0, 1, \ldots, N-1\} \\ 0, & s_N = 0,\ x = N \\ 0, & s_N = 1,\ x = 0 \\ \dfrac{\Phi_{x,1}}{\mathcal{P}_{on}} & s_N = 1,\ x \in \{1, 2, \ldots, N\}. \end{cases} \tag{74}$$

We next consider $\mathcal{P}_{i,s_N}$, the joint probability $s_n = i$ for $i \in \{0, 1\}$ and $s_N \in \{0, 1\}$, which is similar to the calculation for $\mathcal{P}_{i,A}$ in (66),

$$\mathcal{P}_{i,s_N} = \begin{cases} \displaystyle\sum_{x=0}^{N} \Phi_{x,s_N} \frac{N-x}{N}, & i = 0 \\ \displaystyle\sum_{x=0}^{N} \Phi_{x,s_N} \frac{x}{N}, & i = 1. \end{cases} \tag{75}$$

Again we expand (75) to consider the hypotheses separately,

$$\mathcal{P}_{i,s_N} = \begin{cases} \displaystyle\sum_{x=0}^{N-1} \Phi_{x,0} \frac{N-x}{N}, & s_N = 0,\ i = 0 \\ \displaystyle\sum_{x=0}^{N-1} \Phi_{x,0} \frac{x}{N}, & s_N = 0,\ i = 1 \\ \displaystyle\sum_{x=1}^{N} \Phi_{x,1} \frac{N-x}{N}, & s_N = 1,\ i = 0 \\ \displaystyle\sum_{x=1}^{N} \Phi_{x,1} \frac{x}{N}, & s_N = 1,\ i = 1. \end{cases} \tag{76}$$

We note that in (76) only the limits of the summations were modified from (75) when considering the hypothesis separately.

The last probability we consider is the conditional probability $\mathcal{P}_{i|s_N}$. We again use the Kolmogorov definition so that

$$\mathcal{P}_{i|s_N} = \frac{\mathcal{P}_{i,s_N}}{\Pr\{s_N\}} = \begin{cases} \dfrac{\mathcal{P}_{0,0}}{\mathcal{P}_{off}}, & s_N = 0 \;\; i = 0 \\ \dfrac{\mathcal{P}_{1,0}}{\mathcal{P}_{off}}, & s_N = 0 \;\; i = 1 \\ \dfrac{\mathcal{P}_{0,1}}{\mathcal{P}_{on}}, & s_N = 1 \;\; i = 0 \\ \dfrac{\mathcal{P}_{1,1}}{\mathcal{P}_{on}}, & s_N = 1 \;\; i = 1. \end{cases} \tag{77}$$

In this case no combinations simplify when expanding the equation.

Finally, as in (69) we use the conditional probabilities in (77) to evaluate the expected number of samples collected during the sensing period that correspond to a given PU state to be $i \in \{0, 1\}$ at SU sampling instant $n \in \{1, 2, \ldots, N\}$ given that the PU state at the end of the sampling period is $s_N \in \{0, 1\}$ to be

$$N_{i|s_N} = \mathcal{P}_{i|s_N} \cdot N. \tag{78}$$

As is the case for $N_{i|A}$ in (69), $N_{i|s_N}$ is not necessarily an integer.

In Chapter 5 the probabilities described in this chapter are used to derive expressions for $\mathcal{P}_d$ and $\mathcal{P}_f$ using the dynamic PU hypotheses. However, before calculating the sensor performance probabilities, we first verify the mathematical dynamic PU model using simulation.

4.5 VERIFICATION OF DYNAMIC PRIMARY USER MODEL

Because the probabilities in this chapter build upon each other, it is not necessary to verify all probabilities listed in Tables 2 and 3. We instead verify the Φ_x where the theoretical formula is provided by (55) and the conditional values of N, $N_{i|A}$ and $N_{i|s_N}$ respectively defined in (70) and (78).

In order to verify the PU model and conditional values of N we simulated a dynamic PU for the equivalent of $1,000,000$ sampling periods where each sampling period consisted of $N = 20$ samples. Four trials were run, in each the dynamic PU was characterized by an average OFF period $\rho = 50$ while the average ON period $\tau \in \{5, 10, 20, 50\}$ varied between trails.

Figure 31 provides the theoretical versus simulated results for Φ_x. The simulated results closely

match the theoretical results calculated using (55) thus verifying the equation for Φ_x and the individual path probabilities p_k in (54). Figure 32 provides the theoretical versus simulated results for $N_{i|A}$. The simulated results closely match the theoretical results calculated using (70) thus verifying the equation for $N_{i|A}$ and the probabilities listed in Table 2 which contributed to $N_{i|A}$. Likewise, Figure 33 provides theoretical versus simulated results for $N_{i|s_N}$. Again, the simulated and theoretical results calculated using (78) match thus verifying the equation for $N_{i|s_N}$ and the probabilities listed in Table 3 which contributed to $N_{i|s_N}$.

4.6 CHAPTER SUMMARY

In CR networks with a static PU the spectrum sensing hypotheses H_0 indicates the signal is absent during the entire sensing period and H_1 indicates the signal is present during the entire sensing period. This chapter considered a dynamic PU that could can be both present and absent during a sensing period and two alternative sets of dynamic PU hypotheses were proposed. The *Any Sample* hypotheses, H_{free} and H_{busy}, are represented by a conservative null hypothesis where H_{free} indicates the PU is OFF during the entire sensing period. In contrast, the N^{th} *Sample* hypotheses, H_{N0} and H_{N1}, considers a more aggressive use of spectrum in which the hypothesis was determined by the PU state at the end of the sensing period.

In order to analyze PU traffic distribution under the proposed dynamic PU hypotheses a mathematical model for describing the dynamic PU activity using a Markov chain was employed. We considered the evolution of the Markov chain over the SU sensing period and derived several joint and conditional probabilities related to the dynamic PU hypotheses. The probabilities described were verified through simulation and will be used in Chapter 5 to formulate a density function for the energy detector output $Y(N)$ and corresponding sensor performance statistics for each of the four hypothesis described in Section 4.3.

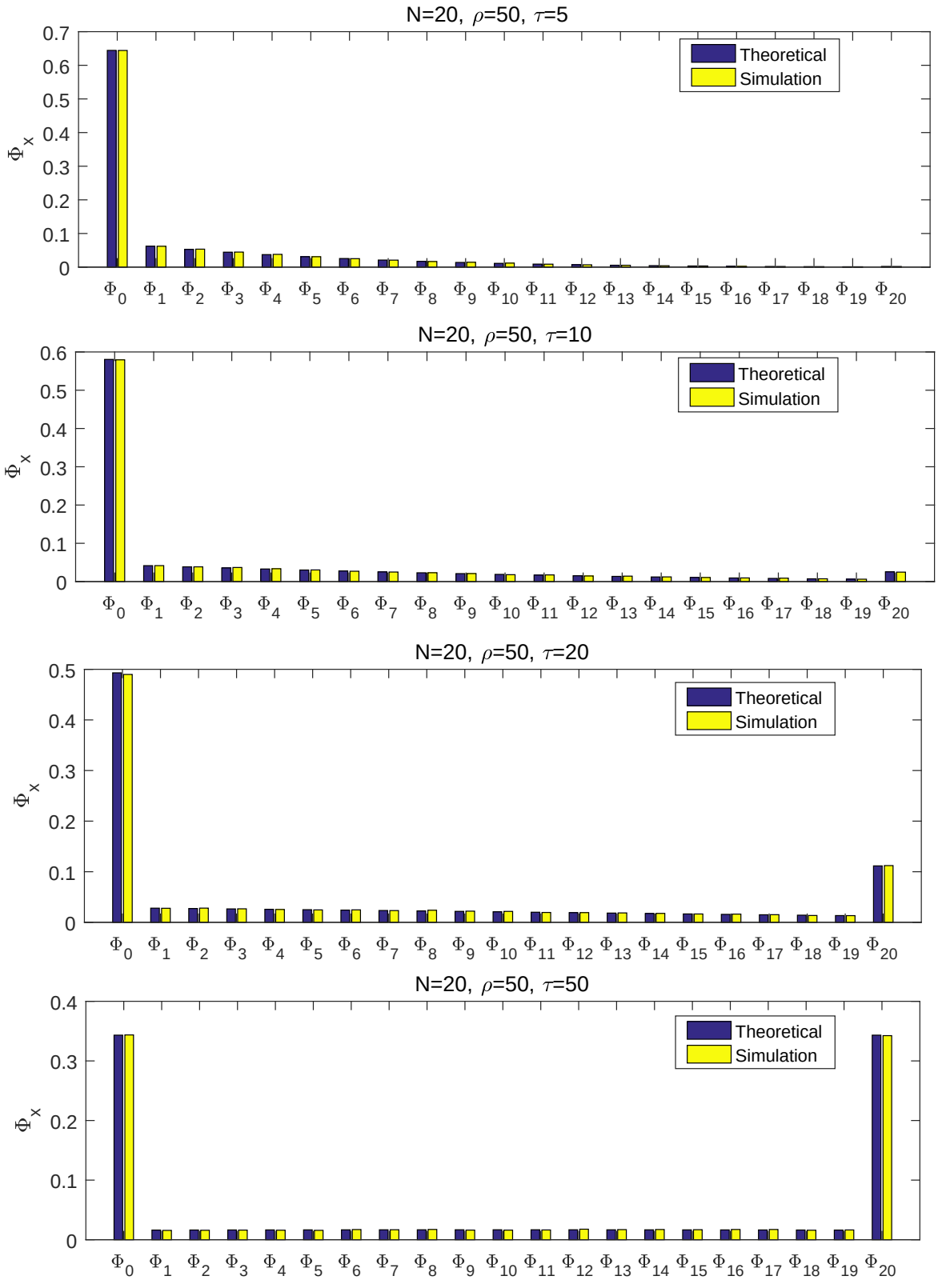

Figure 31. Theoretical vs simulated comparison of Φ_x with $N = 20$, $\rho = 50$, and (a) $\tau = 5$, (b) $\tau = 10$,(c) $\tau = 20$,(d) $\tau = 50$.

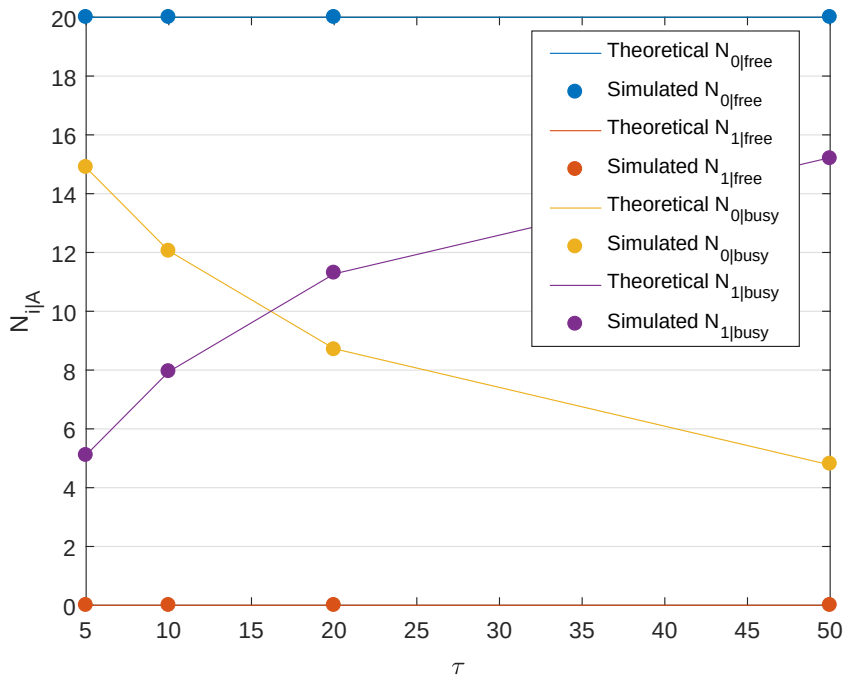

Figure 32. Theoretical vs simulated comparison of $N_{i|s_N}$ with $N = 20$, $\rho = 50$, $\tau \in \{5, 10, 20, 50\}$.

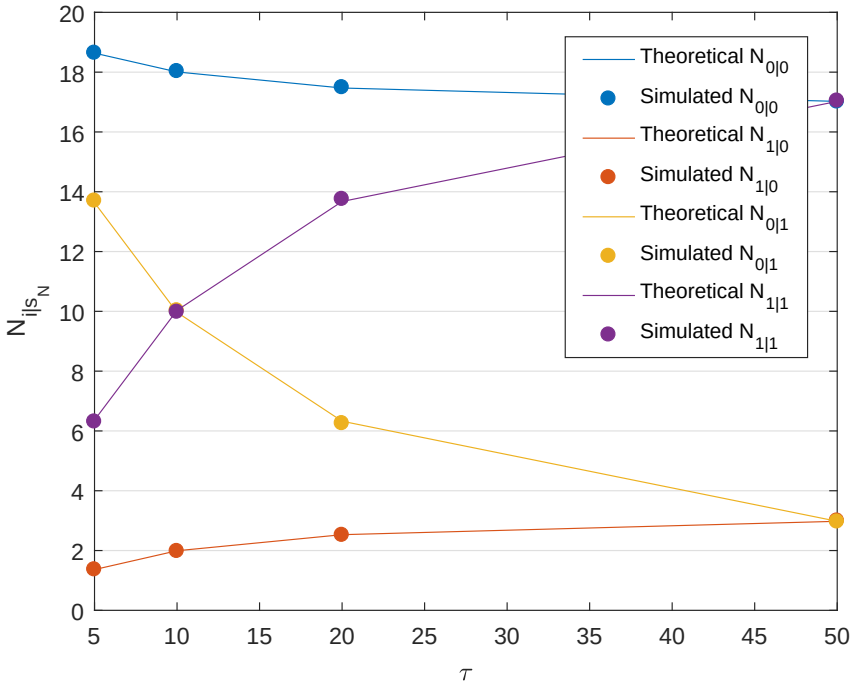

Figure 33. Theoretical vs simulated comparison of $N_{i|A}$ with $N = 20$, $\rho = 50$, $\tau \in \{5, 10, 20, 50\}$.

CHAPTER 5

DYNAMIC PRIMARY USERS SENSING PERFORMANCE

In this chapter analytical expressions for the probabilities of detection $\mathcal{P}_d$ and false alarm $\mathcal{P}_f$ are derived in this context of the PU activity model described in Chapter 4. The expressions for $\mathcal{P}_d$ and $\mathcal{P}_f$ take into account all potential changes in the PU signal. This analysis incorporates the $\mathcal{P}_d$ and $\mathcal{P}_f$ expressions corresponding to the static scenario when the PU signal does not change during spectrum sensing, along with the influence of the dynamic activity of the PU implied by condtional probabilities derived in Chapter 4.

5.1 SPECTRUM SENSING SYSTEM MODEL

We use a similar system model as that presented in Chapter 4 where a PU signal randomly transitions ON and OFF. An SU samples the received signal $r(n)$ where each sample is described by one of the following two possible hypotheses:

$$\begin{aligned} H_0 &\rightarrow \text{PU signal OFF} : r(n) = u(n) \\ H_1 &\rightarrow \text{PU signal ON} : r(n) = s(n) + u(n), \end{aligned} \tag{79}$$

where $u(n)$ is the white Gaussian noise with zero mean and variance σ_u^2 corrupting the signal at the SU receiver. Again,the PU signal $s(n)$ can be real or complex and has variance σ_s^2.

In Chapter 4 a energy detector was considered when describing the PU activity in context to the dynamic PU hypotheses. This was done for clarity and the probabilities and distributions presented in Chapter 4 are independent of the type of sensing technique used. In contrast, the work presented in this chapter is reliant on the SU employing a specific energy detector. Here the SU employs an energy detector to sum the square of each of the N samples in the sensing period [14]

$$Y(N) = \sum_{n=1}^{N} \left| \frac{r(n)}{\sigma_u} \right|^2 . \tag{80}$$

We note that there is an energy detector variant described commonly in CR research which divides the sum of the squares by N, i.e. $(1/N)\sum_{n=1}^{N}|r(n)|^2$, often referred to as a variance estimator. We specifically do not use a variance estimator as will become apparent later in this chapter. The energy detector in (80) also divides each of the squared received samples by the noise variance σ_u^2, thus normalizing the signal $r(n)$. This is done to take advantage of the chi-squared distribution which arises from the sum of the squares of independent standard normal random variables and the noncentral chi-squared distribution which arises from the sum of the squares of independent normal random variables with non-zero means and unit variance [43].

The output of the energy detector $Y(N)$ forms a test statistic which is used to distinguish between two hypotheses. In the next sections we will describe the test statistic distribution with a static PU followed by a derivation of the test statistic distribution under a dynamic PU.

5.2 STATIC PRIMARY USER DETECTION PERFORMANCE

The performance of energy detector with dynamic PU is analyzed in the context of Neyman-Pearson detection theorem where the spectrum sensing decision of the SU maximizes the probability of detection of an active PU for a given probability of false alarm using a likelihood ratio test [43]. Under the assumption that the PU is static and its signal does not change during the entire N sample sensing interval, the energy detector test statistic $Y(N)$ as derived in Chapter 4 is then,

$$Y(N) = \begin{cases} \displaystyle\sum_{n=1}^{N}\left|\frac{u(n)}{\sigma_u}\right|^2, & H_0 \\ \displaystyle\sum_{n=1}^{N}\left|\frac{s(n)+u(n)}{\sigma_u}\right|^2, & H_1. \end{cases} \tag{81}$$

Taking advantage of the specific energy detector defined in (80) the distibutions under H_0 and H_1 follow respectively a chi-squared and noncentral chi-squared distribution [14],

$$Y(N) \sim \begin{cases} \chi_N^2, & H_0 \\ \chi_N^2(N\gamma), & H_1, \end{cases} \tag{82}$$

where χ_N^2 and $\chi_N^2(\cdot)$ denote the central and noncentral chi-squared distributions with N degrees of freedom and a non-centrality parameter implied by the PU SNR at the SU receiver $\gamma = \sigma_s^2/\sigma_u^2$

when the PU is active. The density function corresponding to the test statistic in (82) observed for a time interval $t \to \infty$ is therefore

$$f_Y = \overline{\mathcal{P}_X} \cdot \chi^2_N + \mathcal{P}_X \cdot \chi^2_N(N\gamma) \tag{83}$$

where $\mathcal{P}_X$ is the duty cycle of the PU as described Chapter 3. We note that f_Y is a mixture model which we will discuss in further detail in the next section.

The performance of the energy detector in this static PU scenario, is given by the corresponding probabilities of detection and false alarm, respectively, [14, 15],

$$\begin{aligned} \mathcal{P}_d(\lambda, N) &= Pr\{Y(N) > \lambda | H_1\} \\ &= \int_\lambda^\infty \chi^2_N(N\gamma) \\ &= Q_N(\sqrt{2N\gamma}, \sqrt{\lambda}) \end{aligned} \tag{84}$$

$$\begin{aligned} \mathcal{P}_f(\lambda, N) &= Pr\{Y(N) > \lambda | H_0\} \\ &= \int_\lambda^\infty \chi^2_N \\ &= \frac{\Gamma(N, \lambda/2)}{\Gamma(N)}, \end{aligned} \tag{85}$$

where $\Gamma(\cdot)$ and $\Gamma(\cdot, \cdot)$ are complete and incomplete gamma functions, respectively, $Q_N(\cdot, \cdot)$ is the generalized Marcum Q-function, and λ is the sensing threshold, which is determined from a target $\mathcal{P}_f$ value according to [43, Ch. 5]. We note that the use of a Gaussian approximation discussed in [7] is not applicable in this case as this approximation assumes a large number of samples N in the sensing interval, and we intentionally do not want to place such a restriction on N.

5.3 DYNAMIC PRIMARY USER MIXTURE MODELS

Because of the presence of the dynamic PU we have to revise the distribution of the test statistic to include the fact that the PU signal may be both ON and OFF during the sensing period. A mixture distribution is well suited to this problem. Generally described, a mixture distribution is

a probability density function of the form

$$f(x) = \sum_{k=1}^{K} \alpha_k f(x; \theta_k). \tag{86}$$

Here, K is the number of components in the mixture model. For each k, $f(x; \theta_k)$ is the distribution function of component number k. The scalar α_k is the weight of the component number k. In order for the mixture model to be a proper distribution function, it must be the case that $\sum_k \alpha_k = 1$.

If the PU is dynamic and can be both OFF and ON during a single sampling period, the distribution of $Y(N)$ is dependent on the cumulative number of samples where the PU is ON during a sensing period, x. Therefore, the test statistic for a single sensing interval with a dynamic PU becomes

$$Y(N) \sim \begin{cases} \chi^2_N, & x = 0 \\ \chi^2_N(\gamma), & x = 1 \\ \quad \cdots & \\ \chi^2_N(N\gamma), & x = N. \end{cases} \tag{87}$$

We note that in each case there are N degrees of freedom corresponding to the N samples, but the non-centrality parameter of the corresponding chi-squared distribution depends on the number of samples where the PU was active during the sensing interval. The density function corresponding to the test statistic in (87) observed for a time interval $t \to \infty$ is therefore

$$f_Y = \sum_{x=0}^{N} \Phi_x \cdot \chi^2_N(x\gamma), \tag{88}$$

where Φ_x are the component weights as calculated in (55).

The distribution in (88) is a chi-squared mixture model with $N + 1$ components. Figure 34 illustrates two distinct example chi-squared mixture models. Both mixtures contain five components corresponding to $N = 4$ and have equal compontent weights. Figure 34(a) has a PU signal SNR at the SU receiver $\gamma = 6dB$ while Figure 34(b) has a much lower SNR of $\gamma = -3dB$. As illustrated, when γ is reduced the distributions of the individual components become difficult to distinguish.

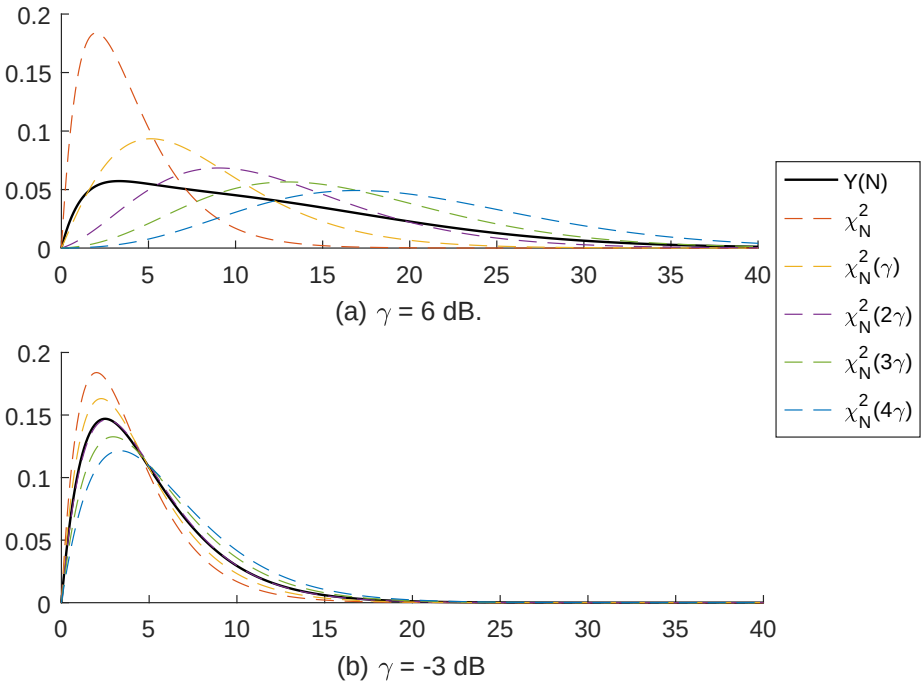

Figure 34. Examples of mixed chi-squared distributions with $N = 4$, weights $\mathbf{\Phi} = \{0.2, 0.2, 0.2, 0.2, 0.2\}$, and (a) $\gamma = 6dB$, (b) $\gamma = -3dB$.

5.4 ANY SAMPLE HYPOTHESES DETECTION PERFORMANCE

In this section we use the chi-squared mixture model for the dynamic PU test statistic in (88) and apply it to the hypotheses H_{free} and H_{busy} described in Chapter 4. Again, H_{free} corresponds to a PU that is OFF during the entire sensing duration and H_{busy} corresponds to a PU that is ON at one or more samples during a sensing period. The dynamic PU test statistic corresponding to the hypotheses is

$$Y(N) \sim \begin{cases} \chi^2_N, & H_{free} \\ \sum_{x=1}^{N} \Phi_{x|b} \cdot \chi^2_N(x\gamma), & H_{busy} \end{cases} \tag{89}$$

where we substituted $\Phi_{x|b}$ for $\Phi_{x|busy}$ for readability. Here, the test statistic for H_{free} is equivalent to H_0 when considering a static PU. The test statistic for $Y(N)$ under H_{busy} is comprised of N components where the component weights are $\Phi_{x|busy}$ defined in (65). We can now calculate the

probability of detection using the distribution for $Y(N)$ under H_{busy} leveraging the expression for $\mathcal{P}_d$ assuming a static PU in (84)

$$\begin{aligned}\mathcal{P}_d &= Pr\{Y(N) > \lambda | H_{busy}\} \\ &= \sum_{x=1}^{N} \Phi_{x|b} \int_{\lambda}^{\infty} \chi^2_N(x\gamma) \\ &= \sum_{x=1}^{N} \Phi_{x|b}\, Q_N(\sqrt{2x\gamma}, \sqrt{\lambda}).\end{aligned} \tag{90}$$

We note that because the test statistic $Y(N)$ under H_{free} is the same as $Y(N)$ under the static H_0. Therefore, the probability of false alarm $\mathcal{P}_f$ under is H_{free} is equivalent to that under H_0 in (85).

With a large number of components, corresponding to longer sensing periods, the distribution under H_{busy} is complex, so we also consider an approximate test statistic $\widetilde{Y}(N)$ which utilizes the conditional value of N, $N_{i|A}$ defined in (70). The approximate test statistic is then

$$\widetilde{Y}(N) \sim \begin{cases} \chi^2_N, & H_{free} \\ \chi^2_N\left(N_{1|b}\,\gamma\right), & H_{busy} \end{cases} \tag{91}$$

where we have substituted the nomenclature $N_{1|b}$ for $N_{1|busy}$ for readability. The test statistic for $\widetilde{Y}(N)$ under H_{busy} is no longer a mixture model but instead a single noncentral chi-square distribution where the non-centrality parameter is determined by SNR γ and the expected number of samples the PU will be ON in a sensing period under the hypothesis H_{busy}. The expression for $\widetilde{\mathcal{P}_d}$ using the approximate distribution $\widetilde{Y}(N)$ under H_{busy} is then,

$$\begin{aligned}\widetilde{\mathcal{P}_d} &= Pr\{\widetilde{Y}(N) > \lambda | H_{busy}\} \\ &= \int_{\lambda}^{\infty} \chi^2_N(N_{1|b}\,\gamma) \\ &= Q_N\left(\sqrt{2\,N_{1|b}\,\gamma}, \sqrt{\lambda}\right)\end{aligned} \tag{92}$$

Again, the distribution of $\widetilde{Y}(N)$ under H_{free} is the same as $Y(N)$ under the static H_0. Therefore, the probability of false alarm $\widetilde{\mathcal{P}_f}$ under H_{free} is equivalent to that under H_0 in (85).

5.5 N$^{\text{TH}}$ SAMPLE HYPOTHESES DETECTION PERFORMANCE

Like the previous section, this section utilizes the chi-squared mixture model for the dynamic PU test statistic in (88) but instead considers the hypotheses H_{N0} and H_{N1} described in Chapter 4. Again, H_{N0} corresponds to the PU being OFF at the end of the sensing period and H_{N1} corresponds to a PU that is ON at the end of the sensing period. The test statistic $Y(N)$ for both H_{N0} and H_{N1} has samples that are both OFF and ON and therefore is similar to $Y(N)$ for H_{busy} in (89)

$$Y(N) \sim \begin{cases} \sum_{x=0}^{N-1} \Phi_{x|0} \cdot \chi^2_N(x\gamma), & H_{N0} \\ \\ \sum_{x=1}^{N} \Phi_{x|1} \cdot \chi^2_N(x\gamma), & H_{N1}. \end{cases} \tag{93}$$

The resulting distributions are again chi-squared mixtures where the mixture weights are $\Phi_{x|s_N}$ provided in (74). The corresponding probabilities of detection and false alarm are respectively,

$$\begin{aligned} \mathcal{P}_d &= Pr\{Y(N) > \lambda | H_{N1}\} \\ &= \sum_{x=1}^{N} \Phi_{x|1} \int_{\lambda}^{\infty} \chi^2_N(x\gamma) \\ &= \sum_{x=1}^{N} \Phi_{x|1}\, Q_N\left(\sqrt{2x\gamma}, \sqrt{\lambda}\right). \end{aligned} \tag{94}$$

$$\begin{aligned} \mathcal{P}_f &= Pr\{Y(N) > \lambda | H_{N0}\} \\ &= \sum_{x=1}^{N} \Phi_{x|0} \int_{\lambda}^{\infty} \chi^2_N(x\gamma) \\ &= \sum_{x=1}^{N} \Phi_{x|0}\, Q_N(\sqrt{2x\gamma}, \sqrt{\lambda}). \end{aligned} \tag{95}$$

We again consider an approximate test statistic $\widetilde{Y}(N)$ which utilizes the conditional value of

N, $N_{i|s_N}$ defined in (78). The approximate test statistic is then

$$\widetilde{Y}(N) \sim \begin{cases} \chi^2_N\left(N_{1|0}\,\gamma\right), & H_{N0} \\ \\ \chi^2_N\left(N_{1|1}\,\gamma\right), & H_{N1} \end{cases} \tag{96}$$

The performance of the energy detector with a dynamic PU evaluated using the test statistic $\widetilde{Y}(N)$ that follows the mixture distribution (96) is implied by the respective probabilities of detection and false alarm expressions

$$\begin{aligned} \widetilde{\mathcal{P}_d} &= Pr\{\widetilde{Y}(N) > \lambda | H_{N1}\} \\ &= \int_{\lambda}^{\infty} \chi^2_N(N_{1|1}\,\gamma) \\ &= Q_N\left(\sqrt{2\,N_{1|1}\,\gamma}, \sqrt{\lambda}\right) \end{aligned} \tag{97}$$

$$\begin{aligned} \widetilde{\mathcal{P}_f} &= Pr\{\widetilde{Y}(N) > \lambda | H_{N0}\} \\ &= \int_{\lambda}^{\infty} \chi^2_N(N_{1|0}\,\gamma) \\ &= Q_N\left(\sqrt{2\,N_{1|0}\,\gamma}, \sqrt{\lambda}\right) \end{aligned} \tag{98}$$

5.6 VERIFICATION OF DYNAMIC SENSING PERFORMANCE

In this section we present numerical results obtained from simulations illustrating receiver operating characteristic (ROC) curves for the energy detector with dynamic PU in various scenarios. Simulated results are compared to theoretical ROC curves implied by the analytical expressions for the probabilities of detection and false alarms. To evaluate the performance degradation implied by the presence of a dynamic PU we have also included in the comparison the ROC curves implied by the analytical expressions of the probabilities of detection and false alarm (84) and (85), which correspond to PU signals that are constant for the entire duration of the sensing window. Each experiment was simulated twice, once considering the dynamic hypotheses H_{free} and H_{busy} and again considering the dynamic hypotheses H_{N0} and H_{N1}.

For the hypotheses H_{free} and H_{busy} simulation results compare:

- Theoretical Constant ROC implied by $\mathcal{P}_d$ (84) and $\mathcal{P}_f$ (85)
- Theoretical Dynamic ROC implied by $\mathcal{P}_d$ (90) and $\mathcal{P}_f$ (85)
- Approximate Dynamic ROC implied by $\widetilde{\mathcal{P}_d}$ (92) and $\mathcal{P}_f$ (85)
- Simulated Dynamic ROC.

For the hypotheses H_{N0} and H_{N1} simulation results compare:

- Theoretical Constant ROC implied by $\mathcal{P}_d$ (84) and $\mathcal{P}_f$ (85)
- Theoretical Dynamic ROC implied by $\mathcal{P}_d$ (94) and $\mathcal{P}_f$ (95)
- Approximate Dynamic ROC implied by $\widetilde{\mathcal{P}_d}$ (97) and $\widetilde{\mathcal{P}_f}$ (98)
- Simulated Dynamic ROC.

The simulated PU activity consisted of a 4-QAM modulated signal with an amplitude equivalent to the square root of the signal variance σ_s as implied by the specified SNR γ and a variance of 1 for the AWGN. The first two simulations compare the output of the energy detector to the threshold λ implied by the target $\mathcal{P}_f$ values which ranged from .01 to 1. The simulation considered $100,000$ sensing intervals, each with $N = 20$ samples.

The first simulation examined the impact of the SNR on the performance of the energy detector with a dynamic PU. We considered a dynamic PU characterized by average values $\rho = 50$, and $\tau = 10$ for the OFF and ON periods, respectively, and for SNR values $\gamma = 0$, -6, -12dB. The results utilizing the hypotheses H_{free} and H_{busy} are shown in Figure 35. We can see that the simulated ROC results for the dynamic PU closely match the theoretical dynamic PU ROC for all values of γ. Additionally, the simulated and approximate ROCs closely matches for $\gamma = -6$ and -12 dB. However, for $\gamma = 0$ the approximated ROC is no longer accurate. Finally, as expected the theoretical constant PU ROC and the various dynamic PU ROCs diverge as the SNR increases. The results of the first simulation considering the hypotheses H_{N0} and H_{N1} are shown in Figure 36. Here again the simulated ROC closely matches the theoretical dynamic PU ROC for all values of γ. As with the hypotheses H_{free} and H_{busy} in Figure 35, the approximated ROC is not a good fit at $\gamma = 0$ but is a good approximate at lower SNRs.

In the second experiment we examined the impact of the average duration of the dynamic PU activity on the performance of the energy detector. Specifically, we take the SNR $\gamma = -6$ dB and the average duration of the PU OFF period of $\rho = 50$ and consider average ON periods of $\tau = 5$, 25, and 50. These results considering the hypothesis H_{free} and H_{busy} are shown in Figure 37. The figure shows that the simulated results match the theoretical and approximate ROCs for PU activity levels examined; however, the approximated ROC does slightly diverge as the value of τ increases. Finally, as expected the theoretical constant PU ROC and the various dynamic PU ROCs diverge as the value of τ decreases. The results for the second experiment utilizing the hypotheses H_{N0} and H_{N1} are shown in Figure 38 and results similar to those for H_{free} and H_{busy} in Figure 37 can be seen.

5.7 CHAPTER SUMMARY

In this chapter we studied the performance of energy detector for spectrum sensing by SU in scenarios with a dynamic PU that switch from active to idle randomly during spectrum sensing. Building up, the two-state Markov chain PU activity developed in Chapter 4 we considered the probability of each possible evolution of these model to establish closed-form expressions for the probabilities of detection and false alarm using mixtures of chi-squared distributions for the energy detector test statistic. The expressions obtained for the single PU scenario examined are corroborated with numerical simulations results. Thus, if the characteristics of the dynamic PU activity, implied by parameters ρ, τ, and γ, are known, then the SU can accurately predict the performance of the energy detector. In the next chapter we propose the use of an incremental EM algorithm to estimate the energy detector performance when ρ, τ, and γ are unknown to the SU.

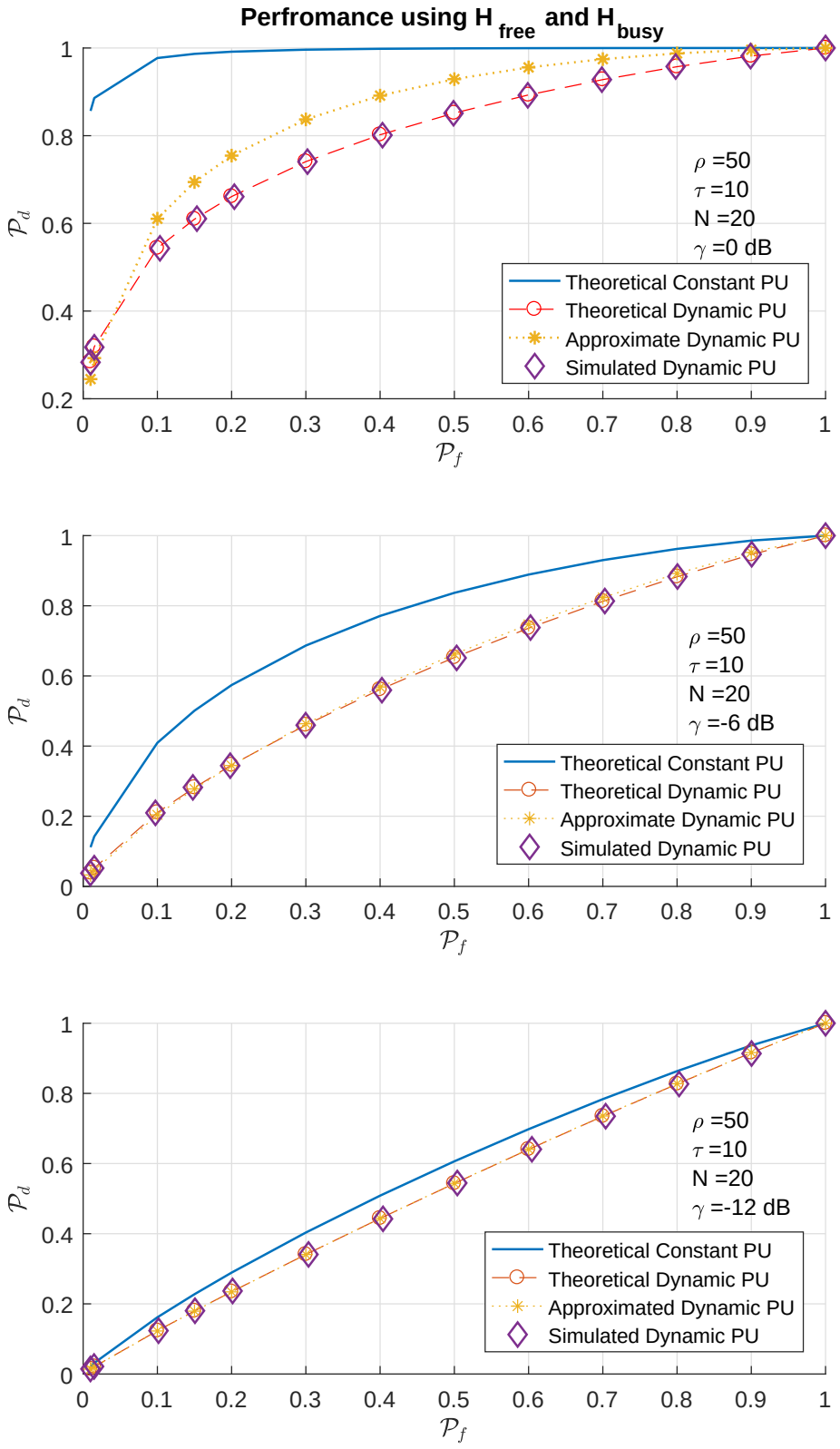

Figure 35. H_{free} and H_{busy} dynamic PU ROC with $\rho = 50$,$\tau = 10$, $N = 20$ and SNR values (a) $\gamma = 0$dB, (b) $\gamma = -6$dB, and (c) $\gamma = -12$dB.

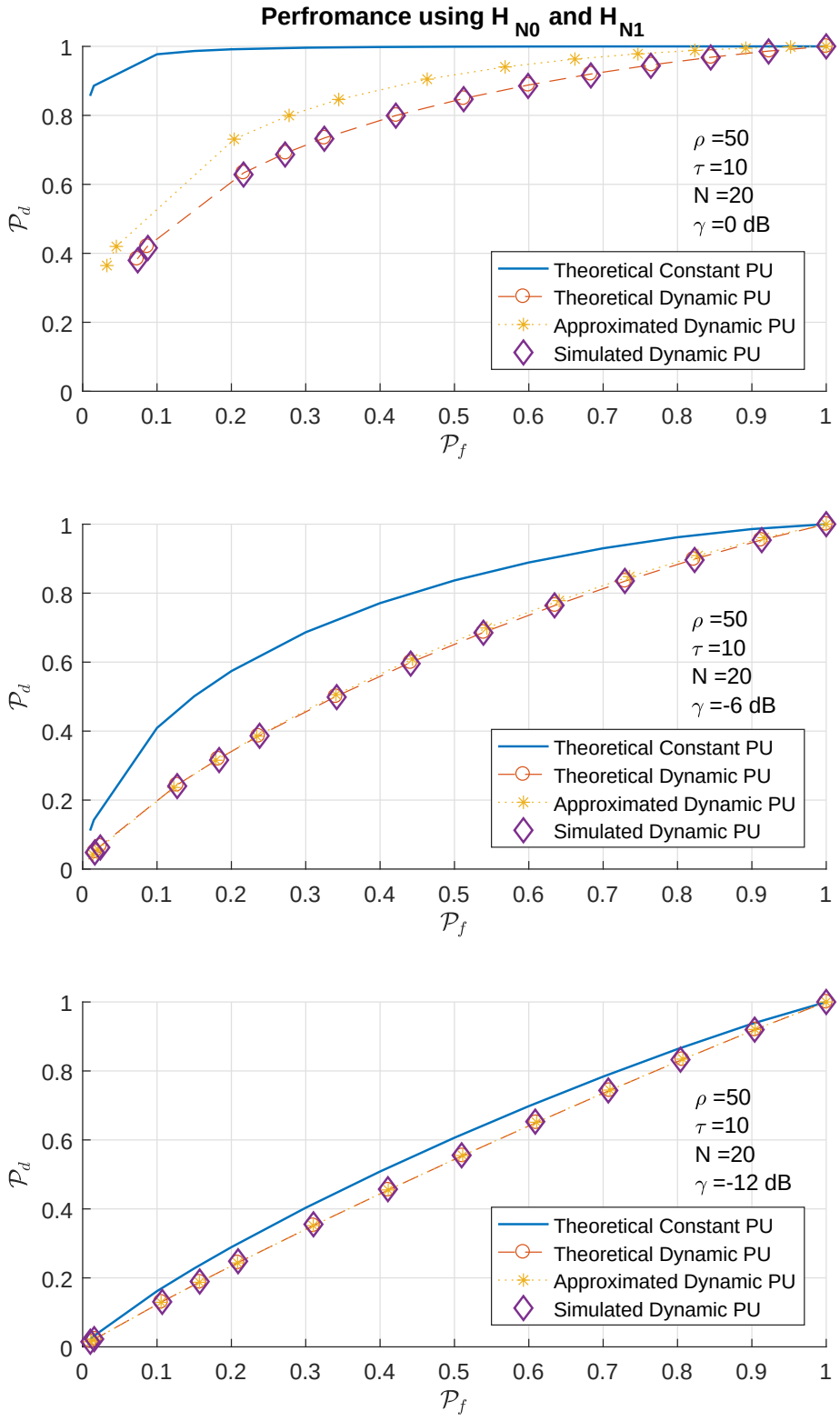

Figure 36. H_{N0} and H_{N1} dynamic PU ROC with $\rho = 50$,$\tau = 10$, $N = 20$ and SNR values (a) $\gamma = 0$dB, (b) $\gamma = -6$dB, and (c) $\gamma = -12$dB.

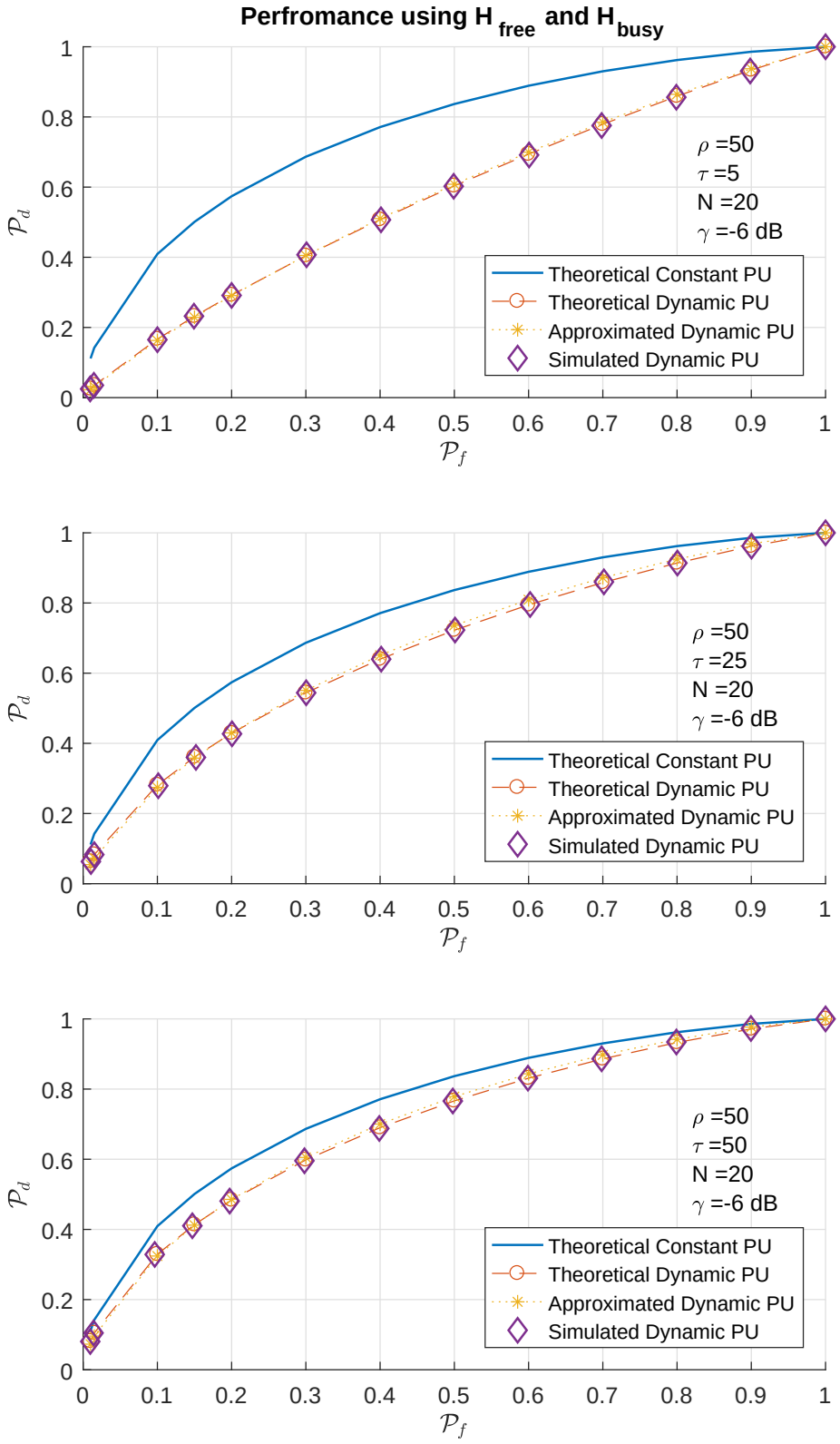

Figure 37. H_{free} and H_{busy} dynamic PU ROC with $\rho = 50$,$\tau = 10$, $N = 20$ and SNR values (a) $\gamma = 0$dB, (b) $\gamma = -6$dB, and (c) $\gamma = -12$dB.

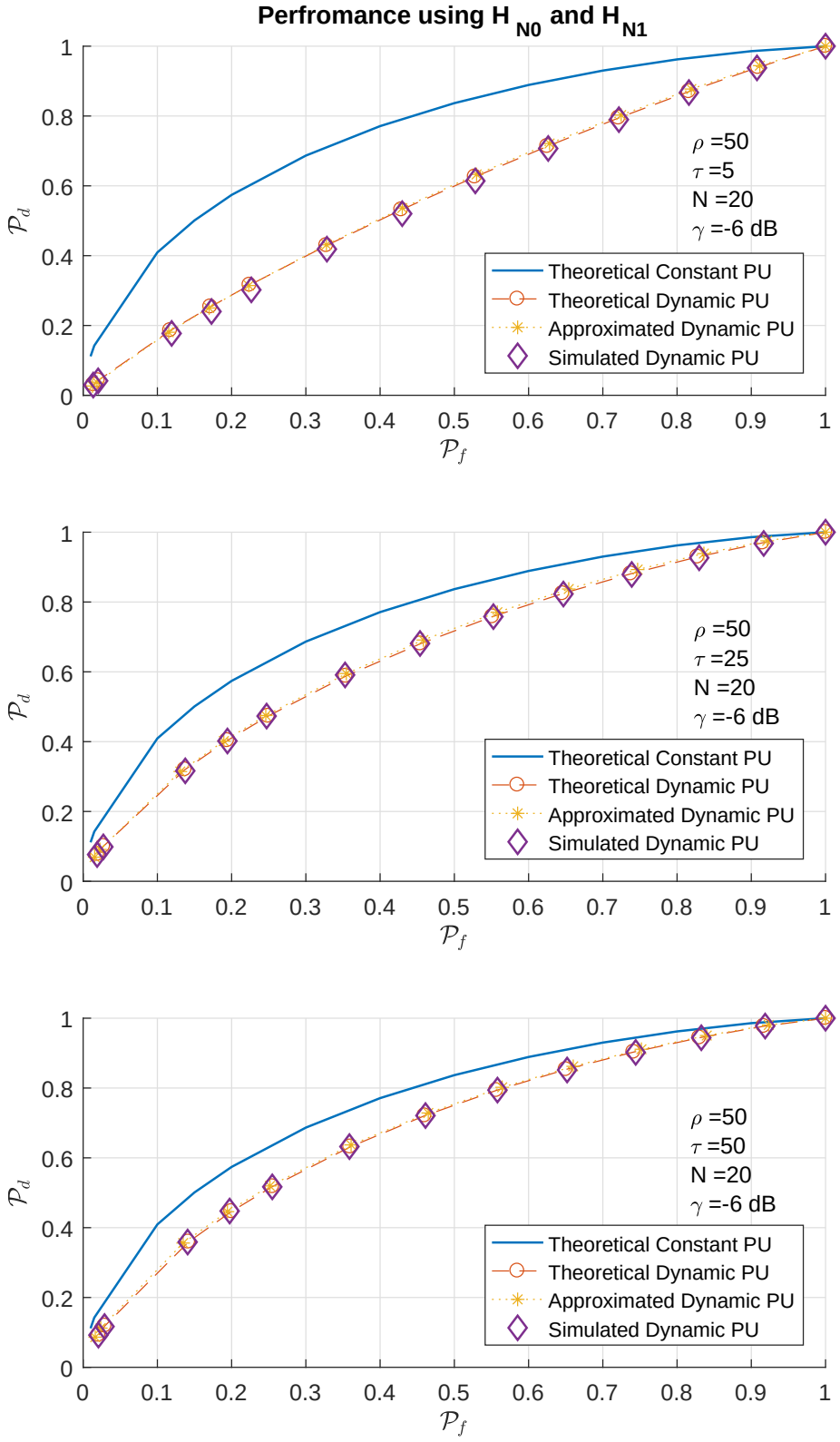

Figure 38. H_{N0} and H_{N1} dynamic PU ROC with $\rho = 50$,$\tau = 10$, $N = 20$ and SNR values (a) $\gamma = 0$dB, (b) $\gamma = -6$dB, and (c) $\gamma = -12$dB.

CHAPTER 6

ESTIMATING SENSING PERFORMANCE

In Chapter 4 we used a two-state Markov chain to model the dynamic activity of a PU. The verified PU activity model was used to establish a chi-squared mixture model for the energy detector output and in Chapter 5 closed-form expressions were derived and verified for SU sensor performance statistics $\mathcal{P}_d$ and $\mathcal{P}_f$ in the context of the dynamic PU activity. The expressions for sensor performance are derived from the parameters limiting the dynamic PU activity, specifically the mean PU ON and OFF durations respectively τ and ρ, and the SNR of the PU signal at the SU receiver γ. In this chapter we consider an SU that does not have knowledge of the dynamic PU activity parameters or SNR. We develop a novel incremental expectation maximization (EM) algorithm to estimate the chi-squared mixture parameters from a set of energy detector observations.

6.1 PERFORMANCE ESTIMATION SYSTEM MODEL

We consider a dynamic PU with the activity model described in Chapter 4 where the PU switches between idle and active randomly with an average idle period of ρ and an average active period of τ. The SU employs the energy detector described in detail in Chapter 5 to formulate a test statistic $Y(N)$,

$$Y(N) = \sum_{n=1}^{N} \left| \frac{r(n)}{\sigma_u} \right|^2. \tag{99}$$

In the case of a dynamic PU the distribution of $Y(N)$ is a mixed chi-squared distribution as derived in Chapter 5,

$$f_Y = \sum_{x=0}^{N} \Phi_x \cdot \chi^2_N(x\gamma). \tag{100}$$

We assume that the SU does not know the extent to which the PU is dynamic and our goal is to determine analytical expressions for $\mathcal{P}_d$ and $\mathcal{P}_f$ that take into account the volatility of the PU

signal. This is accomplished by first observing the output of the energy detector over M sensing periods.

6.2 INCREMENTAL EXPECTATION MAXIMIZATION ALGORITHM

The goal of the EM algorithm is to estimate unknown parameters of a probability distribution function from a set of observations [44]. The EM algorithm is often used for Gaussian mixture models where the unknown parameters are the component weights as well as the mean and variance for each distribution. We note that the chi-square mixture in (100) describing the activity of the dynamic PU is similar to a Gaussian mixture with the following distinctions:

- The distribution $f_{Y_0} = \chi^2_N$ and has mean and variance equal to N and $2N$, respectively.
- The remaining distributions $f_{Y_x} = \chi^2_N(x\gamma)$, have mean $N + x\gamma$ and variance $2N + 4x\gamma$, for $x = 1, \ldots, N$.

Thus, instead of finding the mean and variance of each distribution, as is done in the case of Gaussian mixtures, only the SNR γ and the component weights in $\mathbf{\Phi}$ need to be estimated.

The standard EM algorithm has three steps: initial parameter estimation, expectation, and maximization. The algorithm iterates between the expectation and maximization steps until it converges on a solution. We note that, in general, the EM algorithm converges to a local optimum rather than the global one, and its performance can be poor when the number of components in the mixture is large. However, for low values of the SNR γ a larger N can increase distance between the means of χ^2_N and $\chi^2_N(N\gamma)$ and provides a better estimate for γ. Thus, we propose a incremental EM algorithm in which the distribution in (100) is approximated by $f_Y^{(L)}$ that includes only a subset $x^{(L)}$ of components. With each increment, more components are added until the full set of $N + 1$ components are used,

$$\begin{aligned} f_Y^{(L)} &= \sum_{x^{(L)}} \Phi_x \chi^2_N(x\gamma), && x^{(L)} \subset x^{(L-1)} \\ &\ldots \\ f'_Y &= \sum_{x'} \Phi_x \chi^2_N(x\gamma), && x' \subset x \\ f_Y &= \sum_{x} \Phi_x \chi^2_N(x\gamma), && x = \{0, 1, \ldots N\}. \end{aligned} \tag{101}$$

With this incremental approach the solution from one increment provides the initial parameter

estimation for the next increment. The solution from the final increment, which includes all components, is the full solution.

We note that the incremental EM algorithm performs better than a standard EM algorithm that has one increment containing all the components, since the incremental solution avoids convergence to a local optimum by gradually adding components. We note that the proposed algorithm is similar to the incremental component splitting algorithm proposed in [45] in which for each increment a component is split and variational update equations are applied only to the parameters of the two components resulting from the split. In contrast, the proposed algorithm applies variational update equations to the full set of components in each increment.

This approach is illustrated in Figure 39, for a mixture with $N = 10$ components: the first increment of the EM algorithm is denoted by f_Y'' and is composed of three components, χ^2_{10}, $\chi^2_{10}(5\gamma)$, and $\chi^2_{10}(10\gamma)$; the second increment is denoted by f_Y' and is composed of the original three components plus two additional ones, $\chi^2_{10}(3\gamma)$, and $\chi^2_{10}(8\gamma)$; the final increment includes all eleven components. In the next section we formally describe the three steps of the incremental EM algorithm.

6.2.1 INITIAL PARAMETER ESTIMATION

The initial parameter estimation step is different for the first increment than for subsequent increments. For the first increment the initial estimate for component weights, $\hat{\mathbf{\Phi}}_x \forall x \in x^{(L)}$, should leverage any a priori knowledge of the PU parameters ρ and τ. If there is no a priori knowledge of PU activity the component weight estimates can be initialized to equal values; if this is done the number of components in $x^{(L)}$ should be minimized to improve performance, i.e $x^{(L)} = \{0, N/2, N\}$.

After determining the initial component weight estimates, and estimated SNR $\hat{\gamma}$ can be determined as

$$\hat{\gamma} = \frac{\mu - N}{\sum_{x^{(L)}} x\, \hat{\Phi}_x}, \tag{102}$$

where μ is the sample mean of the M observations and is approximated by

$$\begin{aligned} \mu &\approx \hat{\Phi}_0\hat{\mu}_0 + \hat{\Phi}_1\hat{\mu}_1 + \ldots \hat{\Phi}_N\hat{\mu}_N \\ &\approx \hat{\Phi}_0 N + \hat{\Phi}_1(N + \hat{\gamma}) + \ldots \hat{\Phi}_N(N + N\hat{\gamma}) \\ &\approx N(\hat{\Phi}_0 + \hat{\Phi}_1 + \ldots \hat{\Phi}_N) + \hat{\gamma}((\hat{\Phi}_1 + 2\hat{\Phi}_2 + \ldots N\hat{\Phi}_N)). \end{aligned} \tag{103}$$

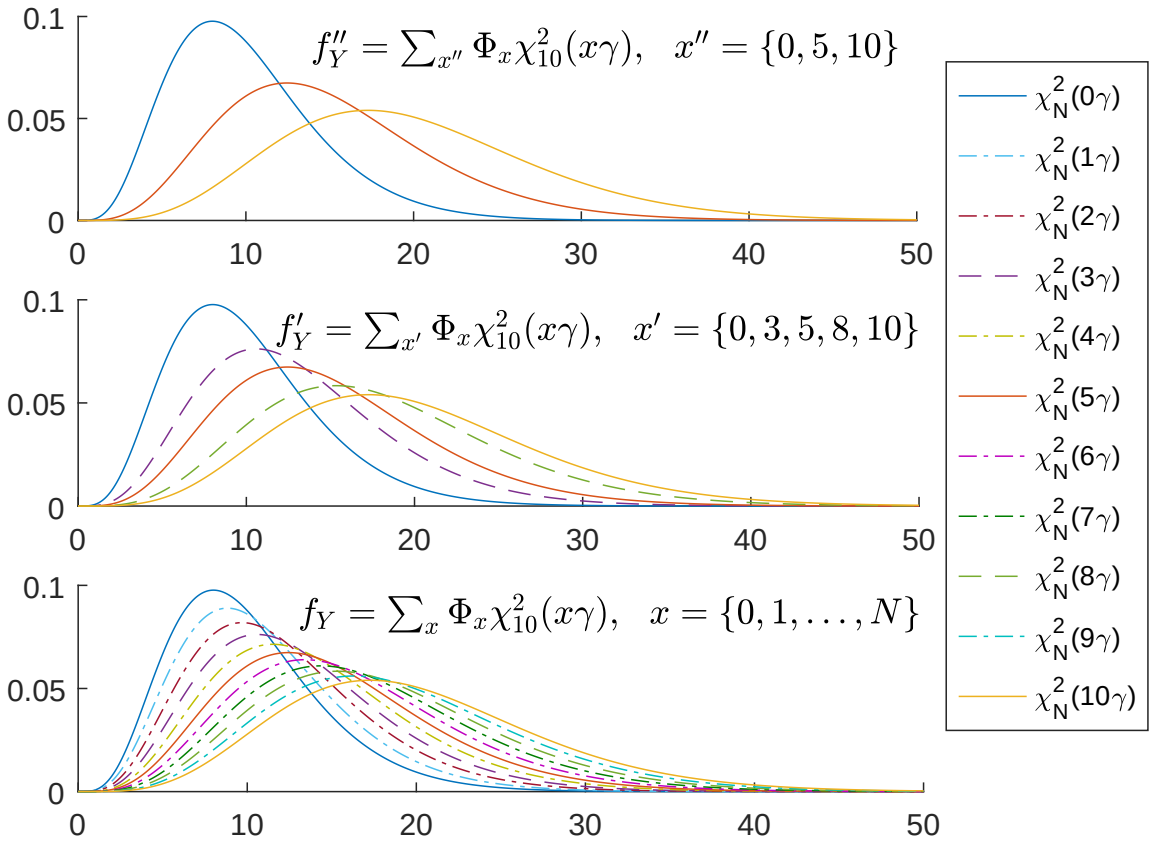

Figure 39. Illustrating different subsets of a chi-squared distribution with a total of $N = 10$ components.

In subsequent increments the solutions from the prior increment are used as an initial parameter estimate. Both the γ and component weights are used as initial parameters. The weights for the components added to the increment are set to ≈ 0.

6.2.2 EXPECTATION

The expectation step uses the same process for all increments. Using the initial parameter estimates for the increment, individual distributions $f_{\hat{Y}_x}$ are formed as well as the appropriate mixture distribution from (101). Partial membership values $\phi_{x,m}$ for each observation y_m are calculated as

$$\phi_{x,m} = \frac{\hat{\Phi}_x f_{\hat{Y}_x}(y_m)}{f_{\hat{Y}}(y_m)} \quad \forall\, x \in x^{(l)}. \tag{104}$$

The partial membership value $\phi_{x,m}$ is the probability that observation y_m is a member of, or generated by distribution $f_{\hat{Y}_x}$, therefore $\sum_{x^{(l)}} \phi_{x,m} = 1$.

6.2.3 MAXIMIZATION

Like the expectation step, the maximization step uses the same process for all increments. Using the partial membership values computed in the expectation step, new estimates for the unknown parameters $\hat{\mathbf{\Phi}}$ and $\hat{\gamma}$ are made. The component weights and means are calculated as with a standard EM algorithm,

$$\hat{\Phi}_x = \frac{1}{M} \sum_{m=1}^{M} \phi_{x,m} \quad \forall\, x \in x^{(l)} \tag{105}$$

$$\hat{\mu}_x = \frac{\sum_{m=1}^{M} \phi_{x,m} y_m}{\sum_{m=1}^{M} \phi_{x,m}} \quad \forall\, x \in x^{(l)}. \tag{106}$$

We then take advantage of the fact that we know $\mu_0 = N$ to find an error factor,

$$\epsilon = N - \mu_0. \tag{107}$$

The error factor ϵ is used to calculate a new estimate for γ,

$$\hat{\gamma} = \frac{1}{N} \sum_{x^{(l)}} \frac{\mu_x + \epsilon + N}{x} \tag{108}$$

The new parameter estimates $\hat{\mathbf{\Phi}}$ and $\hat{\gamma}$ are then used in the expectation step to formulate new partial membership values. The expectation and maximizations steps are repeated iteratively until the solutions for $\hat{\mathbf{\Phi}}$ and $\hat{\gamma}$ converge. The converged solutions are either used as input to the next increment or in the case of the final increment are the terminating solutions.

6.3 ESTIMATING PERFORMANCE STATISTICS

The output of the proposed incremental EM algorithm is an vector of estimated chi-squared mixture component weights $\hat{\mathbf{\Phi}}$ and an estimated SNR $\hat{\gamma}$. We use the estimated component weights to then calculate conditional component weights relative to the dynamic PU hypotheses under consideration which are then used to estimate sensing performance.

For the *Any Sample* hypothesis an estimate of $\hat{\Phi}_{x|A}$ using the expression in (65) is calculated using $\hat{\mathbf{\Phi}}$. Using the estimated $\hat{\gamma}$ from the incremental EM algorithm along with the values of $\hat{\Phi}_{x|A}$ we calculate the estimated $\widehat{\mathcal{P}_d}$ leveraging the expression for $\mathcal{P}_d$ in (90),

$$\widehat{\mathcal{P}_d} = \sum_{x=1}^{N} \hat{\Phi}_{x|b}\, Q_N(\sqrt{2x\hat{\gamma}}, \sqrt{\lambda}). \tag{109}$$

For the *Any Sample* hypotheses it is not necessary to estimate $\mathcal{P}_f$ under H_{free} as the test statistic is the same as that of the static PU hypothesis H_0 and is not reliant on γ.

When considering the N^{th} *Sample* hypothesis an estimate of $\hat{\Phi}_{x|s_N}$ using the expression in (74) is calculated using $\hat{\mathbf{\Phi}}$. The values of $\hat{\gamma}$ and $\hat{\Phi}_{x|s_N}$ are used to calculate an estimated $\widehat{\mathcal{P}_d}$ leveraging the expression for $\mathcal{P}_d$ in (94)

$$\widehat{\mathcal{P}_d} = \sum_{x=1}^{N} \hat{\Phi}_{x|1}\, Q_N\left(\sqrt{2x\hat{\gamma}}, \sqrt{\lambda}\right) \tag{110}$$

and an estimated $\widehat{\mathcal{P}_f}$ leveraging the expression for $\mathcal{P}_d$ in (95)

$$\widehat{\mathcal{P}_f} = \sum_{x=1}^{N} \hat{\Phi}_{x|0}\, Q_N(\sqrt{2x\hat{\gamma}}, \sqrt{\lambda}). \tag{111}$$

In the next section we verify the proposed incremental EM algorithm through simulation and compare the estimated values of $\hat{\mathbf{\Phi}}$, $\hat{\gamma}$, and $\widehat{\mathcal{P}_d}$ for the *Any Sample* hypotheses to the known values.

6.4 INCREMENTAL EXPECTATION MAXIMIZATION VERIFICATION

In this section we present results from two simulated experiments that evaluated the incremental EM algorithm in its ability to estimate the component weights of the chi-squared mixture and the γ parameter. For each simulation we used $M = 100,000$ energy detector test statistic observations, each with $N = 20$ samples. Using the incremental EM algorithm the first increment components were $x'' = \{0, 10, 20\}$, the second increment included $x' = \{0, 5, 10, 15, 20\}$, and the final increment utilized all components $x = \{0, 1, \ldots 20\}$. We assumed an initial component weight of $\hat{\Phi}_0 = \hat{\Phi}_{10} = \hat{\Phi}_{20} = \frac{1}{3}$.

The first simulation considered a dynamic PU characterized by average values $\tau = 10$ and $\rho = 50$ and we considered SNR values $\gamma = -12$, -9, -6, -3, and 0 dB. The results of the simulation are shown in Figures 40 through 42. The estimated $\hat{\gamma}$ values for each iteration are shown in Figure 40. Because in each increment the EM algorithm iterates until the solution has converged, the varying simulations require a varying number of iterations. The discontinuities in the curves in Figure 40 occur at the start of an increment when additional components are included. Figure 41 illustrates the final solution for the estimated component weights for the various γ values. From this figure it appears that the incremental EM algorithm provides more accurate values for $\hat{\mathbf{\Phi}}$ at higher γ values. Here we note that the weight $\hat{\Phi}_0$ is overestimated for all γ values and $\hat{\Phi}_{20}$ is consistently overestimated with the exception of $\gamma = 3$ dB. This is assumed to be an artifact of the incremental approach but the results warrant future research. Finally, Figure 42 compares the estimated ROC calculated using (109) to the ROC calculated using (90) and the known dynamic PU parameters τ, ρ, and γ. As shown, the combined estimates of $\hat{\gamma}$ and $\hat{\mathbf{\Phi}}$ result in a good estimation of sensor performance; however, the accuracy of the estimation is reduced when γ is reduced.

The second simulation considered a less dynamic PU characterized by average values $\tau = 50$ and $\rho = 50$ and again considered SNR values $\gamma = -12$, -9, -6, -3, and 0 dB. The results of the simulation are shown in Figure 43 through Figure 45. The estimated $\hat{\gamma}$ values for each iteration are shown in Figure 43. In comparison to the results for the more dynamic PU in Figure 40 the incremental EM results for less dynamic PU is both more accurate and converges more rapidly. Figure 44 illustrates the final solution for the estimated component weights for the various γ values and once again the estimates are superior to those for the more dynamic PU in Figure 41. Like

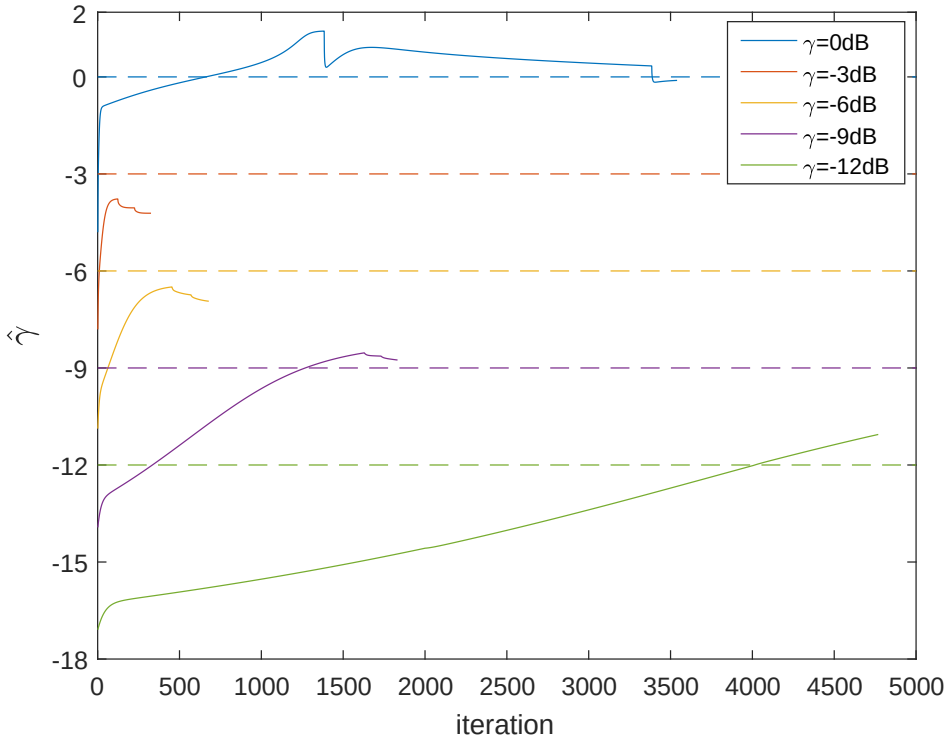

Figure 40. $\hat{\gamma}$ for $N=20$, $\rho=50$, $\tau=10$, and $\gamma=-12$, -9, -6, -3, and 0 dB.

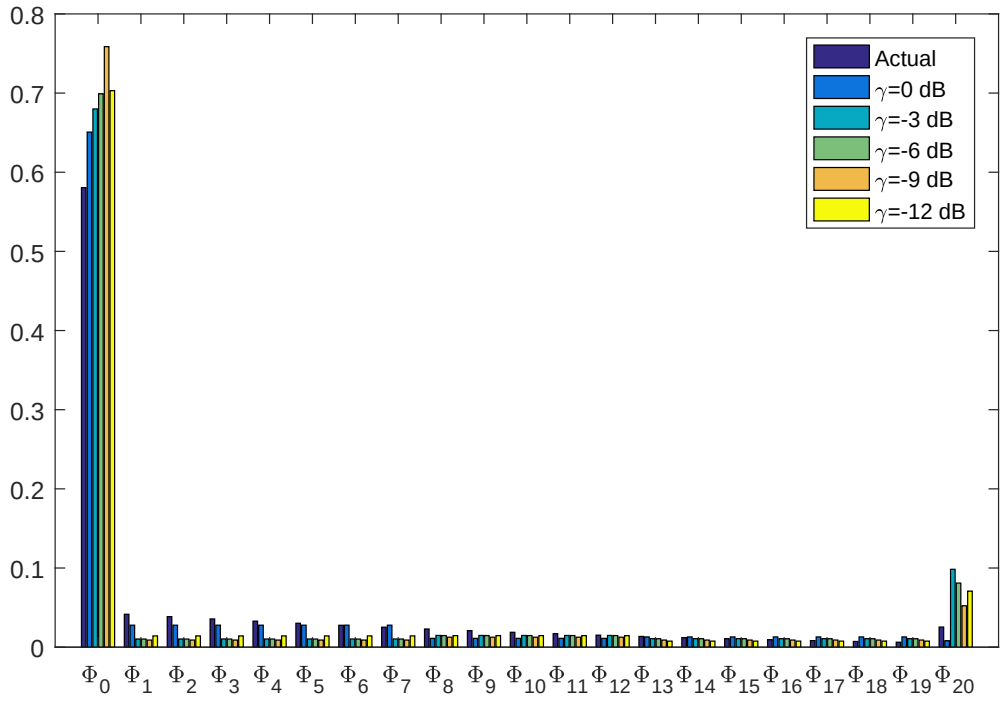

Figure 41. $\hat{\mathbf{\Phi}}$ for $N=20$, $\rho=50$, $\tau=10$, and $\gamma=-12$, -9, -6, -3, and 0 dB.

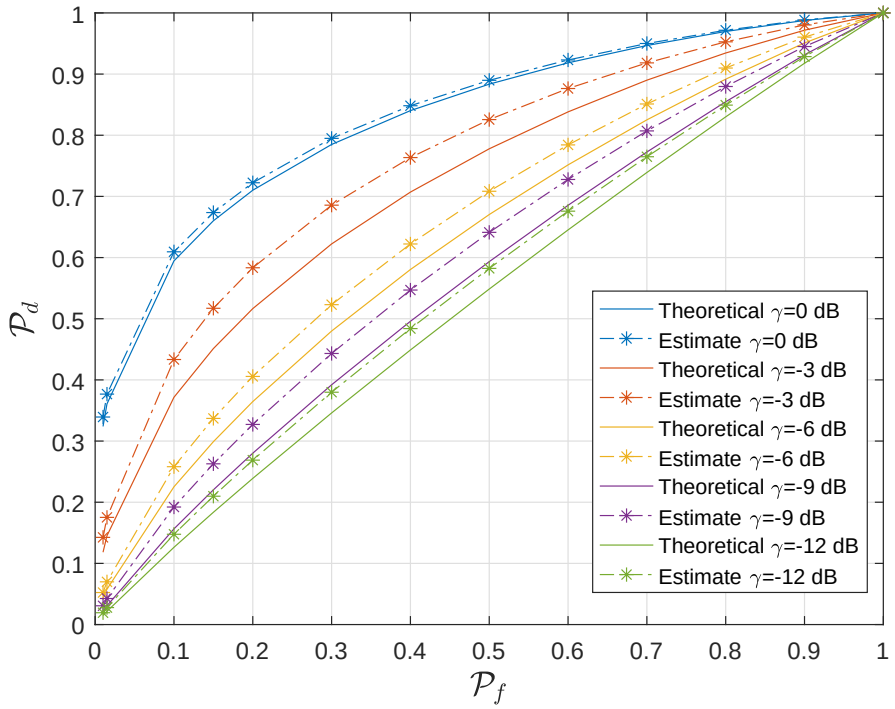

Figure 42. Estimated ROC for for $N = 20$, $\rho = 50$, $\tau = 10$, and $\gamma = -12$, -9, -6, -3, and 0 dB.

the first simulation, the incremental EM algorithm provides more accurate values for $\hat{\mathbf{\Phi}}$ at higher γ values; however in this simulation the weights of $\hat{\Phi}_0$ and $\hat{\Phi}_{20}$ are not consistently overestimated. This is an indication that the superior performance of the second simulation may be an artifact of the initial component weight of $\hat{\Phi}_0 = \hat{\Phi}_{10} = \hat{\Phi}_{20} = \frac{1}{3}$ which are considerably more accurate for the second simulation than the first. Finally, Figure 45 compares the estimated ROC calculated using (109) to the ROC calculated using (90) and the known dynamic PU parameters τ, ρ, and γ. Here, the combined estimates of $\hat{\gamma}$ and $\hat{\mathbf{\Phi}}$ provide an excellent estimation of sensor performance even for low values of γ.

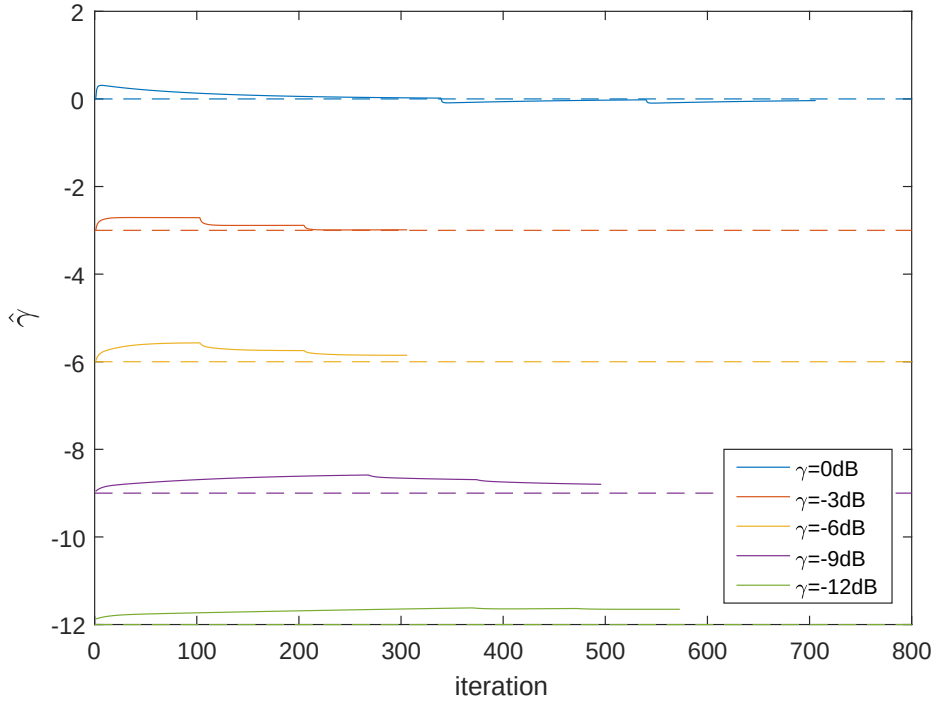

Figure 43. $\hat{\gamma}$ for $N=20$, $\rho=50$, $\tau=50$, and $\gamma=-12$, -9, -6, -3, and 0 dB.

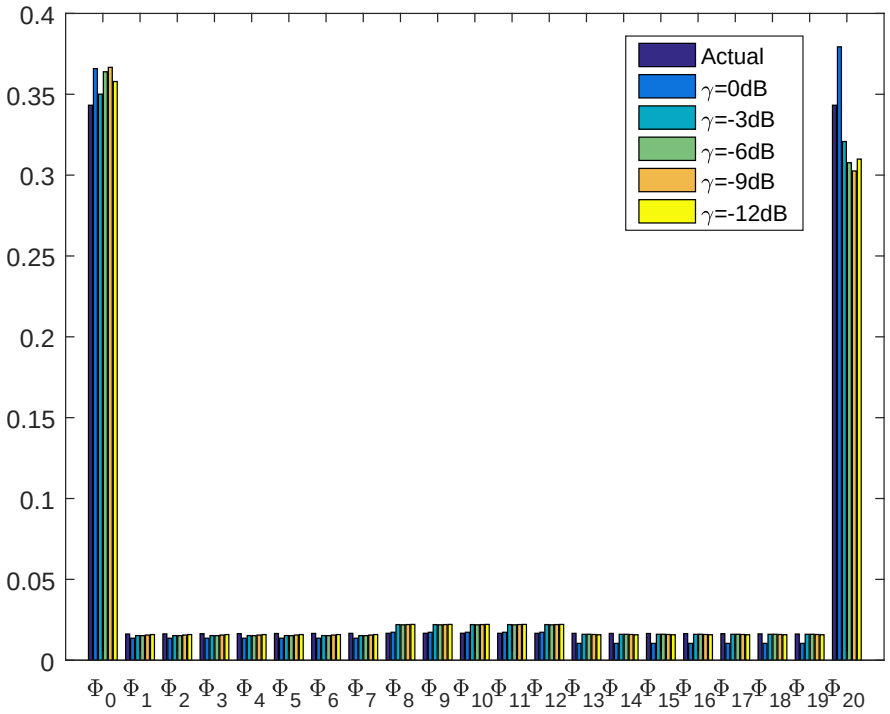

Figure 44. $\hat{\mathbf{\Phi}}$ for $N=20$, $\rho=50$, $\tau=50$, and $\gamma=-12$, -9, -6, -3, and 0 dB.

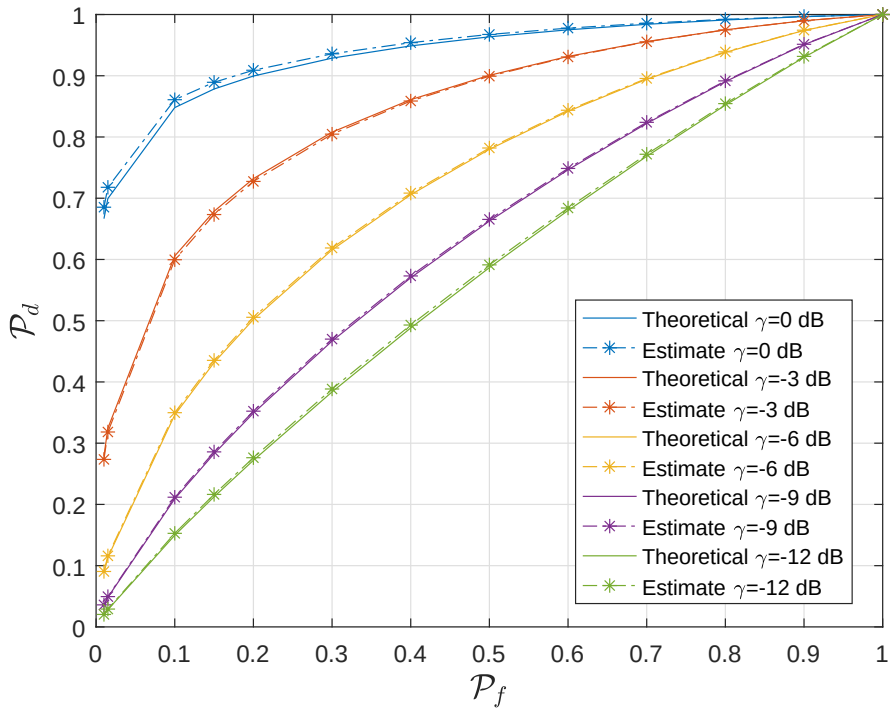

Figure 45. Estimated ROC for $N=20$, $\rho=50$, $\tau=50$, and $\gamma=-12$, -9, -6, -3, and 0 dB.

6.5 CHAPTER SUMMARY

In this chapter we proposed a novel incremental EM algorithm to estimate the sensor performance from a set of observations. Numerical results obtained illustrate that the proposed incremental EM algorithm provides a good estimate of the energy detector test statistic distribution and corresponding performance in the presence of volatile PU with unknown parameters. Further research should include optimization of the initial weights for the first increment as well as weights for components added to subsequent increments. Finally, analysis should be done on how to properly utilize the estimated test statistic distribution to adjust and optimize the sensing window duration.

CHAPTER 7

CONCLUSIONS AND FUTURE RESEARCH

The ever increasing demand for bandwidth within the finite RF spectrum has prompted the need to consider innovative methods to more efficiently use limited spectral resources. CR networks are commonly considered to be a key technology that will enable more efficient use of the RF spectrum in the future. While the last decade has brought significant research and advancements related to CR networks, there has been limited research concerning CR networks with dynamic PUs. The work presented in this dissertation addressed the performance of CR networks with dynamic PU signals, and the system model considered throughout this dissertation specifically considered that the PU could potentially switch state from ON to OFF randomly during an SU sensing period. This chapter summarizes the major conclusions of this dissertation and explores several areas of future research.

7.1 CONCLUSIONS

Several challenges arise when attempting to exploit unused spectrum licensed to highly dynamic PUs. First and foremost the current spectrum sharing paradigms do not adequately support exploiting spectrum licensed to a dynamic PU. The simulation results provided in this dissertation and supported in prior research reveal that the sensing performance with dynamic PUs is less that what is considered acceptable for CR networks. While exploring methods to improve sensing performance is important, it is equally important to consider how CR networks could potentially operate when sensing performance is reduced. A hybrid framework for spectrum sharing with suboptimal sensing performance is presented. The proposed framework requires that the PU calculate an SU operating boundary based on its own level of acceptable information error. The PU then only needs to share this boundary with potential SUs, thus limiting the information the PU is required to share about its own operation. The level of PU waveform obfuscation provided by the proposed framework is critical as it is increasingly the case where spectrum licensed to military systems is considered for spectrum sharing.

A second challenge addressed by this dissertation is the quantification of sensing performance in the presence of dynamic PUs. Prior mathematical expressions relating dynamic PU behavior to sensing performance have been proposed, but all place restrictions on the PU dynamics. The closed-form expressions provided for sensing performance in this dissertation remove these limitations and are shown to be valid regardless of the SNR or PU dynamics. This expression provides a theoretical upper limit on SU sensing performance that can be utilized in CR network design.

The third challenge addressed by this dissertation is the estimation of dynamic PU activity. The closed-form expressions for sensor performance provided requires knowledge of the parameters dictating PU dynamcis and the SNR. If neither is known it is still important for an SU to estimate its sensor performance. The incremental EM algorithm proposed in this dissertation provides a proof of concept and lays the ground work for future research in dynamic PU activity estimation using machine learning.

This dissertation attempts to address some of the problems that arise in CR networks with highly dynamic PUs and sheds light on other areas yet to be addressed in order to effectively utilize idle spectrum licensed to a dynamic PU. While the research in this dissertation was presented in the context of a CR network where an SU senses spectrum to find transmission opportunities, many of the results are applicable to a range of scenarios where sensing is used to observe or detect a dynamic signal such as biomedical signals, pulsed radar systems, or frequency hopping communication systems.

7.2 FUTURE WORK

Because the topic of CR networks with dynamic PUs has received limited attention there are several major avenues of future work that can be explored based on the advances made in this dissertation. The first major area for future research relates to the proposed hybrid spectrum sharing paradigm. The framework presented in Chapter 3 considers a digital communications PU system. However, radar systems make attractive PU systems as they have low spectral utilization both temporally and geographically. Many radar systems, such as pulsed radar, are also highly dynamic when active. Therefore, the hybrid framework presented in Chapter 3 could readily be extended to a radar system using a track error rate instead of $\mathcal{P}_b$ as an information error measure.

In addition to considering alternative PU systems, the spectrum sharing paradigm presented in Chapter 3 should be expanded to consider queuing at the SU. Additionally, topics such as spectral utilization and SU throughput should be explored in conjunction to the PU performance that the

proposed framework considered. We note that in [24] a hybrid paradigm that allows the SU to transition between the interweave and underlay paradigms based only on spectral utilization is considered and future research should consider how the two hybrid paradigms can be merged.

The dynamic PU model derived in Chapter 4 considered a PU where the transmission and idle periods were both modeled as exponential random processes. While the memoryless property of the exponential distribution is convenient for analysis and often a good approximation, alternative distributions for PU transmissions should be considered with respect to expressions for SU sensing performance in Chapter 5. Alternative PU models can be either analytical or empirical; so long as there is an accurate distribution for the number of PU ON samples per sensing period, the sensing performance expressions from Chapter 5 can be applied.

The work presented in Chapter 5 and in Chapter 6 was reliant on the SU using an energy detector. While energy detectors are convenient in that they do not require that the SU has no knowledge of the PU signal, they do not perform as well as other detectors. Future work should consider alternative detector such as waveform-based detectors, cyclostationary detectors, and correlation detectors. Similarly, within CR network research collaborative sensing amongst SUs is often considered as a method to improving sensing performance. This cooperative SU sensing framework should be considered in the detection of dynamic PUs and estimation of dynamic PU parameters

In addition to the robust theoretical model for sensor performance presented in Chapter 5 approximations were provided for $\mathcal{P}_d$ and $\mathcal{P}_f$. The simulated results showed that the approximations became less accurate as SNR increased. A more thorough analysis of how SNR impacts the approximate performance statistics should be conducted with the goal of providing limits on the applicability of the approximate performance statistics or modifying them to provide a more robust approximate.

Finally, the work presented in Chapter 6 is a preliminary attempt to use machine learning in conjunction with observations from an energy detector to define dynamic PU activity. There is significant opportunity to evolve the proposed incremental EM algorithm and explore methods for providing better initial estimates. Additionally, algorithms such as incremental component splitting [45] and distributed EM for sensor networks [46] should be considered should be considered for estimating dynamic PU parameters.

BIBLIOGRAPHY

[1] Federal Communications Commission, "Notice of Proposed Rule Making and Order: Facilitating Opportunities for Flexible, Efficient, and Reliable Spectrum Use Employing Cognitive Radio Technologies," *ET Docket*, no. 03-108, Feb. 2005.

[2] W. Krenik, A. M. Wyglinsky, and L. Doyle, "Cognitive Radios for Dynamic Spectrum Access," *IEEE Communications Magazine*, vol. 45, no. 5, pp. 64–65, May 2007.

[3] R. Chen, J. Park, and J. H. Reed, "Defense against primary user emulation attacks in cognitive radio networks," *IEEE Journal on Selected Areas in Communications*, vol. 26, no. 1, pp. 25–37, Jan 2008.

[4] T. C. Clancy and N. Goergen, "Security in cognitive radio networks: Threats and mitigation," in *2008 3rd International Conference on Cognitive Radio Oriented Wireless Networks and Communications (CrownCom 2008)*, May 2008, pp. 1–8.

[5] Z. Gao, H. Zhu, S. Li, S. Du, and X. Li, "Security and privacy of collaborative spectrum sensing in cognitive radio networks," *IEEE Wireless Communications*, vol. 19, no. 6, pp. 106–112, December 2012.

[6] R. Tandra and A. Sahai, "SNR Walls for Signal Detection," *IEEE Journal of Selected Topics in Signal Processing*, vol. 2, no. 1, pp. 4–17, 2008.

[7] Y. C. Liang, Y. Zeng, E. C. Peh, and A. T. Hoang, "Sensing-throughput tradeoff for cognitive radio networks," *IEEE Transactions on Wireless Communications*, vol. 7, no. 4, pp. 1326–1337, Apr. 2008.

[8] A. F. Molisch, L. J. Greenstein, and M. Shafi, "Propagation issues for cognitive radio," *Proceedings of the IEEE*, vol. 97, no. 5, pp. 787–804, May 2009.

[9] Y. Zeng and Y. . Liang, "Eigenvalue-based spectrum sensing algorithms for cognitive radio," *IEEE Transactions on Communications*, vol. 57, no. 6, pp. 1784–1793, June 2009.

[10] C. S. Hyder, B. Grebur, L. Xiao, and M. Ellison, "Arc: Adaptive reputation based clustering against spectrum sensing data falsification attacks," *IEEE Transactions on Mobile Computing*, vol. 13, no. 8, pp. 1707–1719, Aug 2014.

[11] Z. Quan, S. Cui, H. V. Poor, and A. H. Sayed, "Collaborative wideband sensing for cognitive radios," *IEEE Signal Processing Magazine*, vol. 25, no. 6, pp. 60–73, November 2008.

[12] W. Zhang, R. K. Mallik, and K. B. Letaief, "Optimization of Cooperative Spectrum Sensing with Energy Detection in Cognitive Radio Networks," *IEEE Transactions On Wireless Communications*, vol. 8, no. 12, pp. 5761–5766, Dec. 2009.

[13] Y. Chen, "Optimum Number of Secondary Users in Collaborative Spectrum Sensing Considering Resources Usage Efficiency," *IEEE Communications Letters*, vol. 12, no. 12, pp. 877–889, Dec. 2008.

[14] H. Urkowitz, "Energy Detection of Unknown Deterministic Signals," *Proceedings of the IEEE*, vol. 55, no. 4, pp. 523–531, April 1967.

[15] F. F. Digham, M.-S. Alouini, and M. K. Simon, "On the Energy Detection of Unknown Signals over Fading Channels," *IEEE Transactions on Communications*, vol. 55, no. 1, pp. 21–24, Jan. 2007.

[16] T. Yucek and H. Arslan, "A survey of spectrum sensing algorithms for cognitive radio applications," *Communications Surveys Tutorials, IEEE*, vol. 11, no. 1, pp. 116–130, Quarter.

[17] H. Tang, "Some physical layer issues of wide-band cognitive radio systems," in *First IEEE International Symposium on New Frontiers in Dynamic Spectrum Access Networks, 2005. DySPAN 2005.*, Nov 2005, pp. 151–159.

[18] S. Haykin, J. Reed, G. Li, and M. Shafi, "Scanning the issue," *Proceedings of the IEEE*, vol. 97, no. 4, pp. 608–611, April 2009.

[19] J. Mitola and G. Q. Maguire, "Cognitive Radio: Making Software Radios More Personal," *IEEE Personal Communications magazine*, vol. 6, no. 6, pp. 13–182, August 1999.

[20] R. Tandra, A. Sahai, and M. Mishra, "What is a Spectrum Hole and What Does it Take to Recognize One?" *Proceedings of IEEE*, vol. 97, no. 5, pp. 824–848, May 2009.

[21] F. Akhtar, M. H. Rehmani, and M. Reisslein, "White space: Definitional perspectives and their role in exploiting spectrum opportunities," *Telecommunications Policy*, vol. 40, no. 4, pp. 319 – 331, 2016.

[22] e. a. Biglieri, Ezio, *Principles of Cognitive Radio.* Cambridge: Cambridge University Press, 2012.

[23] H. K. Y. Han, E. Ekici and O. Altintas, "Spectrum sharing methods for the coexistence of multiple rf systems: A survey," *Ad Hoc Networks*, vol. 53, pp. 53–78, December 2016.

[24] F. Mehmeti and T. Spyropoulos, "Performance analysis, comparison, and optimization of interweave and underlay spectrum access in cognitive radio networks," *IEEE Transactions on Vehicular Technology*, vol. 67, no. 8, pp. 7143–7157, Aug 2018.

[25] J. G. Proakis and D. G. Manolakis, *Digital Signal Processing: Principles, Algorithms, and Applications.* Pearson Prentice Hall, 2007.

[26] T. Wang, Y. Chen, E. L. Hines, and B. Zhao, "Analysis of Effect of Primary User Traffic on Spectrum Sensing Performance," in *Proceedings 2009 Fourth International Conference on Communications and Networking in China*, August 2009.

[27] L. Tang, Y. Chen, E. L. Hines, and M. S. Alouini, "Effect of Primary User Traffic on Sensing-Throughput Tradeoff for Cognitive Radios," *IEEE Transactions on Wireless Communications*, vol. 10, no. 4, pp. 1063–1068, April 2011.

[28] S. MacDonald and D. Popescu, "Impact of Primary User Activity on the Performance of Energy-Based Spectrum Sensing in Cognitive Radio Systems," *Proc. of IEEE Globecom*, December 2013.

[29] F. Penna and R. Garello, "Detection of Discontinuous Signals for Cognitive Radio Applications," *IET Communications*, vol. 5, no. 10, pp. 1453 –1461, 1 2011.

[30] L. Tang, Y. Chen, E. L. Hines, and M. S. Alouini, "Performance Analysis of Spectrum Sensing with Multiple Status Changes in Primary User Traffic," *IEEE Communications Letters*, vol. 16, no. 6, pp. 874–877, June 2012.

[31] Y. Zou, Y.-D. Yao, and B. Zheng, "Outage Probability Analysis of Cognitive Transmissions: Impact of Spectrum Sensing Overhead," *IEEE Transactions on Wireless Communications*, vol. 9, no. 8, pp. 2676 –2688, August 2010.

[32] X. Xing, T. Jing, H. Li, Y. Huo, X. Cheng, and T. Znati, "Optimal spectrum sensing interval in cognitive radio networks," *IEEE Transactions on Parallel and Distributed Systems*, vol. 25, no. 9, pp. 2408–2417, Sep. 2014.

[33] K. W. Choi and E. Hossain, "Estimation of Primary User Parameters in Cognitive Radio Systems via Hidden Markov Model," *IEEE Transactions on Signal Processing*, vol. 61, no. 3, pp. 782–795, February 2013.

[34] *Communications Receiver Performance Degradation Handbook.* Defense Information Systems Agency, October 2010.

[35] *IEEE Recommended Practice for the Analysis of In-Band and Adjacent Band Interference and Coexistence Between Radio Systems.* IEEE Std 1900.2-2008, July 2008.

[36] M. A. Richards, *Fundamentals of Radar Signal Processing, Second Edition.* McGraw-Hill, 2014.

[37] J. M. Eargle, *Electroacoustical Reference Data.* Cambridge University Press, 2002.

[38] A. Goldsmith, *Wireless Communications.* Cambridge University Press, 2012.

[39] J. G. Proakis, *Digital Communications - 4th edition.* McGraw-Hill, 2001.

[40] G. Strang, *Linear algebra and its applications.* Thomson, Brooks/Cole, 2006.

[41] R. D. Yates and D. J. Goodman, *Probability and Stochastic Processes. A Friendly Introduction for Electrical and Computer Engineers*, 1st ed. New York, NY: John Wiley and Sons, 1999.

[42] A. Papoulis and S. U. Pillai, *Probability, Random Variables, and Stochastic Processes.* McGraw Hill, 2002.

[43] S. M. Kay, *Fundamentals of Statistical Signal Processing: Detection Theory.* Prentice Hall, 1998.

[44] T. K. Moon, "The Expectation-Maximization Algorithm," *IEEE Signal Processing Magazine*, vol. 13, no. 6, pp. 47–60, November 1996.

[45] C. Constantinopoulos and A. Likas, "Unsupervised learning of gaussian mixtures based on variational component splitting," *IEEE Transactions on Neural Networks*, vol. 18, no. 3, pp. 745–755, May 2007.

[46] D. Gu, "Distributed em algorithm for gaussian mixtures in sensor networks," *IEEE Transactions on Neural Networks*, vol. 19, no. 7, pp. 1154–1166, July 2008.

[47] S. MacDonald and D. C. Popescu, "A hybrid framework for spectrum sharing with dynamic primary users," *IEEE Communications Letters*, Submitted May 2019.

[48] S. MacDonald, D. C. Popescu, and O. Popescu, "Analyzing the performance of spectrum sensing in cognitive radio systems with dynamic pu activity," *IEEE Communications Letters*, vol. 21, no. 9, pp. 2037–2040, Sept 2017.

[49] S. L. MacDonald, D. J. Krusienski, and D. C. Popescu, "Cyclostationary-based detection of steady-state visually evoked potential signals recorded from eeg," in *2016 IEEE International Conference on Acoustics, Speech and Signal Processing (ICASSP)*, March 2016, pp. 764–768.

[50] D. Treeumnuk, S. L. Macdonald, and D. C. Popescu, "Optimizing performance of cooperative sensing for increased spectrum utilization in dynamic cognitive radio systems," in *2013 IEEE International Conference on Communications (ICC)*, June 2013, pp. 4656–4660.

[51] S. MacDonald, D. C. Popescu, and O. Popescu., "Incremental expectation maximization for estimating energy detection performance with volitile primary users," *Proc. of IEEE Globecom*, Submitted May 2019.

VITA

Sara L. MacDonald
Department of Electrical & Computer Engineering
Old Dominion University
Norfolk, VA 23529

Education

- M.S. Electrical and Computer Engineering, Old Dominion University, May 2013.
- B.S. Electrical Engineering, South Dakota School of Mines and Technology, May 2000.

Publications

- S. MacDonald and D. C. Popescu, "A hybrid framework for spectrum sharing with dynamic primary users," *IEEE Communications Letters*, Submitted May 2019.
- S. MacDonald, D. C. Popescu, and O. Popescu, "Analyzing the performance of spectrum sensing in cognitive radio systems with dynamic pu activity," *IEEE Communications Letters*, vol. 21, no. 9, pp. 2037–2040, Sept 2017.
- S. L. MacDonald, D. J. Krusienski, and D. C. Popescu, "Cyclostationary-based detection of steady-state visually evoked potential signals recorded from eeg," in *2016 IEEE International Conference on Acoustics, Speech and Signal Processing (ICASSP)*, March 2016, pp. 764–768.
- S. MacDonald and D. Popescu, "Impact of Primary User Activity on the Performance of Energy-Based Spectrum Sensing in Cognitive Radio Systems," *Proc. of IEEE Globecom*, December 2013.
- D. Treeumnuk, S. L. Macdonald, and D. C. Popescu, "Optimizing performance of cooperative sensing for increased spectrum utilization in dynamic cognitive radio systems," in *2013 IEEE International Conference on Communications (ICC)*, June 2013, pp. 4656–4660.

Submissions

- S. MacDonald, D. C. Popescu, and O. Popescu., "Incremental expectation maximization for estimating energy detection performance with volitile primary users," *Proc. of IEEE Globecom*, Submitted May 2019.

Typeset using LaTeX.